A STUDY OF MULTILEVEL PARTIAL RESPONSE SIGNALLING FOR TRANSMISSION IN A BASIC SUPERGROUP BANDWIDTH

Neil Raymond Joffe

A thesis submitted to the Faculty of Engineering, University of Cape Town, in partial fulfilment of the requirements for the degree of Master of Science in Engineering.

Cape Town, 1989

DECLARATION

I declare that this thesis is my own, unaided work. It is being submitted for the Degree of Master of Science in Engineering in the University of Cape Town. It has not been submitted before for any degree or examination in any other University.

_____

(Signature of candidate)

29th day of September 1989

ABSTRACT

The work in this thesis is primarily directed toward the design, construction and testing of an experimental multilevel partial response signalling baseband system. The system will find practical application in existing frequency division multiplexed-frequency modulated microwave links. The basic supergroup bandwidth of these links is 240 kHz. The design requires a transmission rate of 1.024 Mb/s in this bandwidth. Class-4 15 partial response signalling is the coding technique suitable to achieve this. A pilot tone scheme is used to facilitate symbol timing recovery at the demodulator. A sixth order Butterworth low-pass filter approximates the ideal raised-cosine Nyquist channel. A theoretical discussion on impairments caused by deviation from this channel is given. Since the experimental system was non-ideal, it produced a degradation in the channel signal to noise ratio. This degradation, coupled with other factors, showed that further development was necessary for the system to be suitable for connection into an existing microwave link.

To my parents, Claude and Hazel Joffe,
who have made all of this possible

ACKNOWLEDGEMENTS

I would like to express my appreciation to:

Dr. R. Braun, my supervisor for his invaluable advice and assistance throughout the course of my research

Steven Schrire, for his excellent technical assistance

Peter Scragg of STC, for many useful discussions

Anne Grant, for word processing the main body of this text

Financial assistance from the Council for Scientific and Industrial Research is gratefully acknowledged

CONTENTS

CONTENTS **Page**

CONTENTS **Page**

CONTENTS **Page**

LIST OF FIGURES

LIST OF TABLES

GLOSSARY

ADC	analog to digital converter
BATE	baseband adaptive transversal equalizer
BER	bit error rate
CCI	co-channel interference
C_{jpp}	peak-to-peak clock jitter
DAC	digital to analog converter
DAV/(DAVID)	data above voice (video)
DIV	data in voice
DUV	data under voice
D_{jpp}	peak-to-peak data transition jitter
FEC	forward error correction
ISI	intersymbol interference
LSB	least significant bit
MB	minimum bandwidth
MLSE	maximum likelihood sequence estimation
MSB	most significant bit
NMB	non-minimum bandwidth
NRZ	non return to zero
P(e)	probability of a symbol error
PLL	phase locked loop
PRBS	pseudorandom bit sequence
PRS	partial response signalling
QAM	quadrature amplitude modulation
QPRS	quadrature partial response signalling
SER	symbol error rate
S/N	signal to noise ratio
STR	symbol timing recovery
VCO	voltage controlled oscillator
α	filter roll-off parameter
ø	phase
σ_i	rms noise level of constructed noise source
σ_o	rms noise level measured at the slicer
τ	group delay

C H A P T E R 1
INTRODUCTION

Hybrid microwave systems [1.1] are used for the simultaneous transmission of time division multiplexed (TDM) data and of frequency division multiplexed (FDM) voice signals. These digital and analog signals share the baseband of a microwave system which was originally designed to carry only FDM signals. For a number of applications, if it is required to carry data at a rate between 1.024 Mb/s and 8.448 Mb/s, it is more economical to modify the existing FDM system into a hybrid system than to install a completely new, dedicated, digital link. For this reason hybrid systems are going to be required as long as FDM microwave systems carry the bulk of voice traffic.

There are three modes of hybrid transmission:

1. data under voice (DUV)
2. data in voice (DIV)
3. data above voice (DAV) or (data above video (DAVID))

DUV data is transmitted below the FDM message. In South Africa [1.2] the lowest FDM supergroup channel extends from 312 kHz to 552 kHz. This is a 240 kHz basic supergroup bandwidth. The bandwidth of the data is compressed below 312 kHz by means of multilevel pulse amplitude modulation (PAM) or partial response signalling (PRS) coding schemes.

In DIV systems, data is transmitted in a basic supergroup bandwidth within the FDM channels. Here quadrature carrier techniques are used. DIV transmission requires the most complex modulation techniques due to the narrow bandwidth in which it transmits.

DAV systems allow much higher transmission rates than DIV and DUV. The data spectrum is translated above the top FDM frequency and occupies a band which is normally unusable for

FDM transmission. An advantage of the DAV approach is that the low end of the bandwidth spectrum does not have to be vacated for data transmission, leaving the FDM channels undisturbed.

Major advantages [1.3] of DUV, DIV and DAV hybrid transmission are:

1. an economical means to transmit one or more data streams over a single FM radio system

2. it is simple to make changes to existing analog routes

3. modems equipped with forward error correction (FEC) achieve excellent BER performance of less than 10^{-8}

4. they require regenerative spans of 1000 km, which is in sharp contrast with dedicated digital radio systems which require regenerative modems typically spaced every 60 km.

5. no selective fade problems for DUV and DIV on account of the narrow bandwidths of transmission - adaptive equalizers easily compensate for transmission impairments

6. higher spectral efficiencies are obtainable as compared to current high capacity digital radio systems

DAV and DUV hybrid 1.544 Mb/s transmission schemes appeared in the literature as early as 1975 [1.4]. By 1981, a number of 1.544 Mb/s - above - 960 FDM capacity DAV systems were operational in Canada. The FDM-FM carrier frequency was 6 GHz and the DAV modulation, quadrature phase shift keying (QPSK) [1.5].

In 1985 [1.3], computer simulations showed that it was possible to transmit 1.544 Mb/s plus overhead bits, i.e., a

total rate of 1.6 Mb/s in a bandwidth of 256 kHz. Hence, a spectral efficiency of 6.25 bits per second per Hertz (b/s/Hz) was required. The DIV modulation was 225 QPRS (quadrature partial response signalling).

In 1986 [1.6], a number of 1.544 Mb/s DIV modems, requiring a basic supergroup bandwidth of 240 kHz, were installed over long distance FDM-FM microwave systems. These modems used 256 QAM (quadrature amplitude modulation) and achieved 6.43 b/s/Hz. At about the same time [1.7], computer simulations investigated the performance of DIV and DAVID systems transmitting 2.048 Mb/s in a 240 kHz basic supergroup. The modulation scheme was 1024 QAM and spectral efficiency, 8.53 b/s/Hz.

Theoretical and experimental results in 1987 [1.8] showed that it was possible to obtain a spectral efficiency of 8.84 b/s/Hz. This experimental DIV system transmitted 2.048 Mb/s plus overhead bits in a basic supergroup of 240 kHz.

A paper published in 1988 [1.9] showed by means of a computer simulation that, by carving out a small bandwidth around DC in a 225 QPRS above Nyquist rate DIV modem, spectral efficiencies above 6.25 b/s/Hz could be obtained in a bandwidth of 256 kHz.

The South African FDM-FM microwave systems are being replaced by 16 QAM dedicated digital radio systems. The transmission rate is 140 Mb/s in 40 MHz of RF bandwidth (3.5 b/s/Hz). DUV, DIV and DAV could well be employed on the existing FDM-FM links. DUV could operate at 1.024 Mb/s, DIV at 2.048 Mb/s and DAV at 8.448 Mb/s.

The work in this thesis is primarily directed toward the design, building and testing of an experimental non-minimum bandwidth (NMB) baseband modem. The term "modem" usually refers to a system incorporating carriers and band-pass

hardware. In this thesis "modem" will refer only to the baseband hardware. The modem uses multilevel PRS to facilitate the transmission of 1.024 Mb/s in a 240 kHz basic supergroup bandwidth. Thus the required transmission spectral efficiency is 4.27 b/s/Hz. The design is best suited to DUV applications where there is no carrier system required for connection into the FDM system. Further design work is required for practical 2.048 Mb/s (8.448 Mb/s) transmission rate DIV (DAV/DAVID) systems.

This thesis is divided into six chapters. Chapter 2 gives the theory which is necessary for understanding the techniques used in the design of the modem. The advantages of PRS over zero-memory coding systems is discussed here. Chapter 3 describes the practical work done in designing and building the experimental modem. Chapter 4 describes the experiments done to evaluate its performance.

The channel, may in practice, have significant effect on the performance of the modem. Chapter 5 gives a theoretical discussion on the most common channel impairments. Adaptive equalizers are used to correct for such transmission impairments. However, the design of an adaptive equalizer is beyond the scope of this thesis.

Chapter 6 is a summary of the developments of the previous chapters. Recommendations for further areas of study are also given in this chapter.

REFERENCES

[1.1] Feher, K. **Digital Communications: Microwave Applications**, Prentice-Hall Inc., Englewood Cliffs N.J, 1981 pp.183-197.

[1.2] Siemens technical brochure, **Transmultiplexer TRMX 2x2/SG**, Siemens AG.

[1.3] Feher, K., Karkar E.M. and Huang J. **On 6.67 b/s/Hz - 256-QAM and 225-QPRS Modems for T1/SG Data-in-Voice (DIV) Applications**, IEEE ICC, June 1985, pp. 453-459

[1.4] Feher, K., Goulet, R. and Morissette S. **1.544 Mb/s Data Above FDM Voice (DAV) and Data Under FDM Voice (DUV) Microwave Transmission**, IEEE Trans. Communications, November 1975.

[1.5] same as reference [1.1] above.

[1.6] Mathiopoulos, P., Feher, K. **Performance Evaluation of 512-QAM Systems in Distorted Channels**, Proc. IEE, Vol.133, Pt.F, No.2, April 1986.

[1.7] Kucar, A.D., Feher K. **On 1.544 Mb/s and 2.048 Mb/s Modems for CCITT Supergroup DIV and DAVID Applications**, IEEE ICC, 1986 pp. 446-451.

[1.8] Feher, K. **1024-QAM and 256-QAM Coded Modems for Microwave and Cable System Applications**, IEEE Vol. SAC 5, No. 3, April 1987.

[1.9] Wu, K., Sasase, I. and Feher K. **Class-IV PRS above the Nyquist Rate**, Proc. IEE, Vol. 135, Pt.F, No.2, April 1988.

CHAPTER 2
BACKGROUND THEORY

2.1 Introduction

This chapter gives the background theory necessary for understanding the techniques used in the design of the experimental modem of Chapter 3. Nyquist's theorems are discussed in the first part of this chapter. Section 2.3 describes the advantages of PRS over zero-memory systems. Theory is developed for PRS schemes with binary input. It is shown how the theory can be extended to multilevel inputs. The final section of this chapter, section 2.5 describes the characteristics of selected PRS schemes as well as precoding and decoding techniques.

2.2 Nyquist's Theorems

A digital transmission system [2.1] is more spectrally efficient if it has a capability of transmitting a greater number of bits per second in a given bandwidth. The bandwidth is frequently normalized to 1 Hz, and the spectral efficiency is expressed in bits per second per Hertz (b/s/Hz).

In his landmark patents on channel characteristics in the 1920s, Nyquist defined the minimum channel bandwidth requirements and also the general characteristics required for intersymbol interference (ISI)-free reception. For data transmission systems, the following are the most frequently used Nyquist theorems.

1. Nyquist's First Theorem (Minimum Bandwidth - Brick-Wall Channel

   If synchronous impulses having a transmission rate of f_s symbols per second are applied to an ideal, linear phase brick-wall low-pass channel having a cutoff frequency of

$f_N = f_s/2$, then the responses to these impulses can be observed independently, that is, without ISI.

Note: For ISI-free transmission of f_s rate rectangular pulses, an (x/sin x)-shaped amplitude equalizer has to be added to the ideal brick-wall channel. Thus it is possible to have an ISI-free transmission rate of 2 symbols/s/Hz.

2. Nyquist's Vestigial Symmetry Theorem (Non-Minimum Bandwidth Channel)

The addition of a skew symmetrical, real-valued transmittance function Y(w) to the transmittance of the ideal low-pass filter maintains the zero-axis crossings of the impulse response. These zero-axis crossings provide the necessary condition for ISI-free transmission. The symmetry of Y(w) about the cutoff frequency w_N (Nyquist radian frequency $w_N = 2\pi f_N$) of the linear-phase brick-wall filter is defined by:

$$Y(w_N - x) = -Y(w_N + x) \qquad 0 < x < w_N \qquad (2.1)$$

In order to visualize the practical importance of these theorems, the ensuing description is presented for the binary case; the Nyquist transmission theorems apply to the multilevel case as well.

Consider the ideal brick-wall channel model of Fig.2.1. The cutoff frequency, also known as the Nyquist frequency, is defined to be $f_N = 1/2T_s = f_s/2$, where T_s is the unit symbol duration. (In binary systems, the symbol rate equals the bit rate, thus $T_s = T$, where T is the unit bit duration. In multilevel systems $T_s = T\log_2 M$, where M is the number of signalling levels). The impulse response of the channel, h(f), is given by the inverse Fourier transform of the transfer function H(f):

$$H(f) = \begin{cases} Ts & |f| \le \frac{1}{2T_s} \\ 0 & |f| > \frac{1}{2T_s} \end{cases} \qquad (2.2)$$

$$h(t) = F^{-1}[\ H(f)\ ] = \int_{-\infty}^{\infty} H(f)e^{-j2\pi ft}\, df \qquad (2.3)$$

$$h(t) = \frac{\sin(2\pi f_n t)}{2\pi f_n t} = \frac{\sin(\pi t/T_s)}{\pi t/T_s} \qquad (2.4)$$

(Note that the phase of H(f) is zero for all frequencies). From this impulse response,

$$h(nTs) = \begin{cases} 1 & \text{for } n = 0 \\ 0 & \text{for } n = \pm 1,\ \pm 2,\ \pm 3, \ldots \end{cases} \qquad (2.5)$$

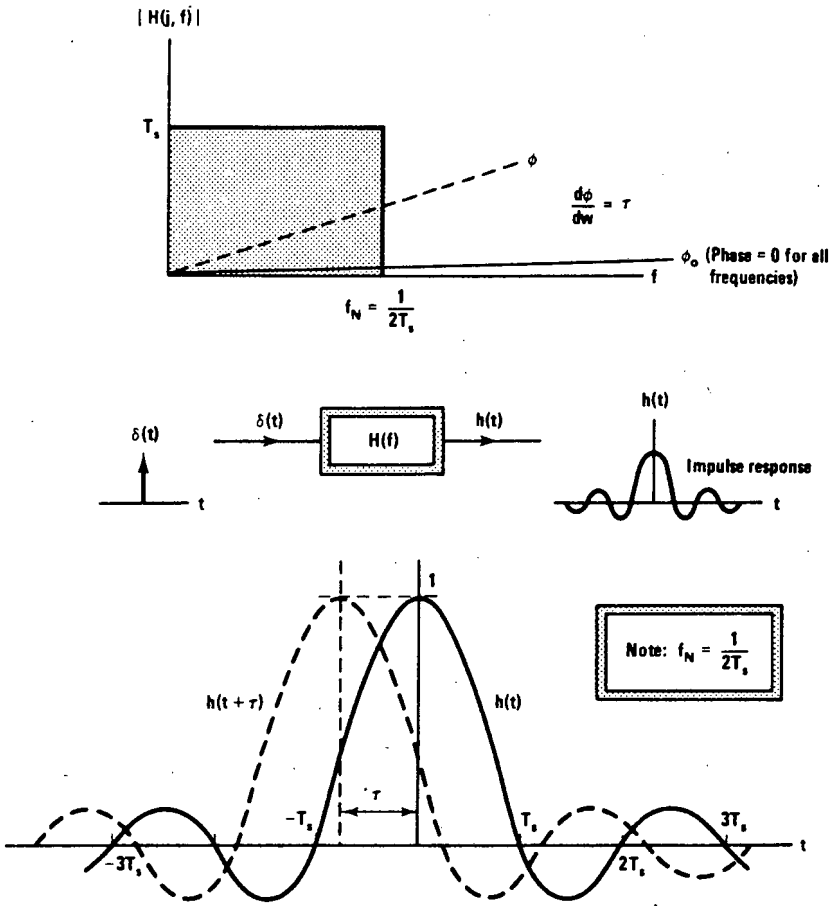

Fig. 2.1 Ideal brick-wall channel and its corresponding impulse response [2.2]

Thus the impulse response attains its full value for $t = nT_s = 0$ and has zero crossings for all other integer multiples of the symbol duration. If the ideal brick-wall channel has a nonzero but linear phase (dashed line in Fig. 2.1), the impulse response is shifted by an amount that equals the channel delay. This delay is = dø/dw; and for linear phase filters, is constant over all frequencies. As the shape of the impulse response is the same as with $\tau = 0$, there will be no further distortion introduced. The sampling instants in the receiver are shifted by τ seconds.

Note that the conceptual channel input (also known as filter excitation), $\delta(t)$, has an infinitesimally short duration, whereas the output (i.e. the impulse response) has an infinite duration. The bandlimited channel stretches the impulse beyond the T_s interval and deforms the input signal. A desirable property of the described impulse response is that it has zero values for integer multiples of T_s. It is now easy to see that in an $f_n = 1/2T_s$ wide brick-wall channel, it is possible to transmit and detect synchronous, random impulses at a rate $f_s = 1/T_s = 2f_N$. Theoretically, the detection of any of these symbols can be performed without any interference from the previously sent or the subsequent patterns. This situation is known as ISI-free transmission.

Unfortunately, the described minimum bandwidth Nyquist channels are not realizable. An infinite number of filter sections would be required to synthesize the infinite attenuation slope of the brick-wall channel. Additionally, the delay in the lobes of the time domain response is very slow. This, in turn, would cause a prohibitively large ISI degradation for smallest filtering or symbol timing imperfections.

To alleviate these problems and to define more practical channel characteristics, Nyquist introduced the vestigial symmetry theorem.

$$H(f) = G(f)(1 - e^{-j4\pi fT})$$
$$= j2T\sin(2\pi fT)\cdot G(f) \qquad (2.10)$$

Thus H(f) has a gradual roll-off to the band edge and can be implemented by practical and realizable analog filtering. The corresponding impulse response h(f) is

$$h(t) = \frac{\sin(\pi t/T)}{\pi t/T} - \frac{\sin[\pi(t - 2T)/T]}{\pi(t - 2T)/T} \qquad (2.11)$$

as shown in Fig.2.3(b). A sample input sequence a_k and the resulting three level ($\pm 2,0$) output sequence, y_k for the class-4 PRS is shown in Fig. 2.3(c).

2.5 Generalized PRS Systems

2.5.1 Impulse and Frequency Response

For a PRS system, the impulse response h(t) is required to pass through 0 at regular T-second intervals with the exception of a period of NT seconds, N being the smallest number of samples that span all the nonzero samples.

The noiseless PRS system is characterized by the samples of the desired impulse response h(t). If x_n, n = 0,1,2,... N-1 are N sample values of h(t) and N is the smallest number of contiguous samples that span all the nonzero samples, the PRS system is described by the system polynomial

$$x(D) = \sum_{k=0}^{N-1} x_k D^k, \qquad x0, xN-1 = 0 \qquad (2.12)$$

where D is the delay operation corresponding to a T second delay. The PRS system can be modelled by a cascade of a tapped delay line with coefficients x_k (a discrete nonrecursive finite impulse response filter) and a filter G(f) as shown in Fig. 2.4.

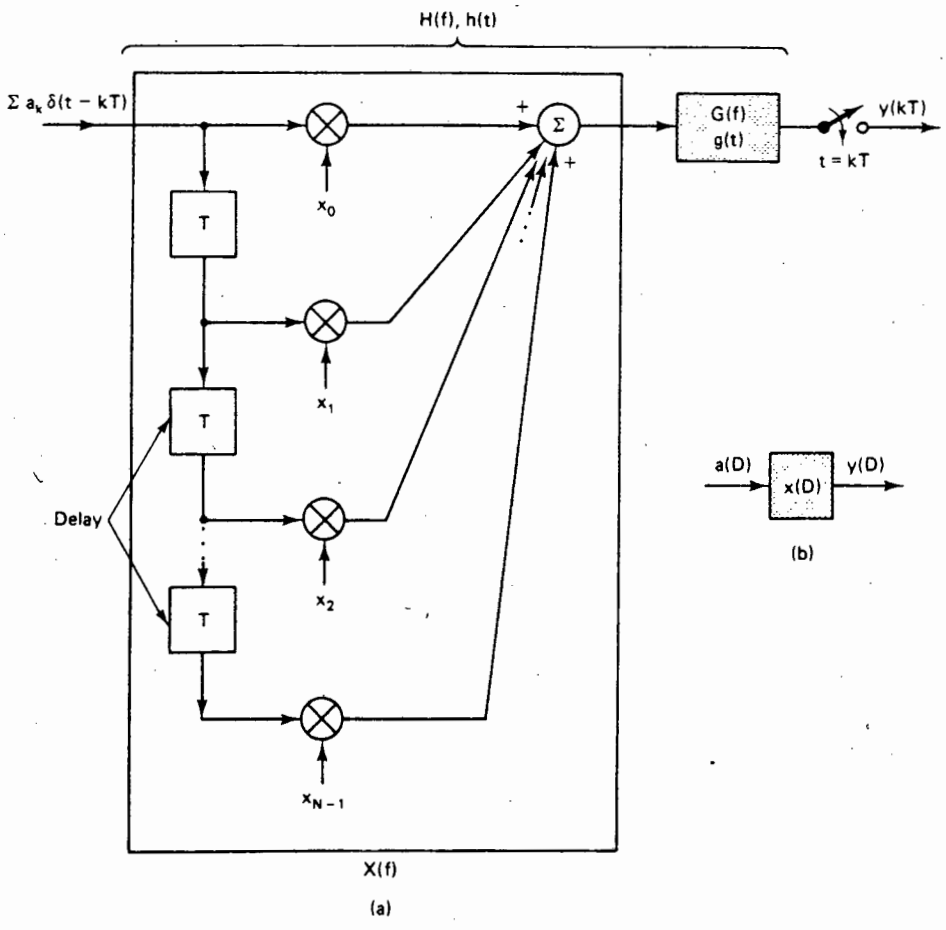

Fig. 2.4 (a) Generalized PRS system model, (b) Discrete system model.

The periodic frequency response of the transversal filter is

$$X(f) = x(D)\Big|_{D = e^{-j2\pi fT}} = \sum_{k=0}^{N-1} x_k e^{-j2\pi kT} \tag{2.13}$$

and the impulse response

$$x(t) = \sum_{k=0}^{N-1} x_k \delta(t - kT) \tag{2.14}$$

The PRS system impulse response thus is

$$h(t) = \sum_{k=0}^{N-1} x_k g(t - kT) \tag{2.15}$$

corresponding to H(f) = X(f)G(f). Thus the PRS system can be visualized as a cascade of two parts: X(f) forces the desired sample value but is periodic whereas the Nyquist filter G(f) preserves the sample values but can be used to bandlimit the resulting system. For a given system polynomial x(D), different choices of G(f) (both minimum and non-minimum bandwidths) result in different H(f), all of which have identical sampled responses.

This separation makes it easier to understand the frequency domain behaviour of the PRS system and its spectral properties such as bandwidth and nulls.

2.5.2 System Bandwidth

From Fig.2.4 it can be seen that the bandwidth is controlled by the choice of G(f). In order to maximize the data rate in the available bandwidth, many PRS systems use the MB G(f). NMB G(f) are also feasible, and are used in DUV systems.

2.5.3 Spectral Nulls

If H(f) is discontinuous (G(f) is the ideal MB brick-wall filter), then h(t) decays slowly as $1/|t|$. This type of system is impractical to use and intolerant to timing perturbations. Therefore, H(f) must be continuous to render the system practical. This implies that X(f) must have a zero at f = 1/2T (where G(f) is discontinuous) for H(f) to be a continuous function. X(f) has a spectral null at f = 1/2T if and only if x(D) has (1 + D) as a factor. For a spectral null at f = 0, it can be shown that (1 - D) must be a factor of x(D). Table 2.2 is a short list of PRS system polynomials. The reader is referred to the paper by Kabal and Pasupathy [2.4] for the extended list. These systems have no nulls or severe ripples in the passband and are therefore good candidates for practical coding schemes.

Table 2.2 Comparison of PRS Coding Schemes

x(D)	PRS Scheme	Spectral Nulls f = 0	Spectral Nulls f = 1/2T
1 + D	class-1	no	yes
1 - D	dicode	yes	no
$1 - D^2$	class-4	yes	yes

2.5.4 Number of Output Levels

The values of a_k do not necessarily have to take on binary values only. For the three PRS systems in Table 2.2, if M is the number of levels of a_k, then the number of output levels in y_k is given by L, where

$$L = 2M - 1 \tag{2.16}$$

This is the extension of PRS to multilevel PRS.

2.5.5 Symbol-by-Symbol Decoders

The sampled output of an ideal noiseless PRS system is given by

$$y_m = x_0 a_m + \sum_{i=1}^{N-1} x_i a_{m-i} \tag{2.17}$$

The second term represents the controlled ISI introduced by the PRS system. The decoder can recover the data a_m by subtracting the effect of previous input symbols. In practice, only estimates of the data are available and these are used to cancel the controlled ISI in the decision feedback decoder structure (Fig. 2.5).

It can be seen that past decision errors can adversely effect subsequent decisions. It can also be shown that class-1, dicode and class-4 PRS systems have identical error performances.

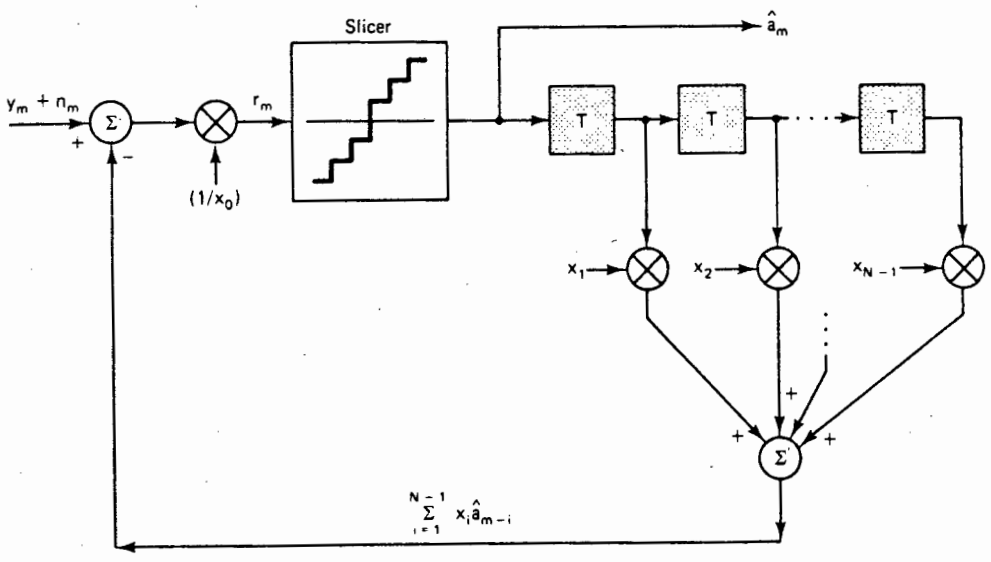

Fig. 2.5 Decision-feedback decoder for PRS [2.3].

2.5.6 Precoding

Precoding is a technique used to eliminate the error propagation problem of the decision feedback decoder. Error propagation was caused by the fact that previous symbols were not available at the decoder and only their estimates were known. The precoder eliminates the effect of previous symbols at the source where they are known precisely. Decisions at the output are then made independently of one another. Figure 2.6 shows the precoding technique as it is applied to the class-4 system for M level input.

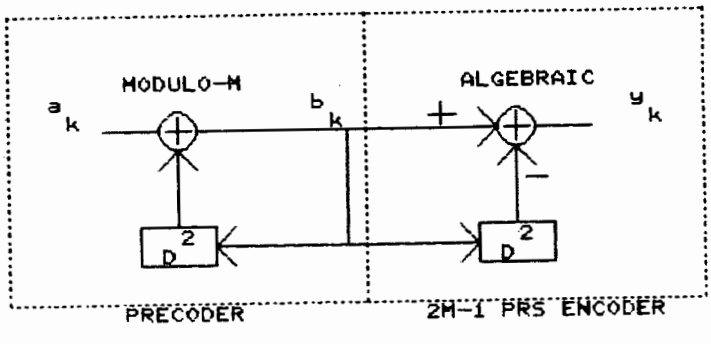

Fig. 2.6 Precoding for class-4 with M level input.

Note that $y_k \equiv a_k$ provided that y_k is interpreted modulo-M. The decoder makes the hard decision modulo-M since y_k does not depend on the symbol two previous to it.

Precoding for dicode and class-1 systems are slightly different to precoding for class-4. They are as simple to implement and are given in reference [2.4].

2.5.7 Viterbi Decoder for PRS

The increase in the number of output levels due to correlation of the a_k symbols results in a S/N degradation. This was seen as the inevitable penalty to be paid in exchange for the increase in data rate and the insensitivity to channel perturbations and variations in transmission rate. This apparent poorer performance is not an inherent drawback of PRS but is due to the non-optimality of the conventional symbol-by-symbol detection method. It was shown that [2.5] maximum likelihood sequence estimation (MLSE), using the Viterbi algorithm, can be used to recover almost all the S/N loss.

REFERENCES

[2.1] Feher, K. and Engineers of Hewlett-Packard, **Telecommunications Measurements, Analysis, and Instrumentation**, Prentice-Hall, Inc. 1987, pp. 10-14.

[2.2] Lender, A. Chapter 7 of Feher K. **Digital Communications: Microwave Applications**, Prentice-Hall, Inc. 1981.

[2.3] Feher, K. **Advanced Digital Communications: Systems and Signal Processing Techniques**, Prentice-Hall Inc. 1987, pp. 433-450.

[2.4] Kabal, P., Pasupathy, S. **Partial-Response Signaling**, IEEE Trans. on Communications, Vol. COM-23, No.9 September 1975.

[2.5] Forney, G.D., Jr. **Maximum-likelihood sequence estimation of digital sequences in the presence of intersymbol interference**, IEEE Trans. on Inform. Theory, Vol. IT-18, May 1972.

C H A P T E R 3
EXPERIMENTAL HARDWARE

3.1 Introduction

This chapter describes the design and construction of an experimental multilevel PRS modem. The chapter starts with a list of the modem specifications. A candidate multilevel PRS scheme is selected based on the specifications. The design and construction is then described in detail.

3.2 Modem Specifications

It is necessary to define a list of specifications for an experimental modem whose performance we wish to investigate.

They are:

1) transmission rate of 1.024 Mb/s in a basic supergroup bandwidth of 240 kHz; spectral efficiency is (1.024 Mb/s)/240 kHz = 4.27 b/s/Hz

2) average BER better than 10^{-8} without FEC (forward error correction)

The specifications are given with the following assumptions:

1) no CCI (co-channel interference)

2) no channel impairments, thus there is no need for a BATE (baseband adaptive transversal equalizer)

Figure 3.1 shows the block diagram of the proposed experimental PRS modem.

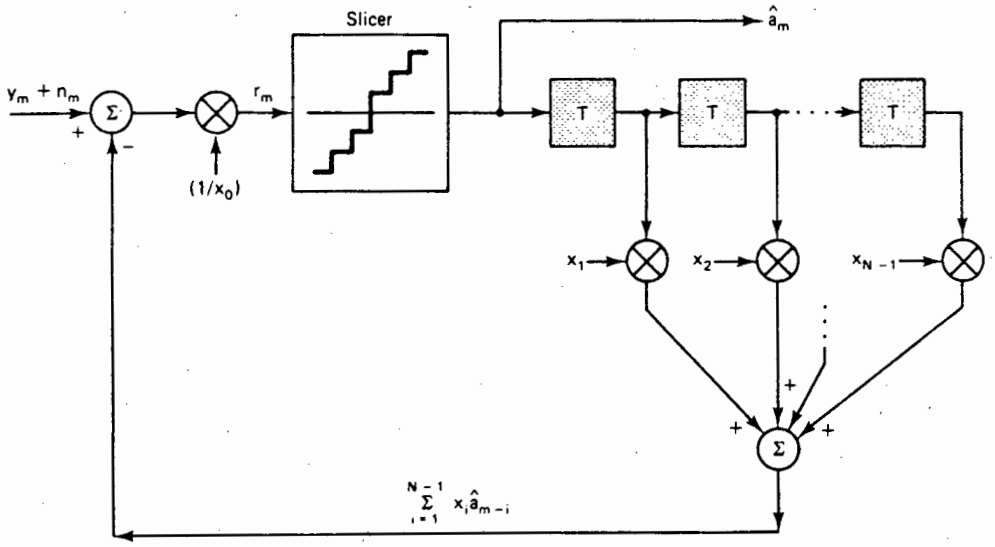

Fig. 2.5 Decision-feedback decoder for PRS [2.3].

2.5.6 Precoding

Precoding is a technique used to eliminate the error propagation problem of the decision feedback decoder. Error propagation was caused by the fact that previous symbols were not available at the decoder and only their estimates were known. The precoder eliminates the effect of previous symbols at the source where they are known precisely. Decisions at the output are then made independently of one another. Figure 2.6 shows the precoding technique as it is applied to the class-4 system for M level input.

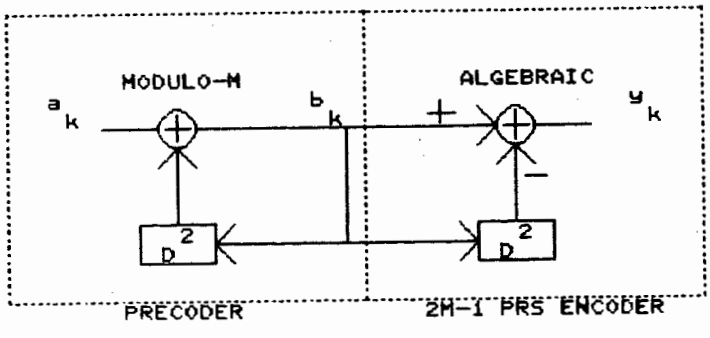

Fig. 2.6 Precoding for class-4 with M level input.

Note that $y_k \equiv a_k$ provided that y_k is interpreted modulo-M. The decoder makes the hard decision modulo-M since y_k does not depend on the symbol two previous to it.

Precoding for dicode and class-1 systems are slightly different to precoding for class-4. They are as simple to implement and are given in reference [2.4].

2.5.7 Viterbi Decoder for PRS

The increase in the number of output levels due to correlation of the a_k symbols results in a S/N degradation. This was seen as the inevitable penalty to be paid in exchange for the increase in data rate and the insensitivity to channel perturbations and variations in transmission rate. This apparent poorer performance is not an inherent drawback of PRS but is due to the non-optimality of the conventional symbol-by-symbol detection method. It was shown that [2.5] maximum likelihood sequence estimation (MLSE), using the Viterbi algorithm, can be used to recover almost all the S/N loss.

REFERENCES

[2.1] Feher, K. and Engineers of Hewlett-Packard, **Telecommunications Measurements, Analysis, and Instrumentation**, Prentice-Hall, Inc. 1987, pp. 10-14.

[2.2] Lender, A. Chapter 7 of Feher K. **Digital Communications: Microwave Applications**, Prentice-Hall, Inc. 1981.

[2.3] Feher, K. **Advanced Digital Communications: Systems and Signal Processing Techniques**, Prentice-Hall Inc. 1987, pp. 433-450.

[2.4] Kabal, P., Pasupathy, S. **Partial-Response Signaling**, IEEE Trans. on Communications, Vol. COM-23, No.9 September 1975.

[2.5] Forney, G.D., Jr. **Maximum-likelihood sequence estimation of digital sequences in the presence of intersymbol interference**, IEEE Trans. on Inform. Theory, Vol. IT-18, May 1972.

C H A P T E R 3
EXPERIMENTAL HARDWARE

3.1 Introduction

This chapter describes the design and construction of an experimental multilevel PRS modem. The chapter starts with a list of the modem specifications. A candidate multilevel PRS scheme is selected based on the specifications. The design and construction is then described in detail.

3.2 Modem Specifications

It is necessary to define a list of specifications for an experimental modem whose performance we wish to investigate.

They are:

1) transmission rate of 1.024 Mb/s in a basic supergroup bandwidth of 240 kHz; spectral efficiency is (1.024 Mb/s)/240 kHz = 4.27 b/s/Hz

2) average BER better than 10^{-8} without FEC (forward error correction)

The specifications are given with the following assumptions:

1) no CCI (co-channel interference)

2) no channel impairments, thus there is no need for a BATE (baseband adaptive transversal equalizer)

Figure 3.1 shows the block diagram of the proposed experimental PRS modem.

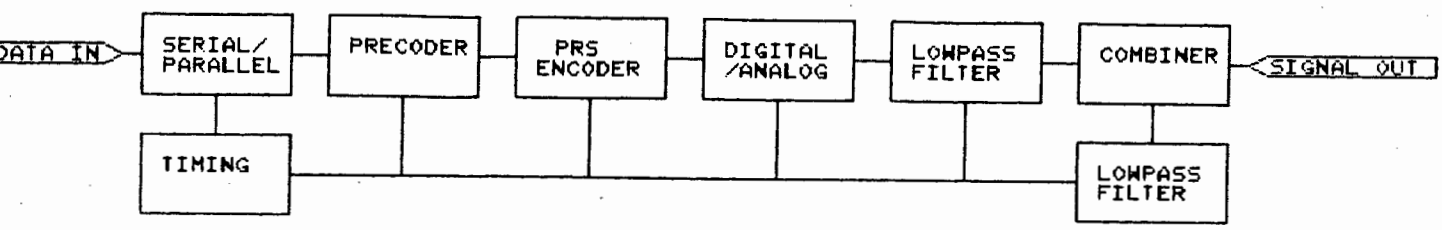

(a)

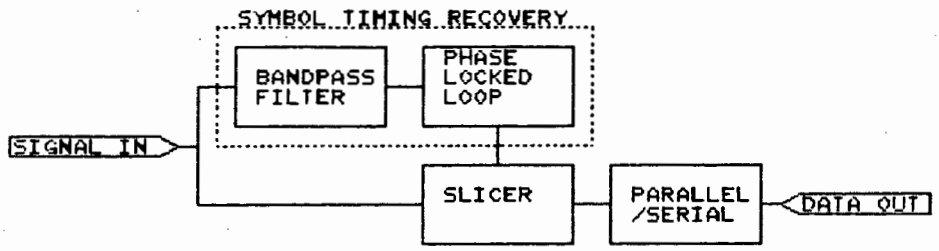

(b)

Fig. 3.1 Modem block diagram: (a) modulator, (b) demodulator.

As discussed in Chapter 1, the design is that of a (non-minimum bandwidth) baseband modem. It is NMB in that the bandwidth is not restricted to the Nyquist frequency (see section 2.5.1). The modem is best suited to DUV applications; carriers are not required for connection of a DUV modem into an existing FDM system.

Although the proposed design is a baseband modem, it is useful to compare its transmission spectral efficiency (measured in a 240 kHz bandwidth) to quadrature carrier systems; the modem achieves the same transmission spectral efficiency as a 225 QPRS modem having two parallel baseband streams carrying independent information each at a rate 512 kb/s. The transmission spectral efficiency is also identical to that obtained in a Q-SSB system having two dependent baseband streams each at a nominal rate of 1.024 Mb/s. This is so because in QPRS systems there are two sidebands and also two independent baseband channels. In Q-SSB systems there is only one baseband stream (the Q baseband stream does not contain independent information) [3.1].

3.3 Candidate PRS Schemes

7 PRS has a theoretical maximum spectral efficiency of 4 b/s/Hz (see Table 2.1). A spectral efficiency of 4.27 b/s/Hz represents an increase of 6.8% above the Nyquist rate. The Nyquist frequency of 7 PRS with a transmission rate of 1.024 Mb/s is 256 kHz. Construction of an above Nyquist rate modem requires spectral chopping of frequencies above 240 kHz. The design is based on Feher's model B [3.2] and requires a low-pass filter with $\alpha < 0.08$.. This is a particularly stringent specification. Construction of a filter of this type requires state-of-the-art technology.

15 PRS has a theoretical maximum spectral efficiency of 6 b/s/Hz. It transmits 3 bits/symbol and has a Nyquist frequency of 170.7 kHz. Constraints on the low-pass filter are far more relaxed than in the case of a 7 PRS scheme. Here α = 240 kHz/170.7 kHz = 0.41. On the other hand 15 PRS has inherently higher ISI.

A third candidate system is 31 PRS. It has a maximum spectral efficiency of 8 b/s/Hz and transmits 4 bits/symbol. The Nyquist frequency for a transmission rate of 1.024 Mb/s is 128 kHz. The required low-pass filter α is 0.875. Although the filter roll-off is the least steep of the three schemes, 31 PRS has the highest amount of ISI and the highest S/N requirement for a given P(e).

A comparison of the three schemes is shown in table form below:

Table 3.1 Comparison of 7, 15 and 31 PRS

Coding Scheme	Input Levels M	Output Levels L	Maximum Spectral Effic-iency (b/s/Hz)	Nyquist Frequency (kHz)	Filter Roll-off α	Required S/N for $P(e)=10^{-8}$ (dB)
7PRS	4	7	4	256	< 0.08	25
15PRS	8	15	6	170.7	0.41	31
31PRS	16	31	8	128	0.875	37

The number of output levels is calculated from (2.16). The required S/N for a P(e) of 10^{-8} are approximate values for S/N in the Nyquist bandwidth which equals half the symbol rate in each case [3.3]. They are determined from the expression

$$P(e) = 2(1 - 1/M^2)\, Q\left[\frac{\pi}{4}\left[\frac{3}{M^2-1}\cdot\frac{S}{N}\right]^{\frac{1}{2}}\right] \qquad (3.1)$$

$$\text{where } Q(x) = \frac{1}{\sqrt{2}\sqrt{\pi}} \int_x^{\infty} e^{-t^2/2}\, dt \qquad (3.2)$$

As the number of output levels increase, so the horizontal and vertical eye openings of the channel are reduced. Thus 31 PRS will be the most sensitive to recovered symbol clock jitter and filter imperfections. For several dBs of degradation (due to performance deviation from the ideal), the practical S/N requirement could be in excess of 40dB.

Table 2.2 gave a list of the characteristics of three PRS coding schemes (class-1, dicode, class-4). Class-1 [3.4] is not suitable for use in SSB modems and carrier systems where reduced low frequency components in the spectrum are required. The main advantage of class-4 over both class-1 and dicode is that class-4 has spectral nulls at both DC and the Nyquist frequency (170.7 kHz).

For systems not restricted to the MB (such as this design), a pilot tone can be inserted in the spectral null, at the Nyquist frequency, to facilitate symbol timing recovery (STR) at the demodulator [3.5].

From the above discussion it can be concluded that class-4 15 PRS is the best candidate for a transmission rate of 1.024 Mb/s in a basic supergroup bandwidth of 240 kHz.

3.4 Modulator

3.4.1 Timing

A 4.096 MHz crystal oscillator circuit is used. All sub-multiples of the crystal frequency required in the modulator are derived by frequency dividing the fundamental square wave. Tuning of the oscillator is achieved by adjusting a 20pF variable capacitor placed in series with the crystal. The circuit diagram is shown in Fig 3.2.

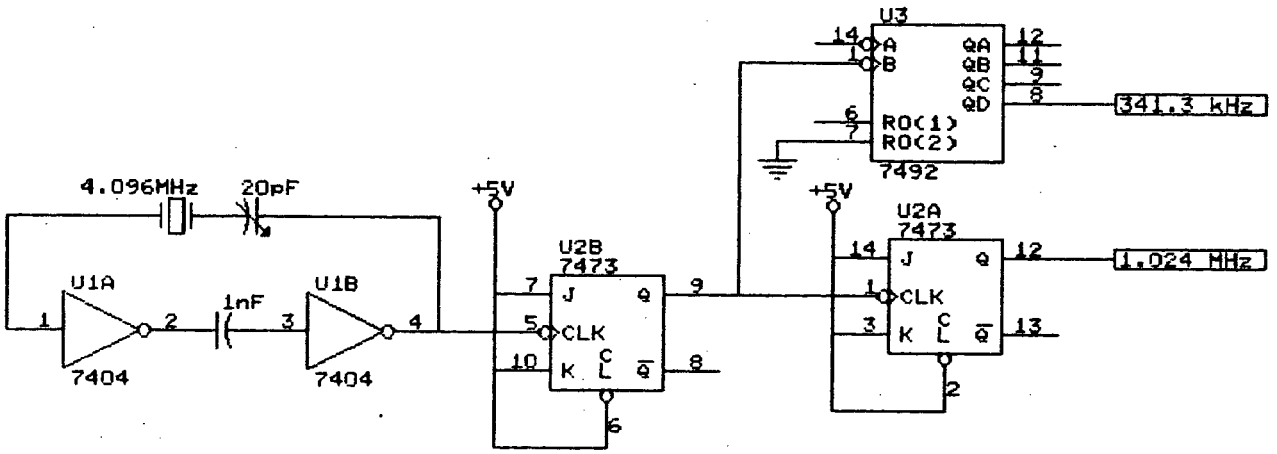

Fig. 3.2 Timing circuit diagram.

3.4.2 Serial to Parallel Converter

The serial 1.024 Mb/s NRZ bit stream is split into three parallel streams by means of shift registers, having a serial input and parallel output configuration. Since the modem transmits three bits/symbol, the symbol rate is (1.024 Mb/s)/(3 bits/symbol) = 341.3 ksymbol/s. With reference to Fig. 3.4, the integrated circuit (IC) suitable for this purpose is a SN7496 (TTL device). Each three bit code (eight-state symbol) is interpreted as a positive binary number with a decimal equivalent from zero to seven.

3.4.3 Precoder and 15 PRS Encoder

Normally Grey coding is performed at the modulator before the precoding operation. Hence, errors in adjacent levels at the decoder correspond to single bit errors. This modem does not have Grey coding with the result that measurements are in terms of SER (symbol error rate) and not BER (bit error rate). This is discussed in detail in Chapter 4.

Precoding (discussed in section 2.5.5) is used to prevent error propagation. Precoding is almost always more effective then decision feedback at the demodulator, except at low values of S/N or when a large portion of filter shaping is done at the modulator [3.6]. Here 100% filter shaping is performed at the modulator. Thus, the precoding operation is more effective.

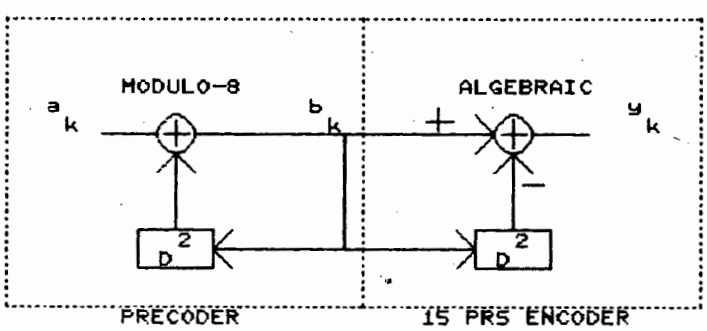

Fig. 3.3 Precoder and 15 PRS encoder.

In mathematical terms, Fig. 3.3 can be expressed as:

$$a_k = b_k (1 - D^2) \qquad \text{modulo-8} \qquad (3.3a)$$

$$\text{or} \quad b_k = a_k + D^2 b_k \qquad \text{modulo-8} \qquad (3.3b)$$

$$\text{and} \quad y_k = b_k (1 - D^2) \qquad \text{algebraic} \qquad (3.3c)$$

A circuit is required to implement expressions (3.3 b and c) which are respectively the precoding and class-4 15 PRS encoding. Referring to Fig. 3.4, each three bit (eight level) code represented by a_k is latched by a positive edge sensitive D-type register at the parallel outputs of the shift registers. Care has to be taken that the latching occurs in the centre of the parallel bits to avoid any edge ambiguities. This is done by using the B input of the divide-by-six counter (Fig. 3.2). Thus the 341.3 kHz clock has a rising edge in the centre of the three bit parallel code.

The D^2 operators are implemented by using a hex D-type latch. The modulo-8 summation (3.3 b) is done by a four bit (7483) summer. The most significant bit - the fourth bit of the sum having an equivalent decimal value of eight - is ignored. Thus the algebraic sum of a_k and $D^2 b_k$ is transformed to a sum in modulo-8.

Table 3.2 Transformation of a_k to y_k

3-bit 8 Level Code, a_k		Corresponding 4-bit 15 Level Code, y_k			
Binary	Decimal	Binary	Decimal	Binary	Decimal
000	0			1000	8
001	1	0001	1	1001	9
010	2	0010	2	1010	10
011	3	0011	3	1011	11
100	4	0100	4	1100	12
101	5	0101	5	1101	13
110	6	0110	6	1110	14
111	7	0111	7	1111	15

Equation (3.3 c) is performed using a modified 2's complement arithmetic. The bits in D^2b_k are complemented, but no sign bit is used to indicate a negative or positive number. The result is that the subtraction of D^2b_k complemented from b_k produces y_k a 15 level code interpreted as positive numbers only. This greatly reduces the complexity of decoding at the demodulator. Table 3.2 shows the transformation of a_k to y_k. Note that all three-bit codes (except for 000) have two possible corresponding transformations to y_k.

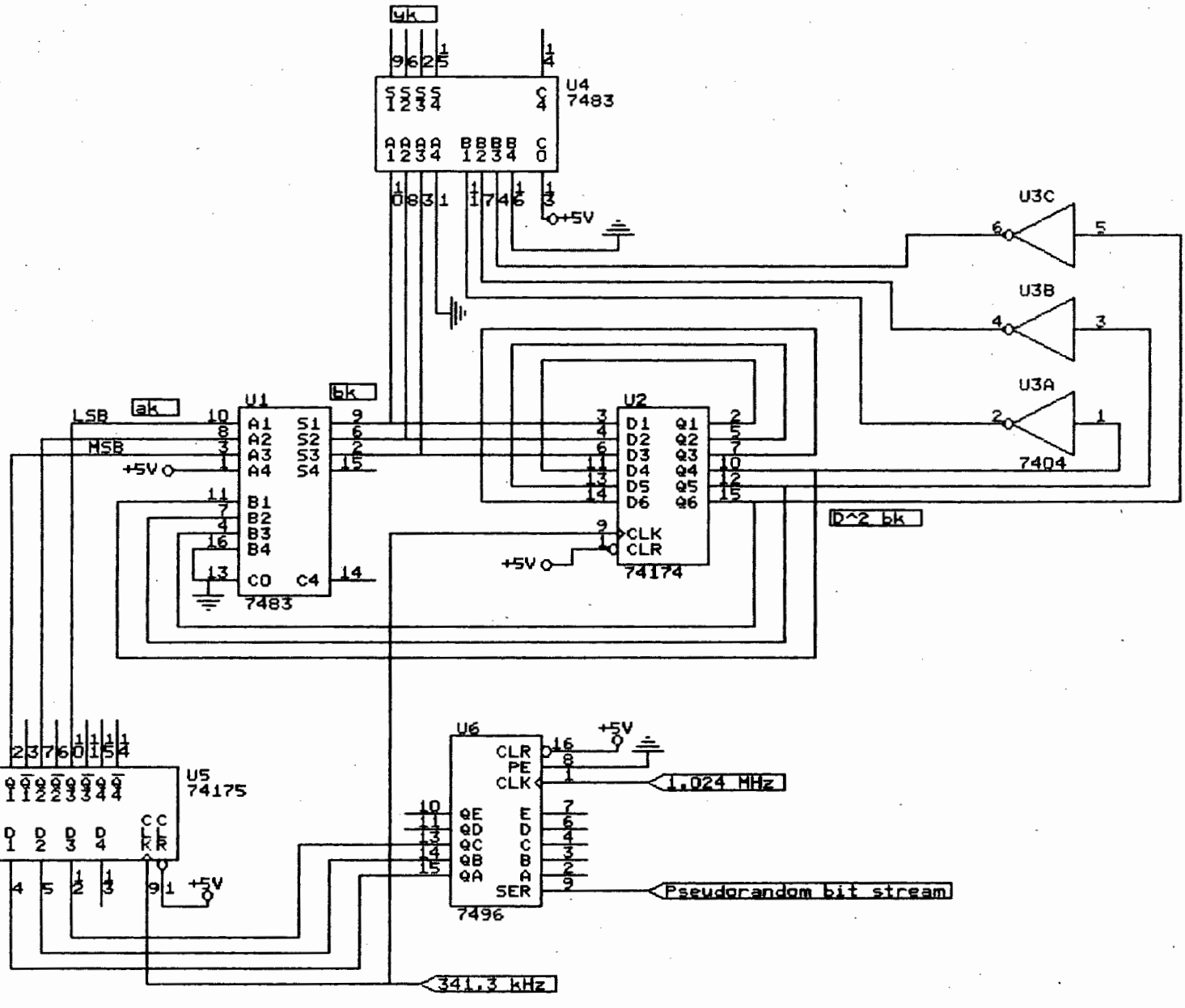

Fig. 3.4 S/P, precoder and 15 PRS encoder circuit diagram.

3.4.4 Impulse Generator

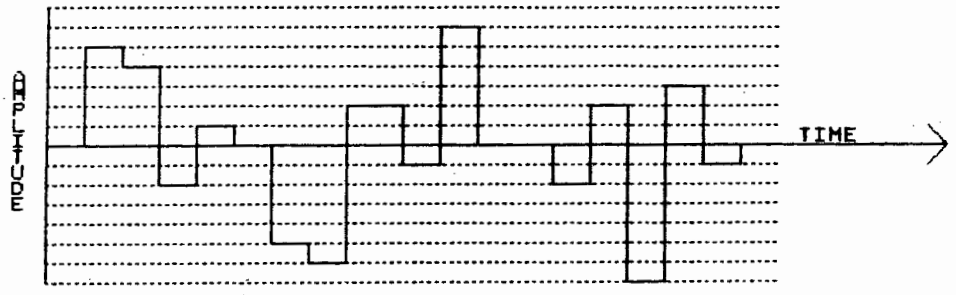

Fig. 3.5 15 Level PRS waveform.

Figure 3.5 shows an example of y_k at the output of the PRS encoder. It consists of synchronous rectangular pulses of width T_s, where $T_s = 1/341.3 = 2.93\mu s$. The spectrum of this waveform is shaped by an envelope of the form

$$\frac{\sin(x)}{x} \qquad (3.3)$$

where $x = wT_s/2$

where w is the angular frequency. The spectral shaping is due to the finite width of the pulses (see section 2.1). An x/sinx amplitude equalizer is normally designed as part of a low-pass filter (equation 2.7). However, this method complicates the design of a low-pass filter to bandlimit the multilevel pulse stream. A second method is to transform the multilevel pulse stream into a multilevel impulse train. This method is one which works particularly well at lower data rates, and provided that the impulse widths are sufficiently narrow. In the modem design, a pulse width of approximately 1/5 T_s was used and this was found to be suitable.

A 74221 monostable is selected to provide narrow pulses which approximate impulses. From the manufacturers design specifications the pulse width, t_w is given as

$$t_w \approx C_{ext}R_{ext}\ln 2 \qquad (3.5)$$

where C_{ext} and R_{ext} are respectively the values of the capacitor and resistor connected to the IC. For a pulse width of $1/5T_s$

$$t_w = \frac{1}{5} \cdot \frac{1}{341.3\ \text{kHz}} = 586\ \text{ns}$$

For C_{ext} = 82pf, the required value of R_{ext} is 10 kΩ. The phase of the narrow pulses are such that they occur at the centre of the parallel data streams of y_k.

The most significant bit of y_k is connected to an OR gate with the impulse signal Q complement (Fig. 3.7). The reason is to force the code 1000 in the time period between two separate symbols of y_k. A code of 1000 at the input to the DAC translates into an output voltage of exactly half the full scale. After level translation this voltage becomes zero volts (ground). The three least significant bits of y_k are connected to an AND gate with the impulse signal Q. Thus the data time is restricted to the impulse width time.

Figure 3.6 shows (on channel 3 & 4), the (Q) waveforms generated by the monostable from the symbol clock (on channel 2). Channel 1 is the 1.024 MHz clock.

3.4.5 Digital to Analog Converter (DAC)

The selection of a DAC is based primarily on its speed of conversion, since the digital pulses at its input are approximately 586 ns wide. An 8-bit monolithic high speed multiplying DAC (AD DAC-08) is used. This device has a fast settling time of approximately 85ns and a linearity error of ± ¼LSB.

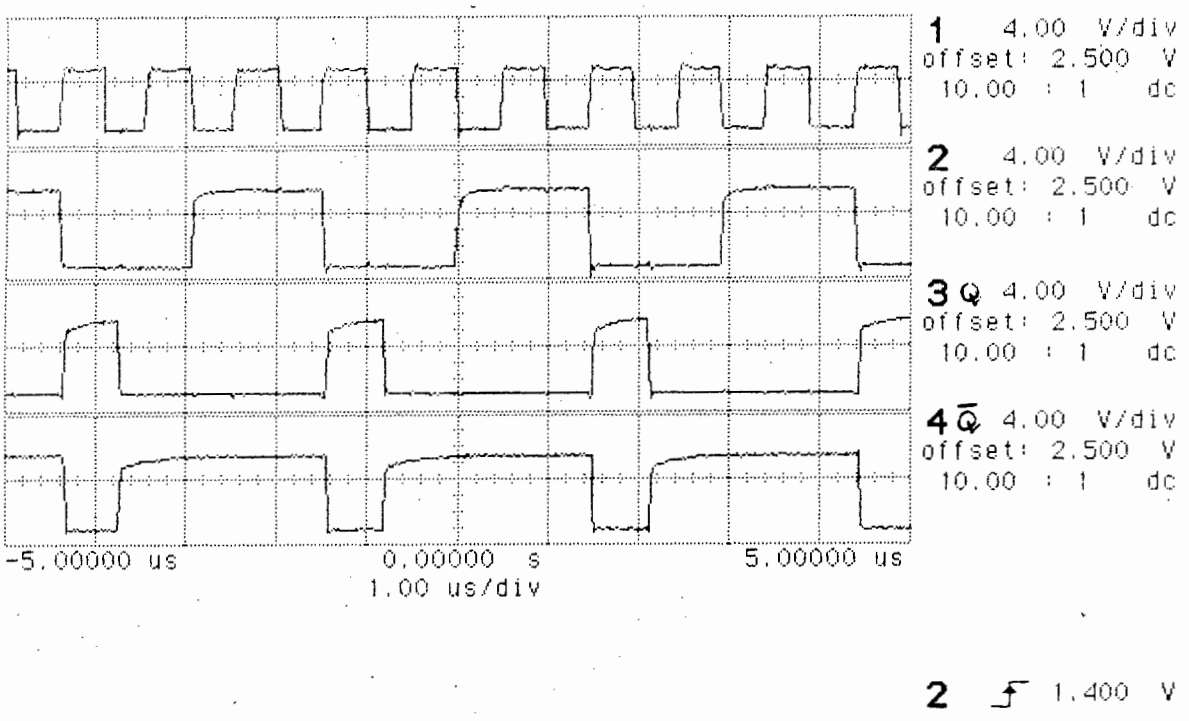

Fig. 3.6 Timing waveforms.

The four most significant bits are used for y_k. The other inputs are grounded. This gives the maximum possible voltage level separation at the output of the DAC. The DAC is used in a trans-resistance configuration (current-to-voltage amplifier). The 10pF capacitor across the op-amp is necessary for stability [3.7]. The DC output capacitance in combination with the 4.7kΩ feedback resistance introduces a lagging phase shift which severely compromises the speed of the op-amp. Thus a high speed op-amp (LM6361) with an input slew rate of 300V/μs and a unity gain frequency of 50 MHz is used for this circuit configuration. A 5kΩ preset resistor is used for level translation. The 15 level impulse train at the output of the op-amp is approximately 8V peak-to-peak. No DC component is present (characteristic of class-4 PRS).

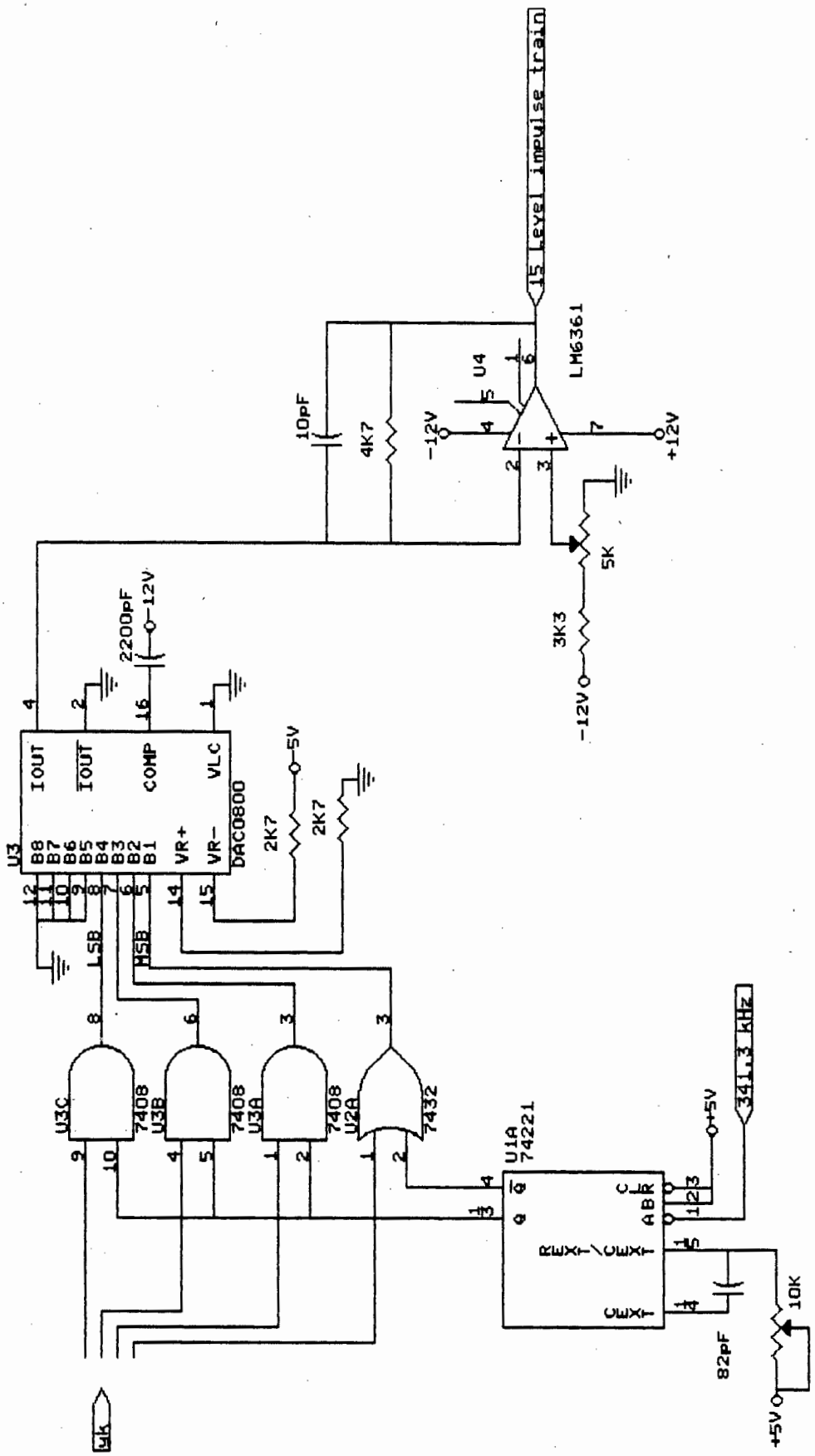

Fig. 3.7 Impulse generator and digital to analog converter.

The sinx/x envelope of the PRS spectrum at the output of the DAC is clear in Fig. 3.8. It can be seen that the envelope has a null at approximately 1.53 MHz. The effective impulse duration is therefore 1/1.53 MHz = 650ns. The lower frequency of the spectrum (frequencies up to 240 kHz), are not attenuated by the envelope. Thus the choice of pulse width is satisfactory.

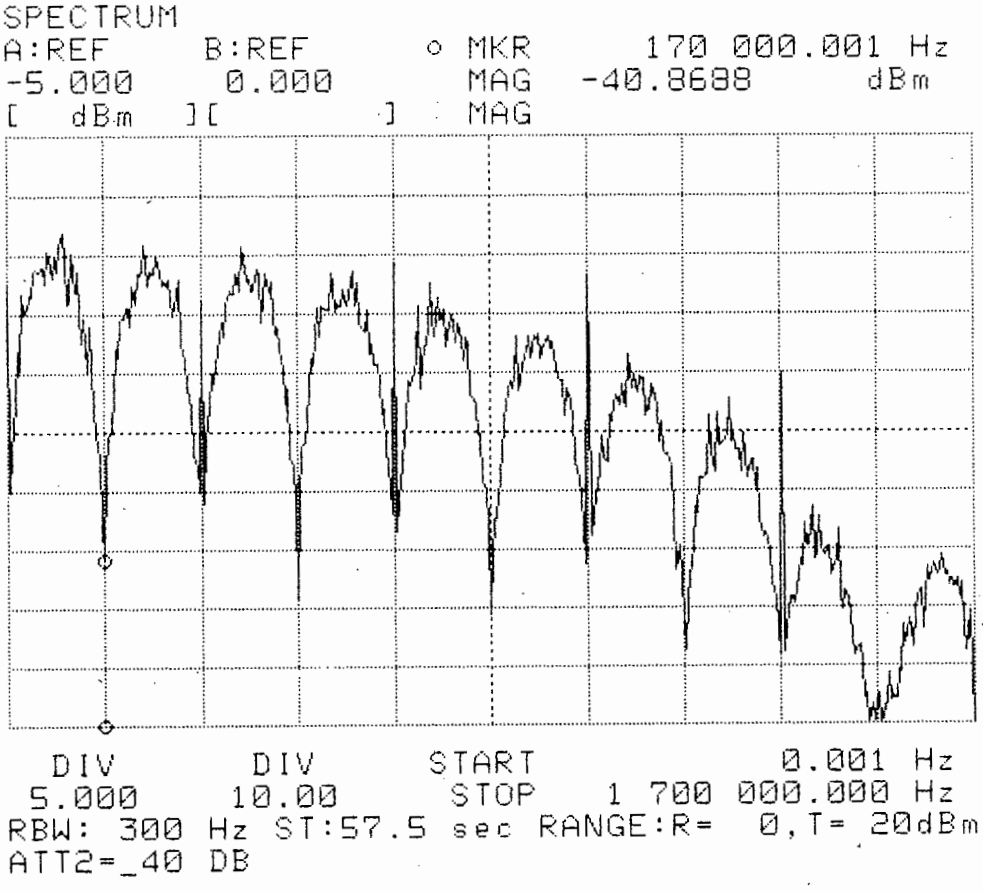

Fig. 3.8 Non-bandlimited class-4 15 PRS spectrum.

The presence of the symbol clock at multiples of 341.3 kHz is due to high power leakage into the spectrum analyzer [3.8]. These clock harmonics are unimportant and should not be confused with the pilot tone which is to be added in the spectral null at 170.7 kHz. The spike below 0.001 Hz

indicates the 0 - Hz start sweep frequency of the spectrum analyzer.

3.4.6 Low-Pass Filter Design

3.4.6.1 Specifications

As stated in Chapter 2, Nyquist filters and overall Nyquist channel response lead to ISI-free transmission systems. An attempt must be made to approximate a Nyquist raised-cosine low-pass filter which has a flat (unequalized) magnitude (for impulse transmission) at low frequencies and a roll-off portion that has a sinusoidal form with odd symmetry about the -3dB cutoff frequency of 170.7 kHz. The filter, in theory must have linear phase across its entire band. Practical filters [3.1] are phase equalized up to the -10 to -15dB attenuation point. They have an out of band attenuation of 20 to 50dB depending on the adjacent CCI. In this modem design, since it has been assumed that there is no CCI, an out of band attenuation of 20dB will be sufficient.

Optimum performance [3.6] of a raised-cosine Nyquist channel is obtained when matched filters are used, i.e. filter shaping is shared equally between the modulator and the demodulator. Each filter has a $\sqrt{\alpha}$ roll-off parameter. In this design, 100% filter shaping is performed at the modulator. The demodulator merely bandlimits the channel noise. This commonly used filter shaping results in about 1dB degradation in S/N with respect to the case in which the filter shaping is optimally divided between the modulator and the demodulator [3.4].

The requirements on performance of the low-pass filter based on the discussion above are:

1. flat passband amplitude response
2. -3dB cutoff frequency of 170.7 kHz
3. minimum out of band attenuation of 20dB at f = 240 kHz

4. skew symmetrical roll-off about the cutoff frequency
5. linear phase up to -10 to -15dB attenuation frequency

3.4.6.2 Filter Types

The Butterworth filter exhibits a maximally flat passband amplitude response. A sixth order Butterworth filter (in theory) gives 17.8dB attenuation at 240 kHz. However phase characteristics of this all-pole filter are poor nearer the cutoff frequency.

An elliptic filter provides excellent out of band attenuation. A filter of minimum order three is required for 20dB attenuation at 240 kHz. This filter exhibits ripples in both the pass- and stopbands. However the filter can be designed to have a small passband ripple which is within acceptable limits. The phase characteristics of an elliptic filter are the most non-linear of all types of filters.

The Chebyshev filter exhibits ripples in the passband and is monotonic in the stopband.

The Bessel filter has a monotonically decreasing amplitude response from DC. High orders of this type of filter exhibit almost perfect linear phase response. However this type of filter does not meet the passband or stopband amplitude requirements.

All-pass filters have flat amplitude characteristics. Their phase may be controlled in such a way as to cancel out or equalize the poor phase characteristics of a filter which meets the amplitude requirements.

Thus it can be said that it is impossible to satisfy all five requirements with one low-pass filter. The final filter will be a hybrid or combination of two or more filters. In practice, this is how a raised-cosine Nyquist filter is best approximated.

Three types of second order sections are considered here. Their characteristics are shown in Table 3.3 below.

Table 3.3 Comparison of 2nd order sections of active filters

Filter Type	Circuit Complex -ity	no. of op-amps	Max Pole Pair Q	Tuning	Variable Component	Stability
VCVS	simple	3	100	easy	resistor	good
biquad	complex	3	100	easy	resistor	excellent
three cap- icitor	complex	3	100	easy	capacitor	good

Note: VCVS is the short form of voltage controlled voltage source

The biquad circuit was selected because of its ease of tuning and excellent stability. However, this circuit was fairly complex in its implementation. A quad op-amp (LF347N) was used for the active filter sections. This device has an input slew rate of 13V/μs and a gain bandwidth product of 4 MHz. It easily meets the specifications for the minimum slew-rate. Both filters were designed for a DC gain of 1. The capacitors were standard 56pF ceramics. Tuning of each second order section was done with 10-turn potentiometers so that good accuracy could be achieved.

3.4.6.4 Elliptic Filter Design

An attempt is made to satisfy requirements 1,2,3 and 4 by means of sixth order elliptic filter. The elliptic filter has an amplitude response that exhibits ripples in both the pass and stopbands (Fig. 3.9), and it is the best of all low-pass filters in that, for a given order and allowed pass and stopband deviation, it has the minimum transition width (TW) = $(w_1 - w_c)$. The pass-band ripples are equal in magnitude and may be characterized by the maximum allowable pass-band

loss. This value is called the pass-band ripple width (PRW) and is given by:

$$PRW = -20\log_{10}A_1 \quad dB \tag{3.6}$$

The stopband ripples are also equal in magnitude (although not necessarily equal to the pass-band ripple magnitude) and are characterized by the minimum stopband loss (MSL).

$$MSL = -20\log_{10}A_2 \quad dB \tag{3.7}$$

A flat pass-band amplitude response is given by requirement no. 1. The minimum obtainable PRW (based on design tables in reference [3.9]) is 0.1dB. The -3dB cutoff frequency of 170.7 kHz is not $f_c = wc/2\pi$ as one would expect. In this case f_c is the -0.1dB cutoff. For a sixth order filter, the theoretical MSL is 50dB at 240 kHz. The filter consists of three cascaded second order sections.

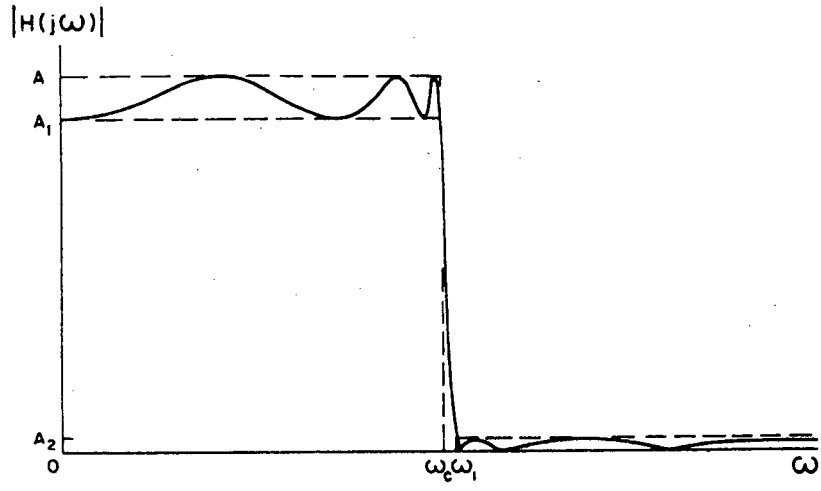

Fig. 3.9 Elliptic sixth order low-pass amplitude response [3.9]

The filter was designed for a -0.1dB cutoff frequency of 168 kHz. This was an attempt to obtain a -3dB cutoff of 170.7 kHz. Thus TW = (240 - 168) kHz = 72 kHz.

Component values and theoretical responses of each second order section were calculated using EUREKA(C) software (see Appendix A). A second order section of the sixth order filter is shown in Fig. 3.10.

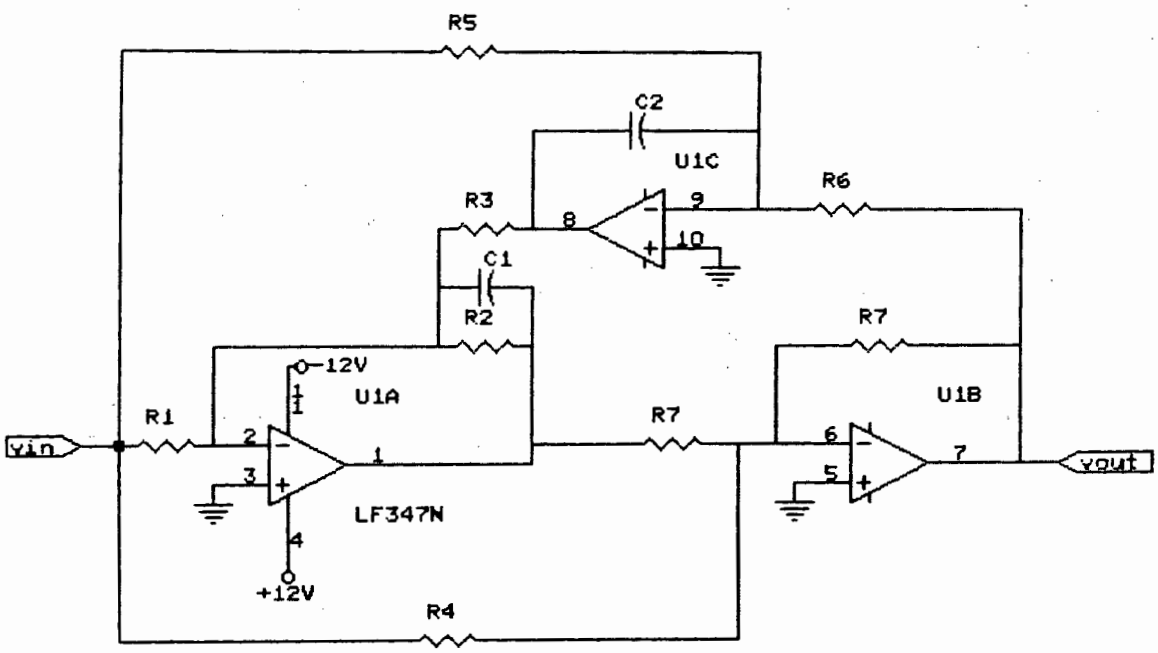

Fig. 3.10 Biquad elliptic second order section

3.4.6.5 Butterworth Filter Design

Here an attempt is made to satisfy requirements 1,2,4 and 5 by means of a 6th order Butterworth low-pass filter. Here f_c is the -3dB cutoff frequency of 170.7 kHz. For a given order n, the attenuation α_2 (dB) at any frequency point f_1 beyond the cutoff f_c is given by

$$\alpha_2 = 10\log\left[1 + \left[\frac{f_1}{f_c}\right]^{2n}\right] \qquad (3.8)$$

For a sixth order filter with f_1 = 240 kHz, α_2 is determined from (3.8) to be 17.8dB. Thus, it can be seen that this filter does not meet the third requirement (20dB attenuation at 240 kHz).

Component values and theoretical responses of each second order section are given in Appendix A. The circuit diagram of a second order biquad Butterworth section is shown in Fig. 3.11.

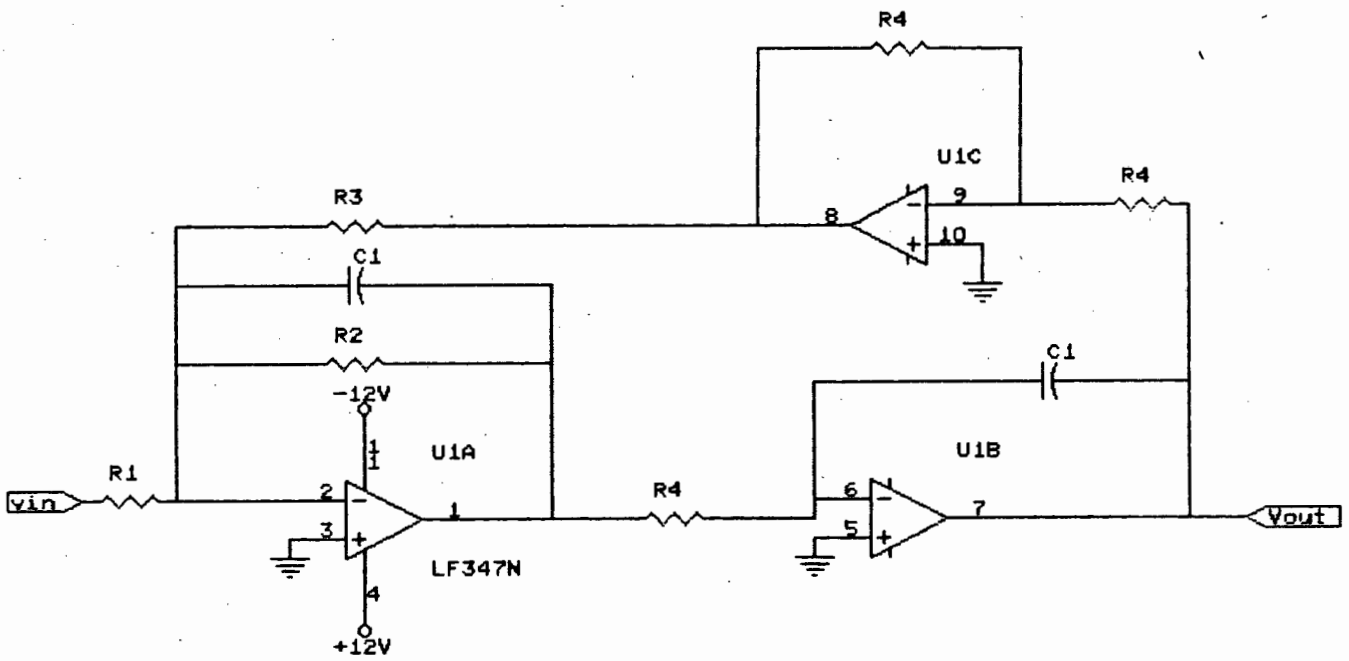

Fig. 3.11 Biquad second order Butterworth section.

3.4.6.6 Results

Magnitude responses of the two filters are shown in Fig. 3.12 (a) and (b). The scale reference of 0dBm is not absolute since an oscilloscope introduced attenuation between the outputs of the filters and the input to the spectrum analyzer. The scale reference is unimportant since it is the shape of response and relative attenuation which are of interest.

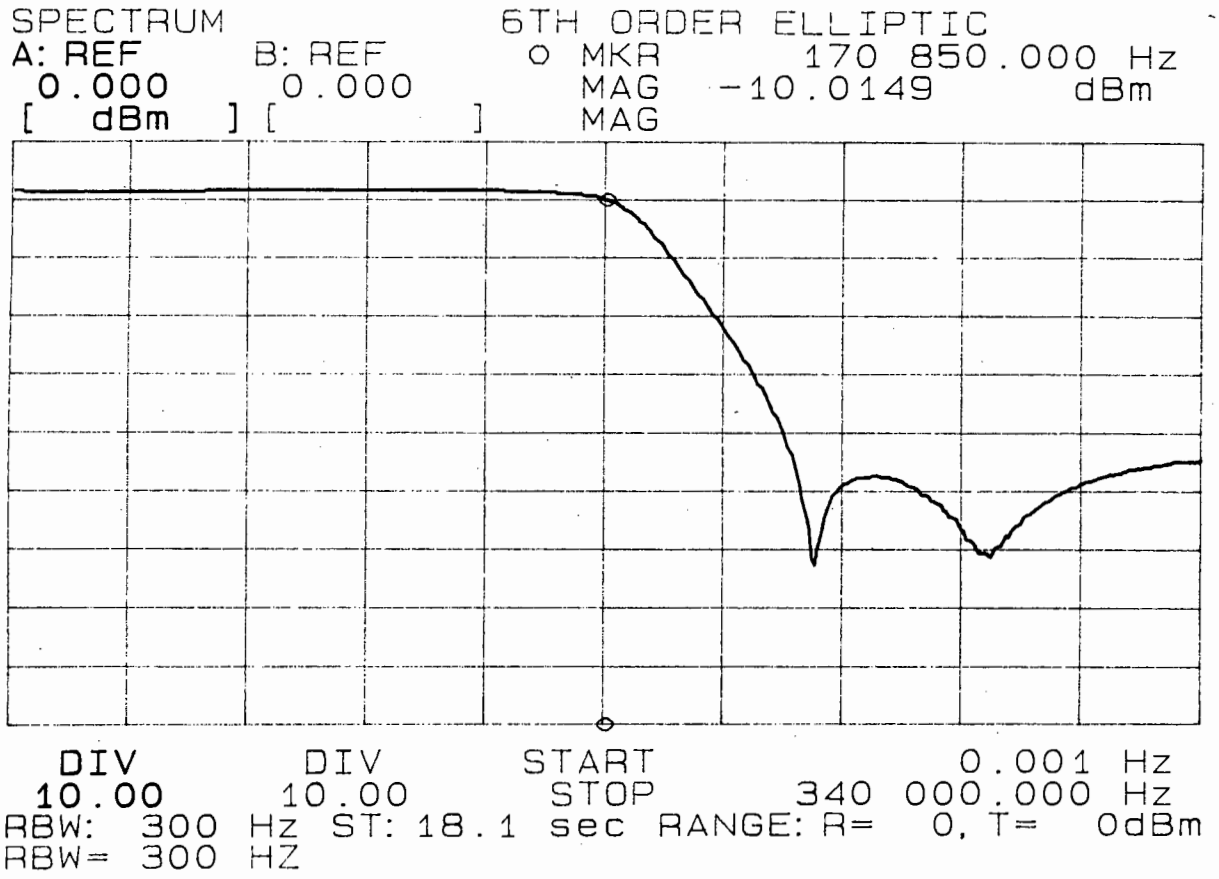

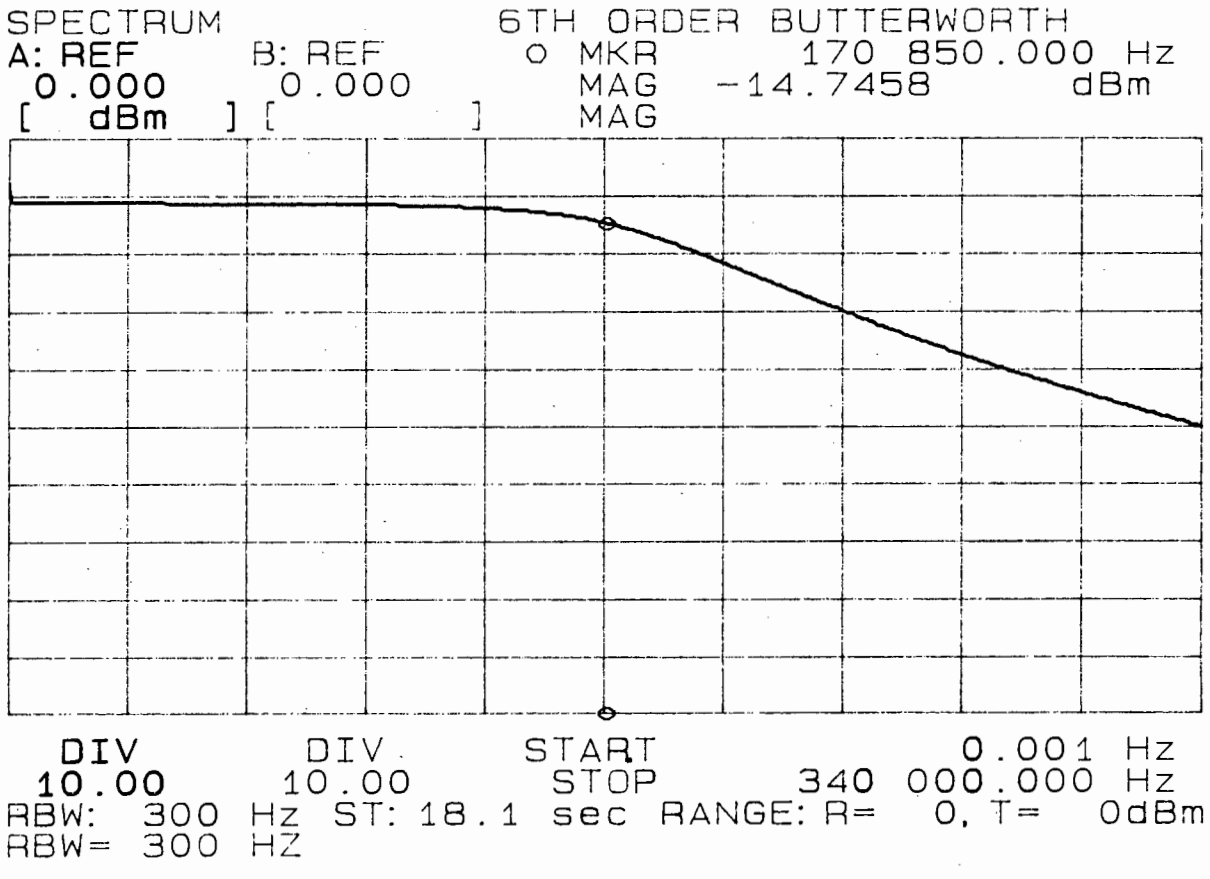

Fig. 3.12 Measured filter magnitude responses: (a) elliptic, (b) Butterworth.

Referring to Fig 3.12, at 240 kHz, the elliptic filter MSL is 45dB (5dB worse than the theoretical). The Butterworth attenuation is 19dB down (1.2dB better than the theoretical). Note how both amplitude responses could be tuned to have accurate -3dB cutoff frequencies of 170.7 kHz. The PRW of the elliptic filter is approximately 0.1dB.

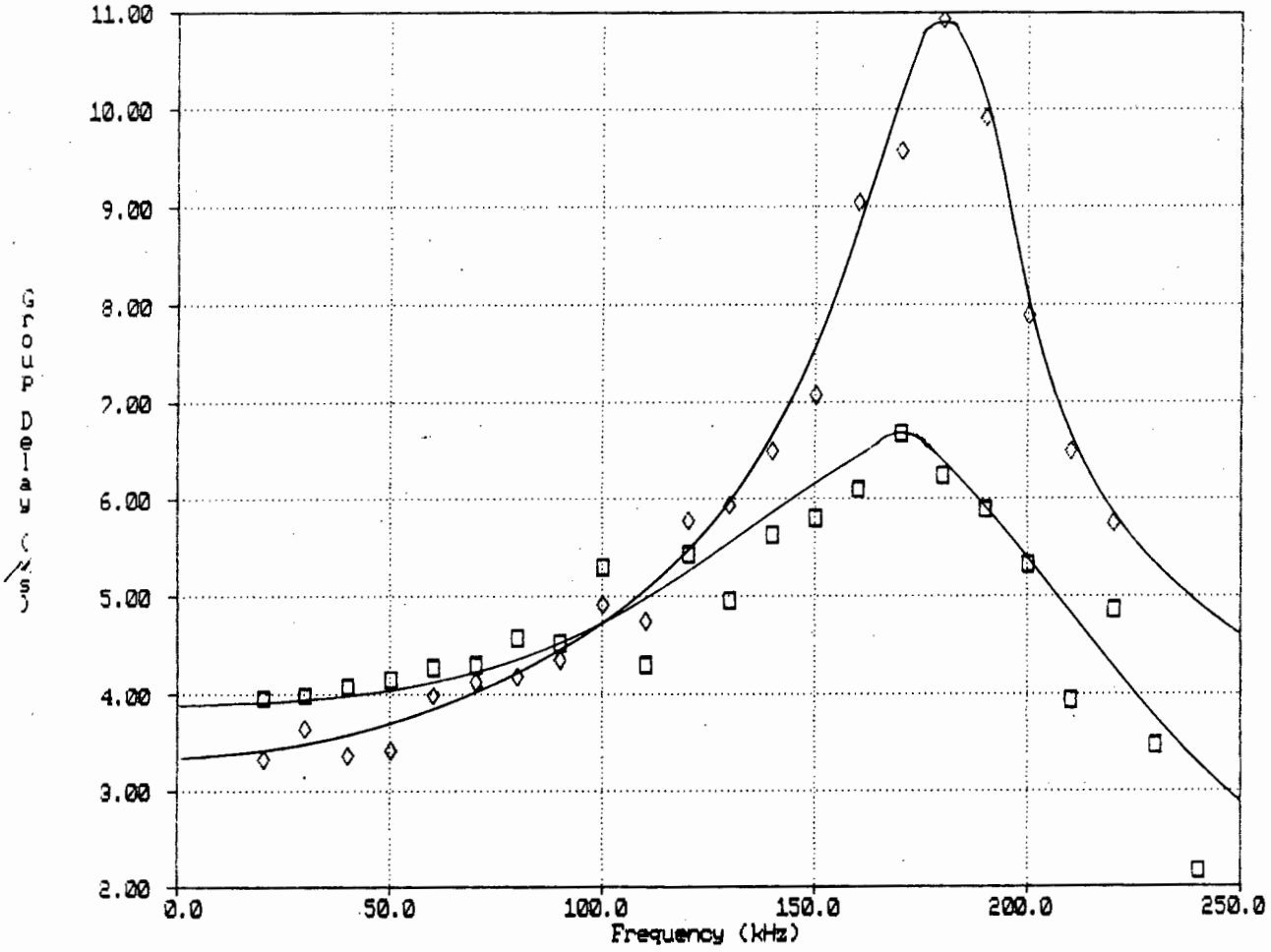

Fig. 3.13 Filter group delays

Group Delay It is better to characterize the filters in terms of their group delays (τ) rather than in terms of phase (ϕ). The group delay is defined as

$$\tau = - \frac{1}{2\pi} \cdot \frac{d\phi}{df} \quad \text{secs} \qquad (3.9)$$

where ϕ is in radians and f in Hz.

Thus perfect linear phase (requirement no.5) across the band gives a constant group delay. A first order finite difference approximation of the form:

$$\tau_i = -\frac{1}{2\pi}\frac{(\phi_{i+1} - \phi_i)}{\delta f} \qquad (3.10)$$

was used to calculate group delay from practical phase measurements. The results of the approximation are shown in Fig. 3.13. Here δf is 10 kHz. It is important to note the extreme deviation from constant group delay in the case of the elliptic filter. The Butterworth filter group delay is a fair approximation to a constant group delay for frequencies less than 120 kHz. It is unsatisfactory around the cutoff frequency.

Discussion Neither of the two filters met all the requirements (this was expected). The Butterworth filter was used in the modem testing because it produced less eye distortion of the channel (see Chapter 4). The elliptic filter gave excellent out of band attenuation but poor group delay response. An elliptic filter with a small PRW and several orders of phase equalization will come closer to meeting all the requirements. The design of a phase equalizer is left for future investigation.

3.4.7 Pilot Tone and Signal combiner

3.4.7.1 Hardware

A 170.7 kHz square wave clock, which is derived from the symbol clock, is filtered by a three pole passive low-pass filter. The -3dB cutoff frequency is 250 kHz. This ensures that all higher order harmonics of the square wave are sufficiently attenuated. This filter has a high frequency roll-off of 6n dB/octave, where n is the number of poles. At 512 kHz the third harmonic of the square wave is

approximately 21dB lower in magnitude than the first harmonic at 170.7 kHz.

Viewed in the frequency domain (Fig. 3.14), the pilot tone sits conveniently in the Nyquist frequency null at 170.7 kHz. At 240 kHz, the Butterworth filtered PRS spectrum is approximately 20dB down on the peak of the main lobe. The spike at DC is present for the reasons discussed in section 3.4.5.

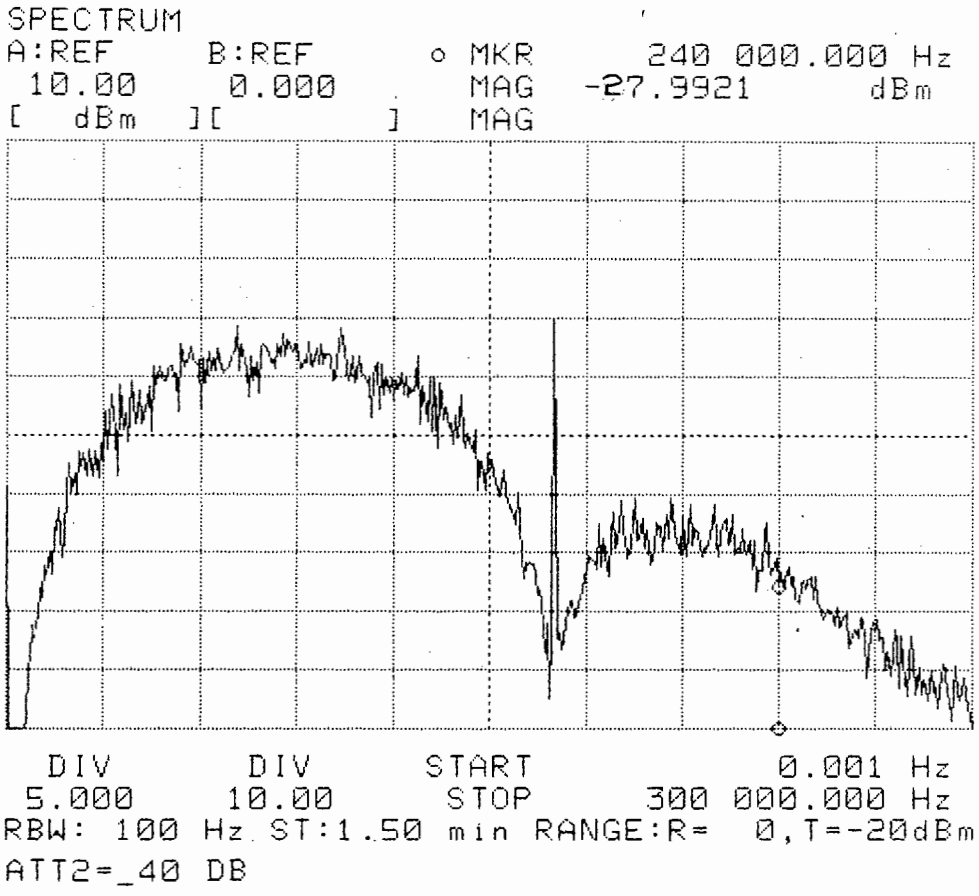

Fig. 3.14 Bandlimited class-4 15 PRS spectrum and pilot tone.

It is necessary to adjust the phase of the pilot tone so that it has its zero crossings at the centre of the eyes (see section 4.5.7). This ensures that at the optimum sampling instant (centre of the eyes), the contribution from the pilot tone is effectively zero.

A 5kΩ 10-turn potentiometer is used to adjust the phase of the pilot tone. This has the effect of slightly varying the cutoff frequency of the low-pass filter and hence the delay of the pilot tone.

A LM351 op-amp is used to combine the signal and the pilot tone. This device has similar specifications to the LF347. The circuit diagram of the combiner is shown in Fig. 3.15.

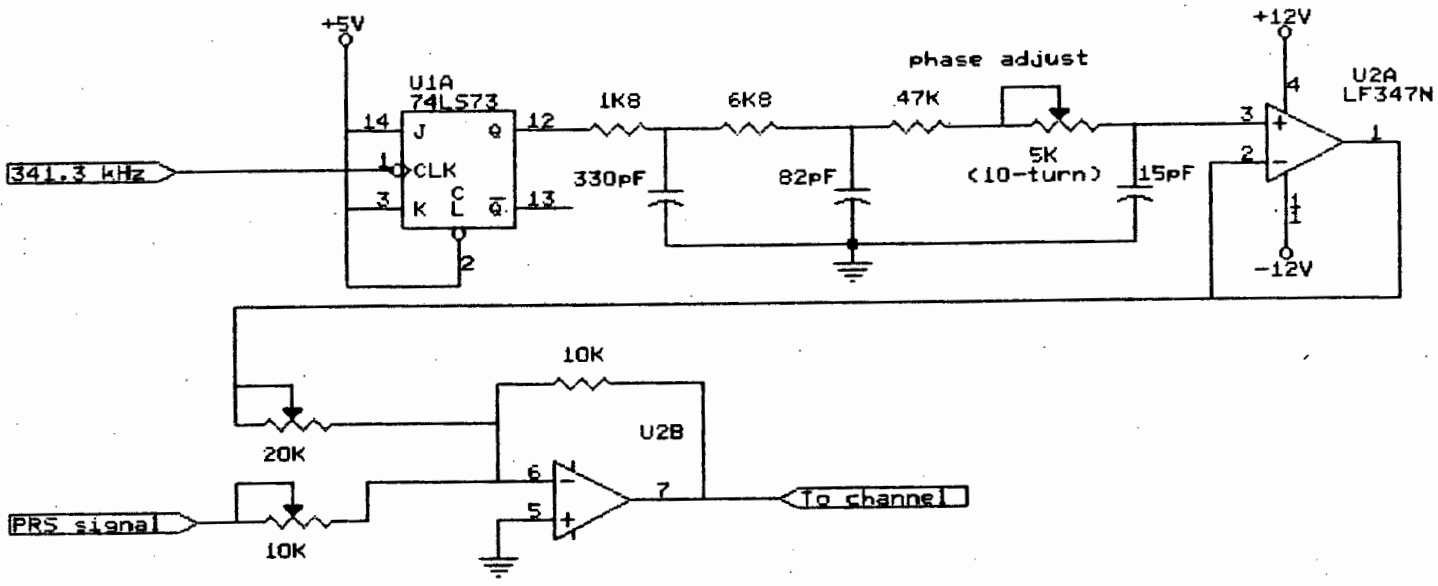

Fig. 3.15 Pilot tone and PRS signal combiner

3.4.7.2 PRS Signal to Pilot Tone Power Ratio

A convenient selection of signal to pilot tone power ratio is 20dB. For increased ratios, the signal degradation caused by addition of the pilot tone is less marked. However the received pilot tone must have sufficient amplitude so that it can be detected by the symbol timing recovery circuits. The measured PRS signal was 1.1V rms and tone, 127mV rms. Therefore the power ratio (in a 1Ω load) = 20log (1.1/0.127) = 18.8dB.

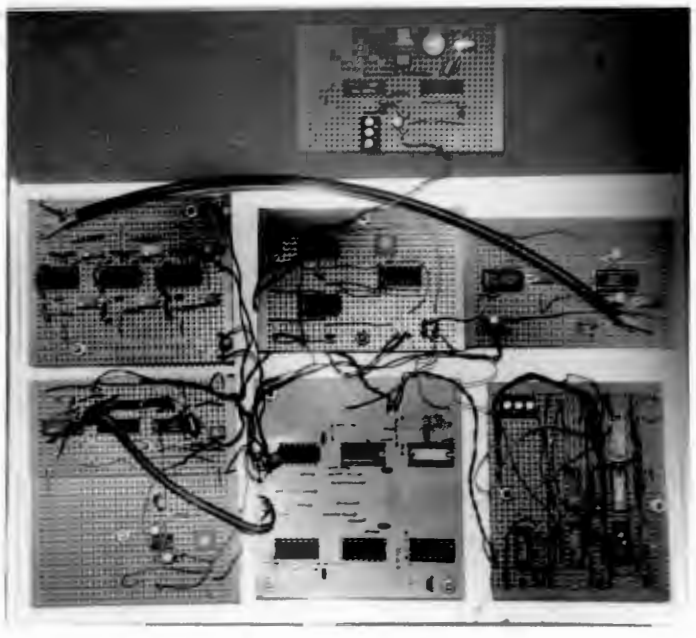

(a)

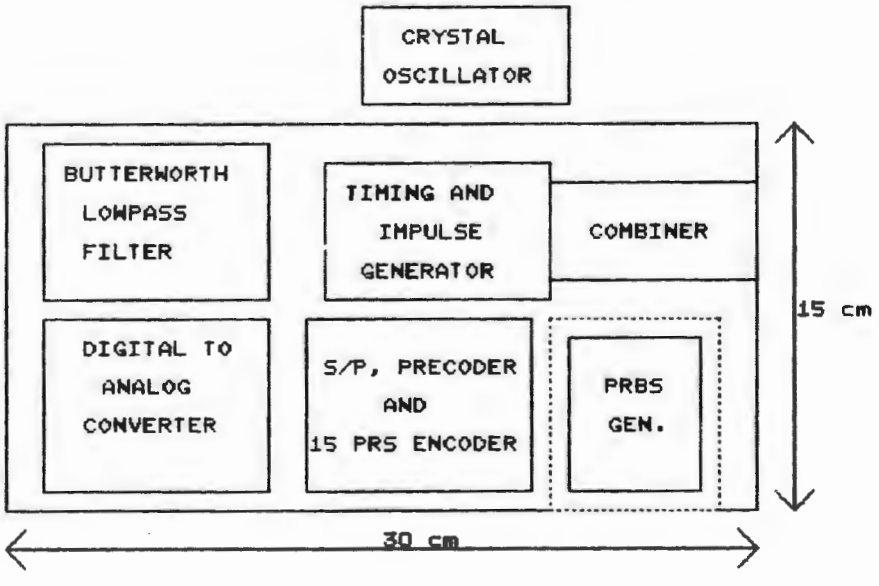

(b)

Fig. 3.16 Modulator: (a) photograph, (b) block diagram (not to scale).

3.5 Demodulator

3.5.1 Symbol Timing Recovery

3.5.1.1 Design

To recover symbol timing from the data at the demodulator, practical PRS systems use a non-linear diode network in conjunction with a band-pass filter or PLL. These are systems which generally operate at or above the Nyquist rate. In this instance, the bandwidth is not restricted to 170.7 kHz. The pilot tone scheme has been used successfully [3.10] and it generally provides better noise immunity than a non-linear network.

Several attempts were made to recover the pilot tone directly using a PLL. Phase noise and AM modulation of the pilot tone caused by the random waveform made it virtually impossible to recover the tone. Instead a narrow band-pass filter (high Q-tuned circuit) at the input to the PLL was used to reduce noise levels around the pilot tone frequency.

3.5.1.2 Tuned Circuit

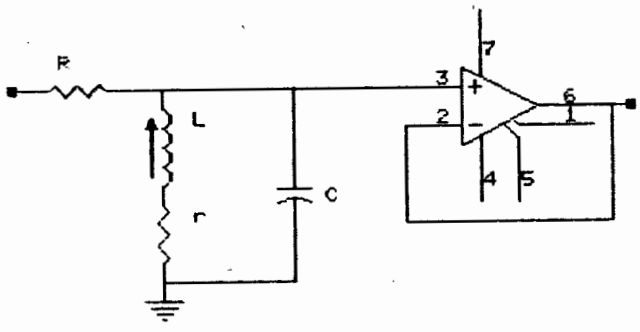

Fig. 3.17 Tuned circuit.

Consider the circuit given in Fig. 3.17 above. The resonant frequency of the parallel branch is given by

$$w_r = \sqrt{\frac{1}{LC} - \frac{r^2}{L^2}} \quad \text{rad/s} \qquad (3.11)$$

The lower case (r) represents a small finite resistance in the coil. If r = 0 then the formula reduces to the well known

$$w_r = 2\pi f_r = \sqrt{\frac{1}{LC}} \quad \text{rad/s} \qquad (3.12)$$

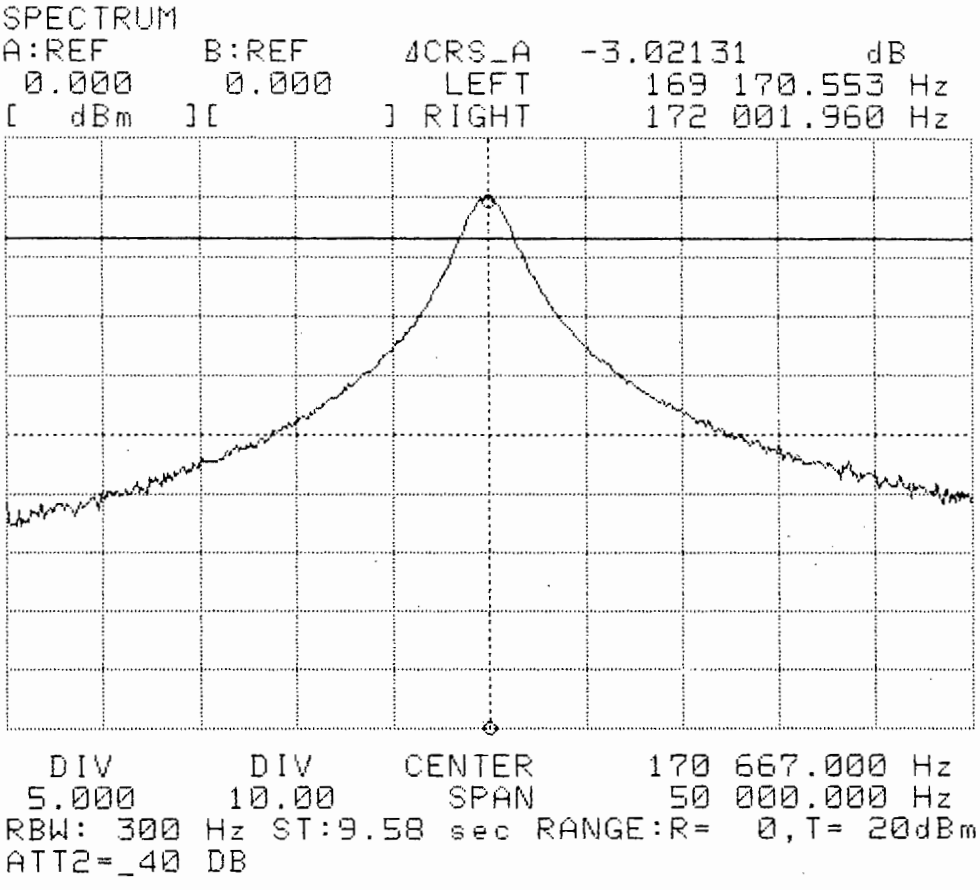

Fig. 3.18 Tuned circuit frequency response.

The series resistance R adjusts the Q (quality factor) of the circuit and signal attenuation. The Q [3.11] is defined as the resonant frequency, f_r divided by the -3dB bandwidth on

either side of f_r. The op-amp prevents loading of the tank circuit and hence degradation of Q.

A 8200pF (2%) capacitor was used in the tuned circuit. For a resonant frequency of 170.7 kHz, the approximate value of L determined from (3.12) is 106μH. The coil was wound on a pot-core. Coil resistance (r) was measured to be less than 0.4Ω . The exact resonant frequency could be obtained by tuning the pot-core. The highest possible Q was experimentally obtained by varying R. The optimum value of R was found to be 33kΩ.

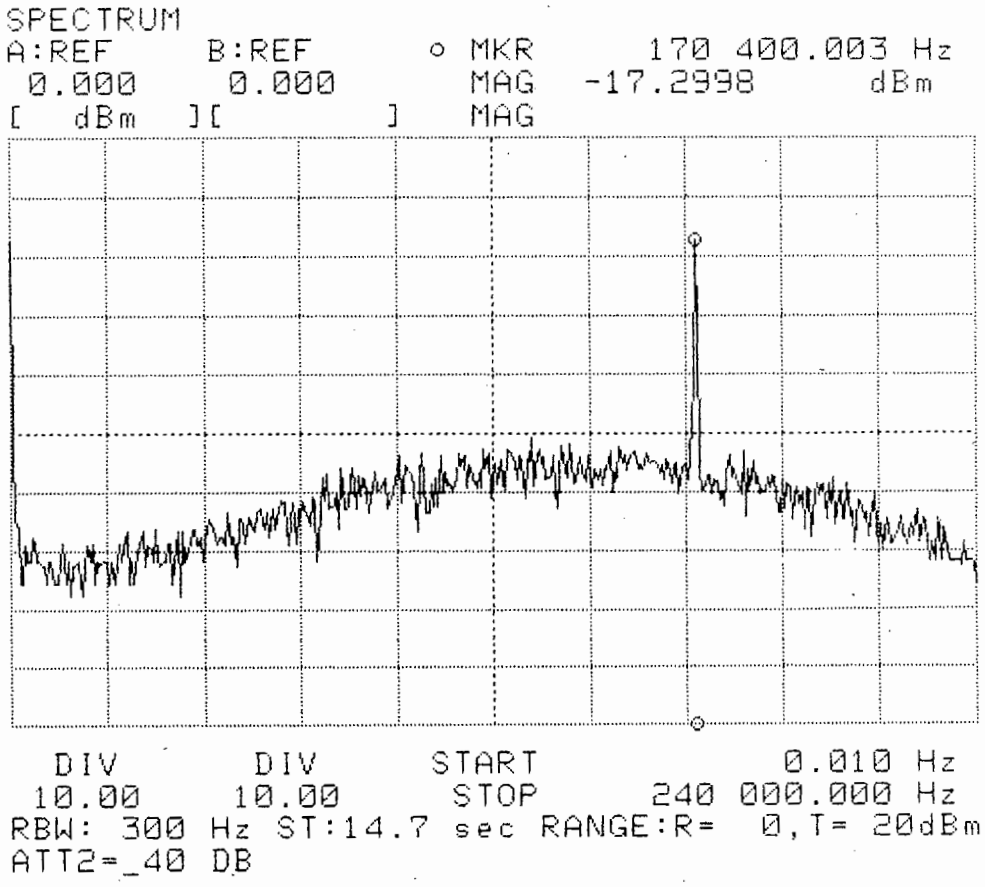

Fig. 3.19 Spectrum at the output of the tuned circuit.

Figure 3.18 shows the measured response of the circuit. From this response, the Q value can be determined:

$$Q = \frac{170.7}{172.0 - 169.2} = 61$$

Figure 3.19 shows the spectrum at the output of the high-Q tuned circuit. Note that the spectral peak is approximately 35dB above the noise level. The continuous noise spectrum is a combination of both AM and PM [3.8]. The total integrated power of the noise spectra is the cause of clock jitter in the recovered symbol timing clock. The tone plus noise power at the output of the tuned circuit was measured to be 64mV rms. (Recall that the power of the tone at the combiner in the modulator was 127mV rms).

3.5.1.3 PLL Design

Here we require recovery of the discrete spectral line at 170.7 kHz, the symbol clock at 341.3 kHz and the serial data clock at 1.024 MHz. Consider the circuit given below. The operation of this circuit configuration is well known, and the theory for it is given in Appendix B.

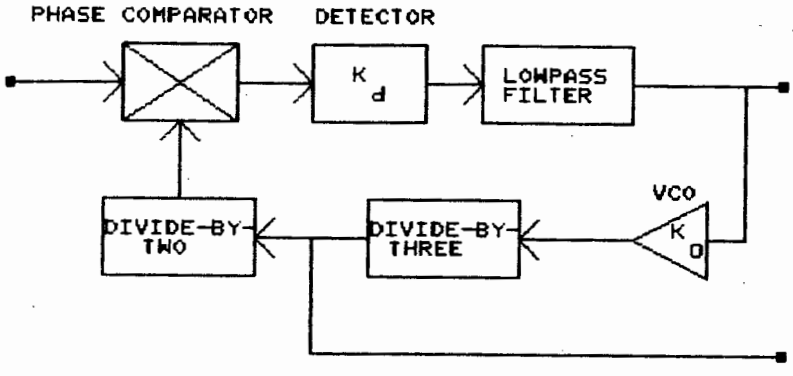

Fig. 3.20 Phase locked loop block diagram.

Two key parameters of the PLL system [3.12] are its lock range and capture range. They can be defined as follows:

1. **Lock range:** the range of frequencies in the vicinity of f_o, over which the PLL can maintain lock with an input signal. It is also known as the tracking range or holding range. Lock range increases as the overall gain of the PLL is increased.

2. **Capture range:** the band of frequencies in the vicinity of f_o where the PLL can establish or acquire lock with an input signal. It is also known as the acquisition range. It is always smaller than the lock range and so related to the low-pass filter bandwidth. It decreases as the filter bandwidth is reduced.

Reduced bandwidth of the low-pass filter gives improved noise immunity. There is, however, a point at which the low-pass filter bandwidth becomes so narrow that the speed of response of the PLL is compromised. There is an optimum low-pass filter bandwidth. This optimum was determined by a simple test (see below).

The PLL is an EXAR 210 device. This device can operate with a free running frequency (f_0) of up to 20 MHz. It interfaces easily with conventional logic. It can lock onto input signals in the range from 300mV rms to 3V rms. It has a VCO fine-tune capability and a frequency stability of 200ppm/°C for a power supply voltage of 12V.

From manufacturer's specifications, the approximate VCO free-running frequency is

$$f_0 \approx \frac{220}{C_0} \left[1 + \frac{0.1}{R_T} \right] \text{ Hz} \qquad (3.13)$$

where C_0 is the VCO timing capacitor (in μF) and R_T, the fine-tune resistor (in kΩ).

The selected value of C_0 was 202pF and R_T, a 10-turn 5kΩ potentiometer (see Fig. 3.25). The free-running frequency was tuned to a value slightly above 1.024 MHz. Thus it was possible to observe when the PLL was in lock.

The VCO conversion gain, K_0 is given by

$$K_0 \approx \frac{700}{C_0 R_0} \quad \text{rad/s/V} \tag{3.14}$$

where R_0 is the lock-range control resistor (in kΩ). The lock range ($2\delta w_L$) was selected to be approximately 40% of the free-running frequency. The required value of R_0 was 4.7 kΩ.

The phase detector conversion gain K_d is constant at 2V/rad for input signals greater than 30 mV rms below which the gain is proportional to the input amplitude. It is important to have a constant conversion gain to keep the capture range constant. $K_d K_0$ is independent of signal amplitude, but inversely proportional to K_0 for signal levels greater than 30mV rms. If saturation or limiting does not occur, half the lock range is equal to the loop gain, i.e., $\delta w_L = K_T = K_d K_0$.

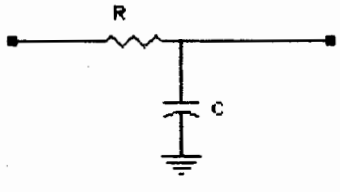

Fig. 3.21 Low-pass lag filter.

Capture range: the capture range is determined by the lock range and the low-pass filter time constant. For a simple lag

filter shown in Fig. 3.21, the capture range can be expressed as

$$2\delta w_C \approx 2\sqrt{\frac{\delta w_L}{T_1}} \quad \text{rad/s} \tag{3.15}$$

where T_1 is the low-pass filter time constant. The -3dB bandwidth (in Hz) of the low-pass filter is given by

$$f_{-3dB} = \frac{1}{2\pi T1} = \frac{1}{2\pi RC} \tag{3.16}$$

It can be seen from (3.16) that selection of the filter time constant directly affects the capture range in (3.15). The phase detector outputs when used in a PLL configuration produce a differential output voltage with a 12kΩ impedance. When these outputs are capacitively loaded (by C), the configuration forms the low-pass loop filter.

Selection of the optimum low-pass loop filter bandwidth was determined by trial and error: the recovered symbol clock waveform was connected to the input of a digitizing oscilloscope. The oscilloscope was set to infinite persistence (to simulate the behaviour of an analog oscilloscope). A static (jitter free) reference clock taken from the modulator, was used to trigger the oscilloscope on another channel. The infinite persistence setting allowed the superimposed display of the transitions of the recovered symbol clock. Thus a measure of the peak-to-peak jitter could be taken. Recovered symbol clock jitter is discussed in detail in Chapter 4. The peak-to-peak jitter was measured for different values of C. The corresponding loop filter bandwidth was calculated from (3.16).

The trend in the curve of Fig. 3.22 is clear. As the low-pass filter bandwidth is decreased below the optimum, the PLL response time is slower and the peak-to-peak jitter on the recovered symbol clock increases. As the bandwidth is increased above the optimum, more of the pilot tone modulation noise is present (wider capture range). The PLL fails to suppress it, and the jitter increases. The capture range for the optimum low-pass filter bandwidth is determined by (3.15) to be 123 kHz. The lock range and optimum capture range are shown graphically in Fig. 3.23.

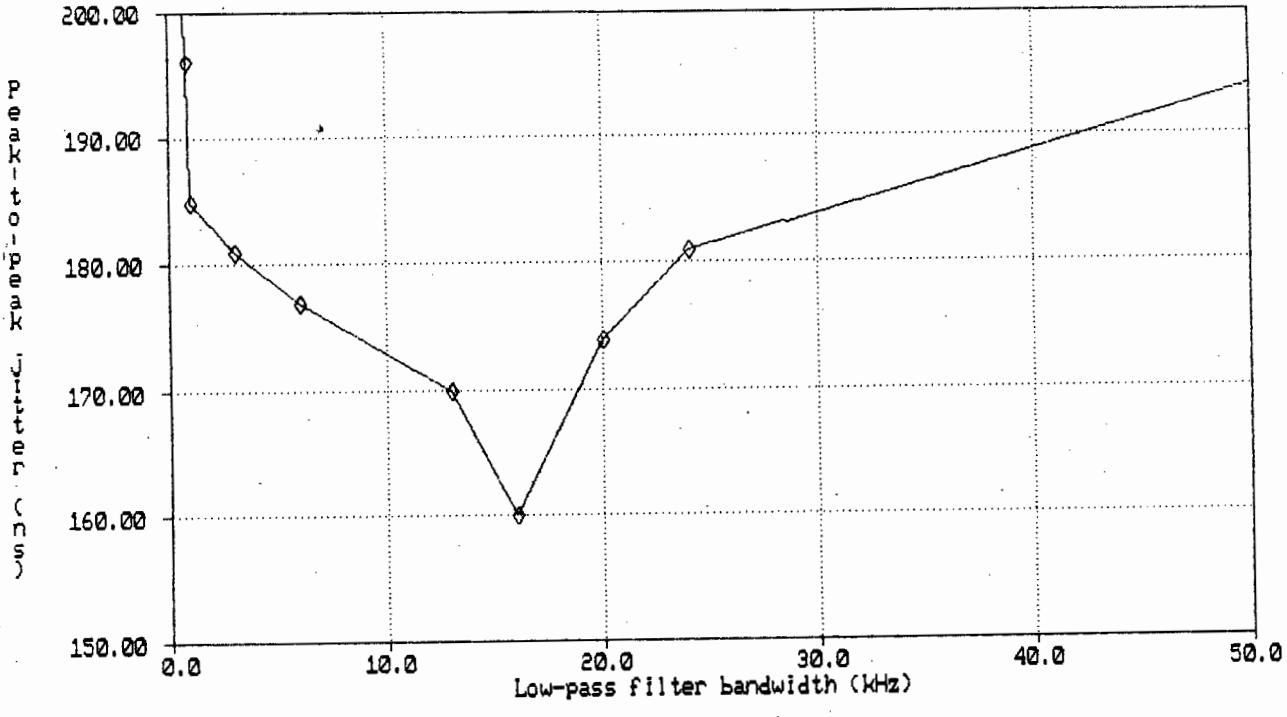

Fig. 3.22 Measured peak-to-peak jitter versus PLL low-pass filter bandwidth.

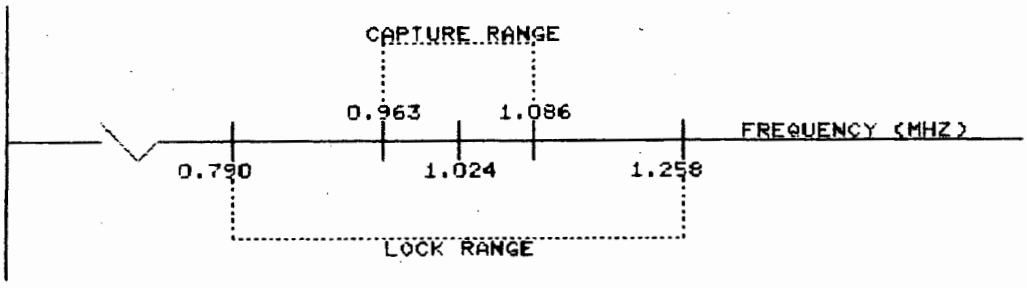

Fig. 3.23 Lock range and capture range.

Note The determination of the optimum low-pass filter bandwidth was performed using a $2^{20}-1$ pseudorandom bit sequence. This value of low-pass filter bandwidth may not necessarily be optimum for other sequences. Different sequences produce different results.

The VCO output produces a 2.5V peak-to-peak square wave. The DC output level is approximately 2V below the 12V supply rail. It is necessary to convert this waveform so that it is suitable for TTL logic. This is achieved by using the circuit shown below.

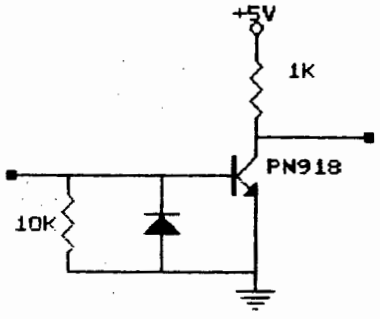

Fig. 3.24 VCO output to TTL level converter.

The 10kΩ resistor (connected to pin 15 of XR210) is used to increase the output drive capability of the VCO. The signal is AC coupled by a 1nF capacitor. The diode conducts on

negative cycles and reverse biases the base-emitter junction of the transistor. On the positive cycle, the diode is reverse biased and the transistor saturates causing the collector voltage to drop to a value slightly above zero volts. Note that this circuit introduces a 180° phase inversion of the signal.

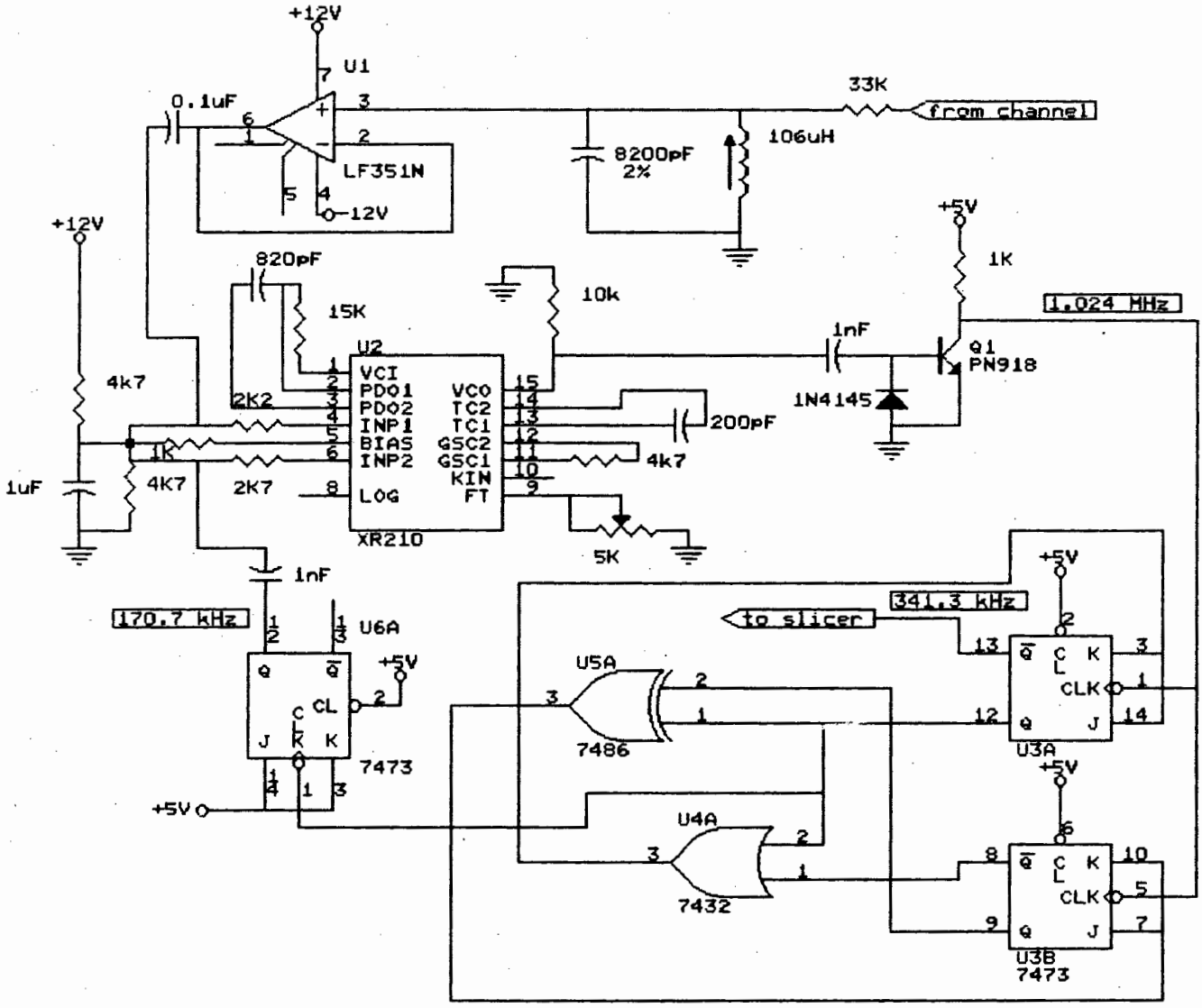

Fig. 3.25 Symbol timing recovery circuit diagram.

With reference to Fig. 3.25, the divide-by-three circuit is designed using two J-K flip flops and two gates. This configuration prevents the circuit from entering one unused

logic state. The 341.3 kHz clock does not have a 50% duty cycle. This is not a necessary feature, since only positive rising edges are required at the sampling instants. The divide-by-two circuit is implemented using a J-K flip flop.

It is necessary to convert the TTL waveform back into the form which the VCO generates, i.e., 2.5V peak-to-peak 2V below the supply voltage. This is done by AC coupling the 170 kHz square wave, attenuating it and providing the correct DC bias.

The PLL attempts to force a 90° phase difference between the input pilot tone and the reference 170 kHz square wave. The recovered clock lines are shown in Fig. 3.26 below.

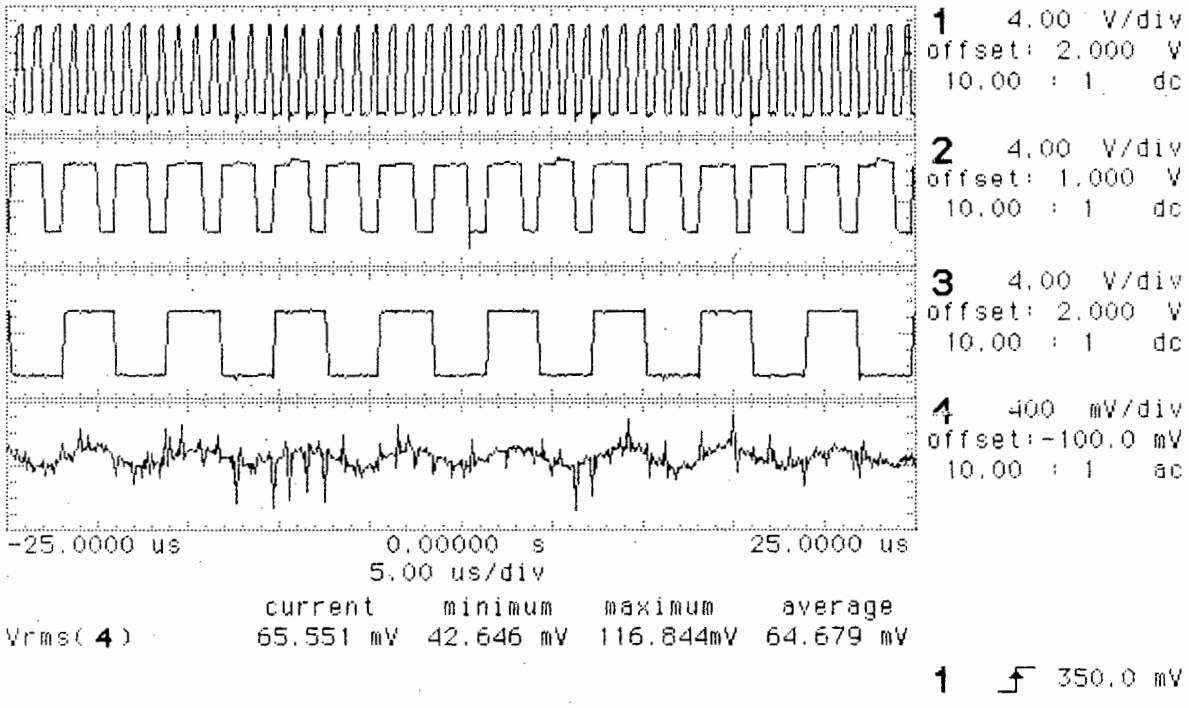

Fig. 3.26 Recovered clock lines

From top to bottom they are respectively 1.024 MHz, 341.3 kHz and 170.7 kHz. The pilot tone measured at the input to the PLL (after the high-Q tuned circuit) is the fourth trace. Note the 90° phase difference between the bottom two traces.

Also note the severe amplitude modulation of the tone and the random noise caused by the data sequence. Phase modulation of the pilot tone is barely discernible since it corresponds to slowly time varying changes in its zero crossings.

3.5.2 Decoder

3.5.2.1 Slicer

Recovery of the data can be done by using symbol-by-symbol detection on account of the precoding operation at the modulator.

We require a four bit slicer (ADC) to convert a 15 level analog waveform into four parallel bit steams. Selection of the appropriate ADC is based on the speed requirements, slew rate and output to indicate the end of a conversion. A MAXIM ADC0820 is selected. It is a high speed analog to digital converter which uses a half-flash technique. It has a conversion time of 600nS. The ADC0820 is an eight bit converter.

3.5.2.2 Threshold Levels

There are 15 possible input levels. Using the four most significant bits (largest level separation), the valid output codes extend from 0001000 to 11110000 inclusive. The unused code below 0001000 is 00001111. Since the ADC is powered by a 5.04V voltage regulator

$$1 \text{ LSB} = \frac{5.04}{256} = 19.69 \text{ mV}$$

There are 16 unused codes extending from 00000000 to 00001111 inclusive. Thus the first threshold level is at 16 x 19.69mV = 0.315V. If the input is above this threshold, then the output code is 00010000. The next valid code (00100000) is 16 LSBs away.

Half the distance between the thresholds (0.1575V) is known as the decision distance, d. The list of threshold voltage levels and the corresponding output codes is shown in Table 3.4.

Table 3.4 ADC Conversion Codes

Threshold Level,V	Output Code (4 MSBs) (if input is above threshold level)
0.315	0001
0.630	0010
0.945	0011
1.260	0100
.	.
.	.
4.410	1110
4.725	1111
5.040	

On account of the manner in which the 15 PRS encoding is performed at the modulator (see section 3.4.3), the recovered data stream can be interpreted modulo-8. If the MSB (leftmost bit) of the output code in Table 3.4 is ignored, the codes reduce exactly to the three-bit codes given in Table 3.2. Hence no decoding logic is required after the slicer. Only parallel to serial conversion is required.

These measurements were validated by performing a simple test on the ADC: the input voltage was varied by means of a potentiometer and the corresponding output code was displayed on a digital counter.

3.5.2.3 Signal Conditioning

3.5.2.4 DC Bias

The input PRS baseband waveform has zero DC component. From the threshold levels of Table 3.4, it can be seen that the ADC0820 requires the input 15 level waveform to have a DC

bias. Referring to Fig. 3.27 biasing is done by means of an LF351 op-amp in the inverting configuration. A 5kΩ 10-turn potentiometer is used to finely adjust the DC offset of the waveform. An inversion of the waveform is necessary since an odd number of inversions were performed at the modulator.

3.5.2.5 Static Phase Adjustment

The pilot tone is delayed by the high-Q tuned circuit. Additionally, there is a 90° phase shift forced between the pilot tone and the 170.7 kHz reference square wave. There is therefore no assurance that the recovered symbol clock at 341.3 kHz has its rising edges at the centre of the eyes.

The PRS waveform is delayed by means of a simple low-pass filter. A delay of approximately 200nS is required to bring the symbol clock into phase. The delay circuit is shown in Fig. 3.27. The 2K 10-turn potentiometer is used to finely adjust the static phase of the rising edge of the symbol clock. The cutoff frequency of the low-pass filter with a delay of 200ns is 796 kHz. This frequency is sufficiently high so as not to introduce attenuation of the PRS waveform. The delay of this filter is very nearly constant in the frequency range of interest.

3.5.2.6 Parallel to Serial Converter

The ADC is used in a mode where the end of a conversion is signified by the logic state of the INT (interrupt) output. The simplest method of parallel to serial conversion is to parallel load three shift registers and then to shift out the bits in serial mode. The recovered 1.024 MHz clock is used as the input shift clock. The INT output from the ADC is used to parallel load the shift registers.

The parallel to serial converter is implemented using CMOS logic. CMOS logic does not load the data bit outputs of the ADC which is the case with TTL logic.

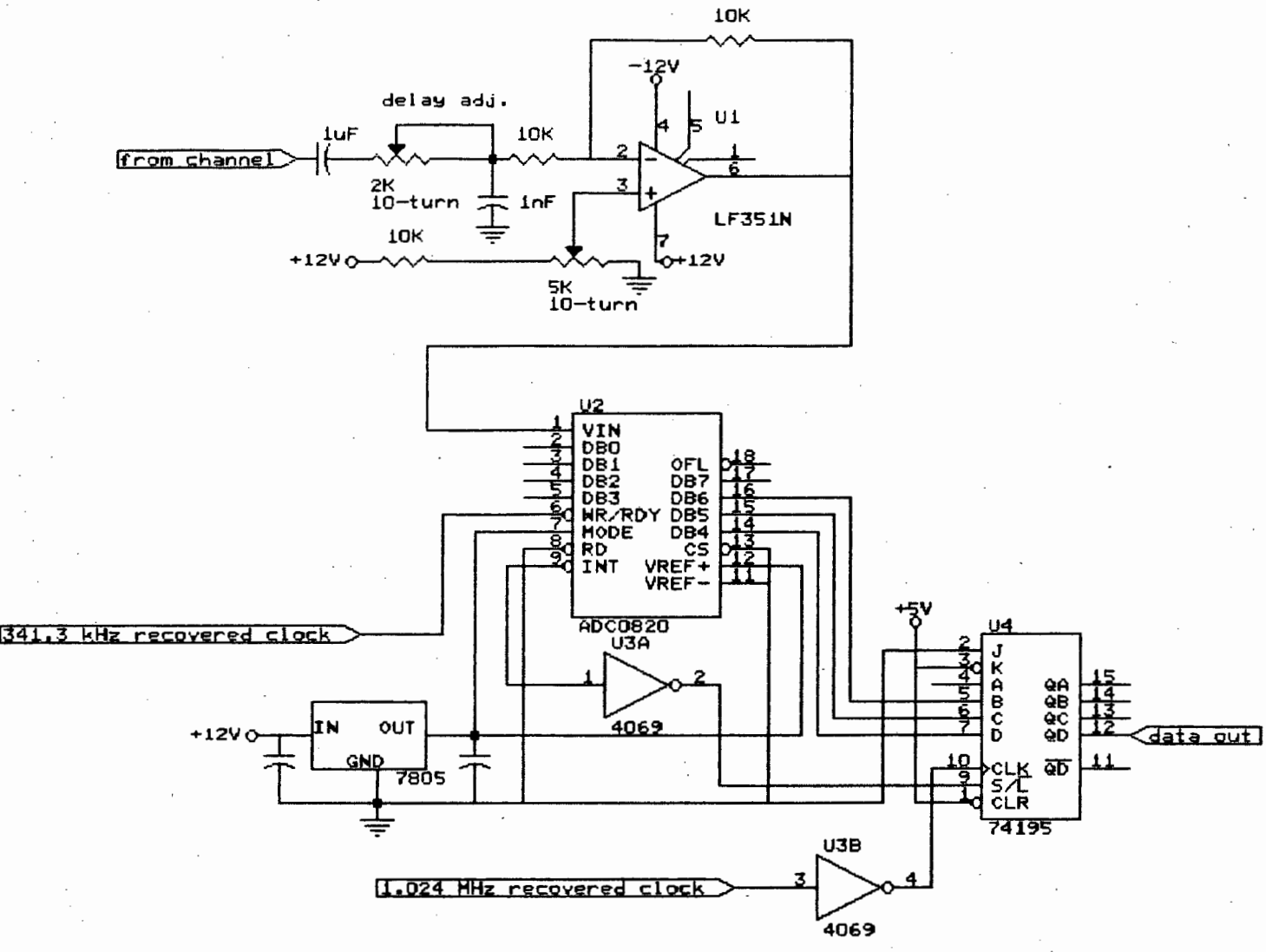

Fig. 3.27 Decoder circuit diagram.

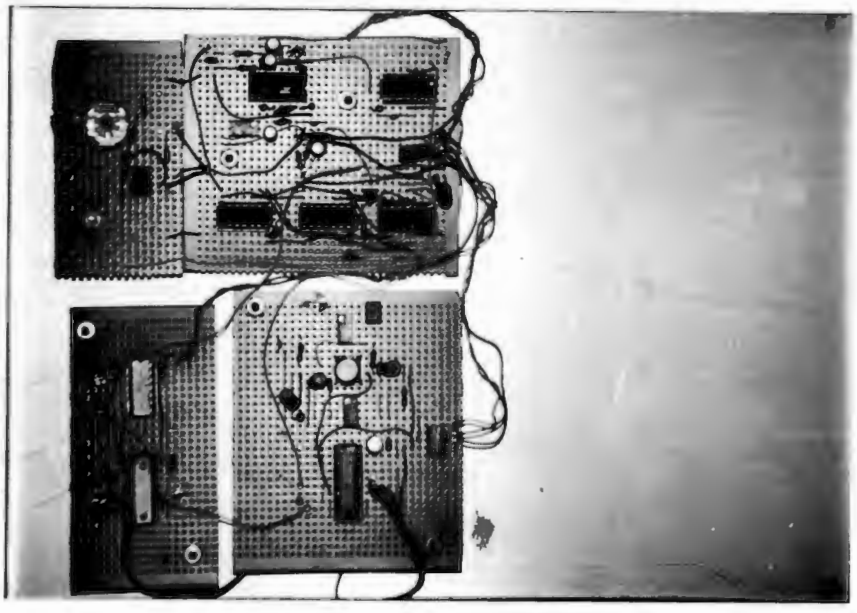

(a)

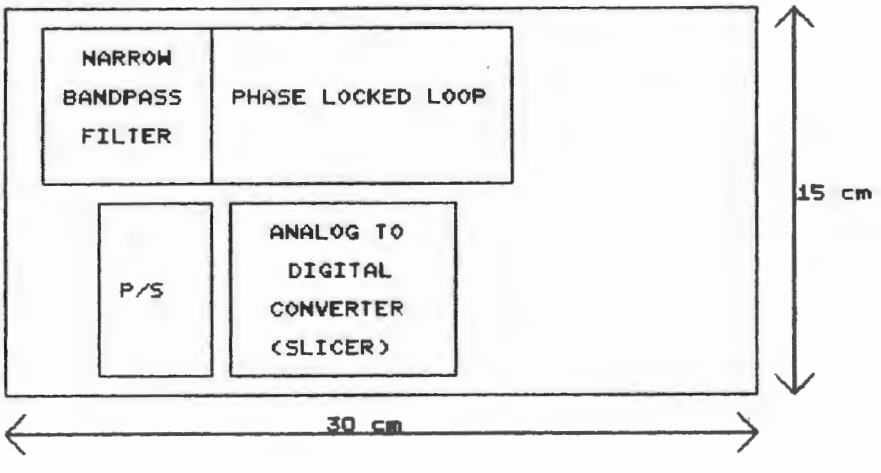

(b)

Fig. 3.28 Demodulator: (a) photograph, (b) block diagram (not to scale).

REFERENCES

[3.1] Feher, K. **Advanced Digital Communications: Systems and Signal Processing Techniques**, Prentice-Hall Inc. 1987.

[3.2] Wu, K. and Feher, K. **Multilevel PRS/QPRS Above the Nyquist Rate**, IEEE Vol. COM-33, No.7, July 1985

[3.3] Feher, K. **Digital Communications: Microwave Applications**, Prentice-Hall Inc. 1981

[3.4] Wu, K., Sasase, I. and Feher, K. **Class-IV PRS above the Nyquist rate**, Proc. IEE, Vol. 135, Pt.F, No.2, April 1988.

[3.5] Baker, D.M. **Analog/digital hybrid radio**, Can. Electron. Eng., pp. 34-38, Feb. 1973.

[3.6] Newcombe, E.A. and Pasupathy, S. **Effects of Filtering Allocation on the Performance of a Modified Duobinary System**, IEEE Vol. COM-28, No.5, May 1980.

[3.7] Horowitz, P. and Hill, W. **The Art of Electronics**, Cambridge University Press, 1980

[3.8] Feher K., and Engineers of Hewlett Packard, **Telecommunications Measurements, Analysis, and Instrumentation**, Prentice-Hall Inc. 1987.

[3.9] Johnson, D.E., Johnson J.R. and Moore H.P. **A Handbook of Active Filters**, Department of Electrical Engineering Louisiana State University.

[3.10] Horwitz, R. **4 Bits per Second per Hertz on a Telephone line**, BSc. Thesis, University of Cape Town, 1988.

[3.11] Bobrow, L. **Elementary Linear Circuit Analysis**, Holt, Rinehart and Winston Inc. 1981.

[3.12] EXAR Data Book, EXAR Corporation, 1982.

CHAPTER 4
TEST MEASUREMENTS

4.1 Introduction

This chapter describes the methods of measurement used to characterize the performance of the modem. The chapter starts with a discussion on the choice of pseudorandom bit sequence generators. Section 4.3 deals with factors which degrade the signal to noise ratio. Section 4.4 is a description of a test done to determine the modem's sensitivity to changes in transmission rate. The next section, section 4.5 discusses error performance of the modem and the experimental methods used to obtain these results.

4.2 Pseudo Random Bit Sequence Generator

Pseudo random bit sequence (PRBS) generators are used to simulate the effects of live data traffic. The performance of the modem depends on the sequence length. Adequate (i.e. close enough) spectral line spacing [4.1] is important when testing systems containing relatively narrow (high Q) clock timing recovery circuits in order to see the jitter contribution of these and its effect on error performance. The choice of shift-register configuration affects the run properties of the PRBS, which, in turn, affects the jitter performance in terms of the length of zero blocks over which phase error is accumulated by the timing recovery circuits [4.2]. This leads to pattern dependent jitter. The run property of the PRBS is a measure of the running binary sum's disparity from zero.

Studies have shown that jitter observed on digital test patterns may be different to that observed on live traffic. This may be due to the unfortunate choice of shift register configuration leading to peculiar run properties of the binary PRBS or a combination of this with the repetitive rate

of the PRBS approaching that of the jitter bandwidth of the system under test.

The important properties of the selected PRBS generator are summarized as follows:

- sequence length in bits
- shift register configuration, which defines the binary run properties
- spectral line spacing, which depends on bit rate

Figure 4.1 shows the general configuration of a PRBS generator.

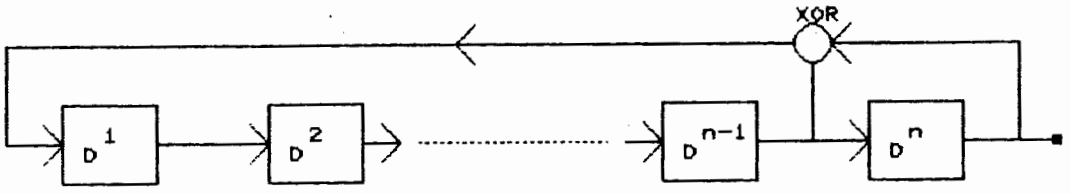

Fig. 4.1 PRBS generator.

The envelope of the power spectral density of the PRBS has a sinx/x shape (Fig.4.2), however the power spectral density consists of discrete spectral lines. The separation of the spectral lines, δf is given by $f_b/2^{n-1}$ (for a maximum length sequence). Here f_b is the bit rate, and n is the total number of shift registers in the PRBS generator.

A sequence length of $2^{20}-1$ was selected for testing the modem. The spectral line spacing $\delta f = (1.024 \text{ Mb/s})/(2^{20} - 1) = 0.98$ Hz. This sequence length gave a good approximation to truly random data traffic. The spectral line spacing was sufficiently narrow so as to adequately test the STR circuits.

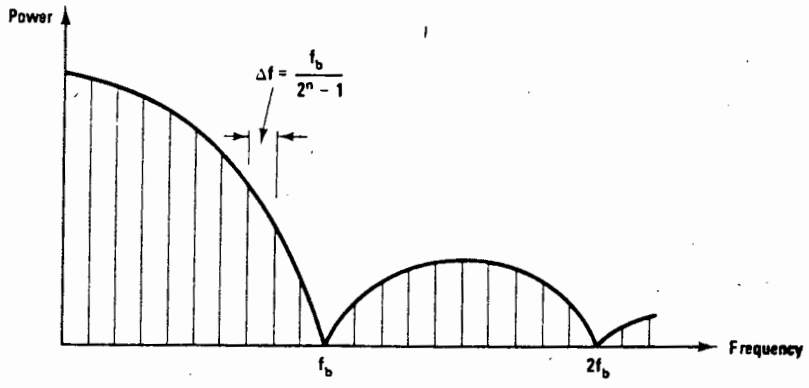

Fig. 4.2 Spectrum of a binary NRZ PRBS [4.1].

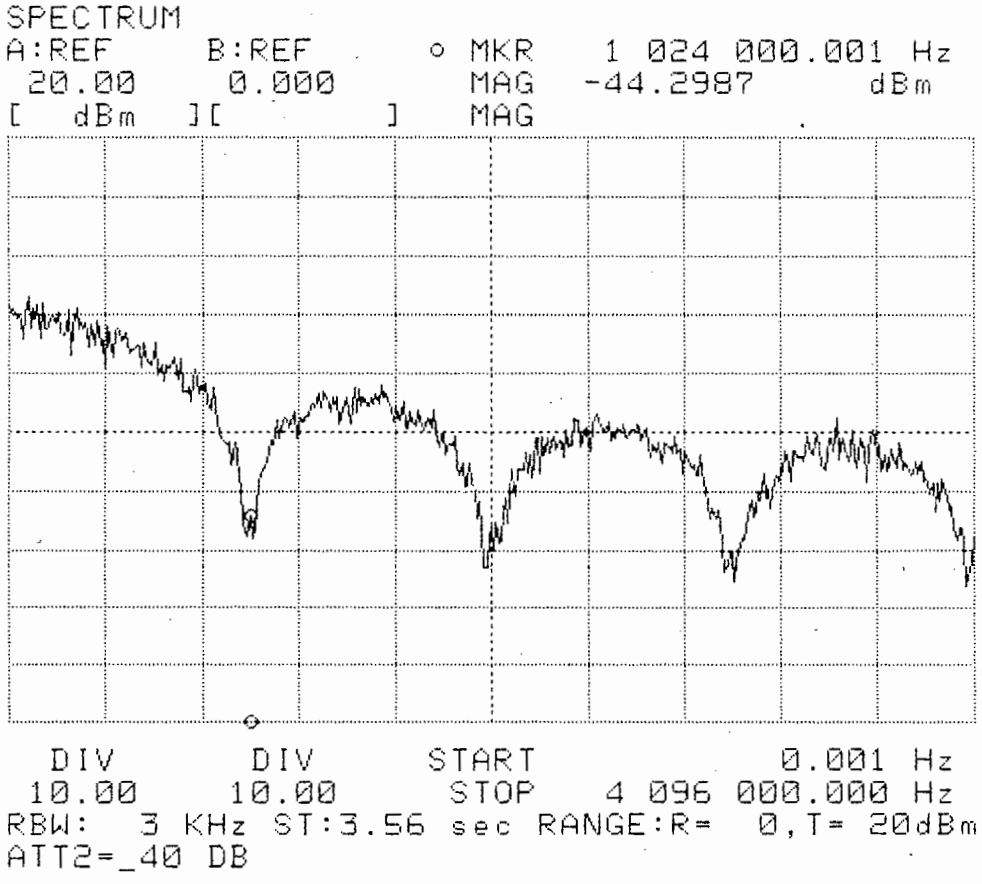

Fig. 4.3 Measured spectrum of 2^{20}-1 PRBS.

Here the run properties of the sequence affected the STR circuits in a different manner to the zero block phase errors discussed above. This is because STR was obtained from the zero crossings of a pilot tone and not from the zero crossings of the data.

A PRBS length of $2^3-1 = 7$ was totally inadequate for simulating live traffic tests. The spectral line spacing of this sequence was 146 kHz, and the repetition time, 6.8μs. This sequence generated a 12 level deterministic signal (no eye diagram). The three centre levels were not present. The use of this short PRBS enabled the modem to operate close to the theoretical optimum (see section 4.5.7).

4.3 Signal to Noise Ratio Degradation

4.3.1 Eye Diagrams

The quality of digital transmission links [4.1] is frequently evaluated by means of eye diagrams. They provide an excellent qualitative means to display system or hardware imperfections and to provide a first-order approximation of system performance.

A back-to-back connection was made between the modulator and the demodulator. The Butterworth filter was used since it produced far less vertical eye closure than the elliptic filter (see section 4.3.3).

During experimentation, for the display of the 15 level eye diagram, an analog oscilloscope was used. The inherent persistence of the cathode-ray tube displayed the superimposed impulse responses of the Butterworth channel. The 15 level eye diagram shown in Fig. 4.4, was obtained from a digitizing oscilloscope. An infinite persistence setting was selected on the digitizing oscilloscope to mimic the behaviour of the analog oscilloscope.

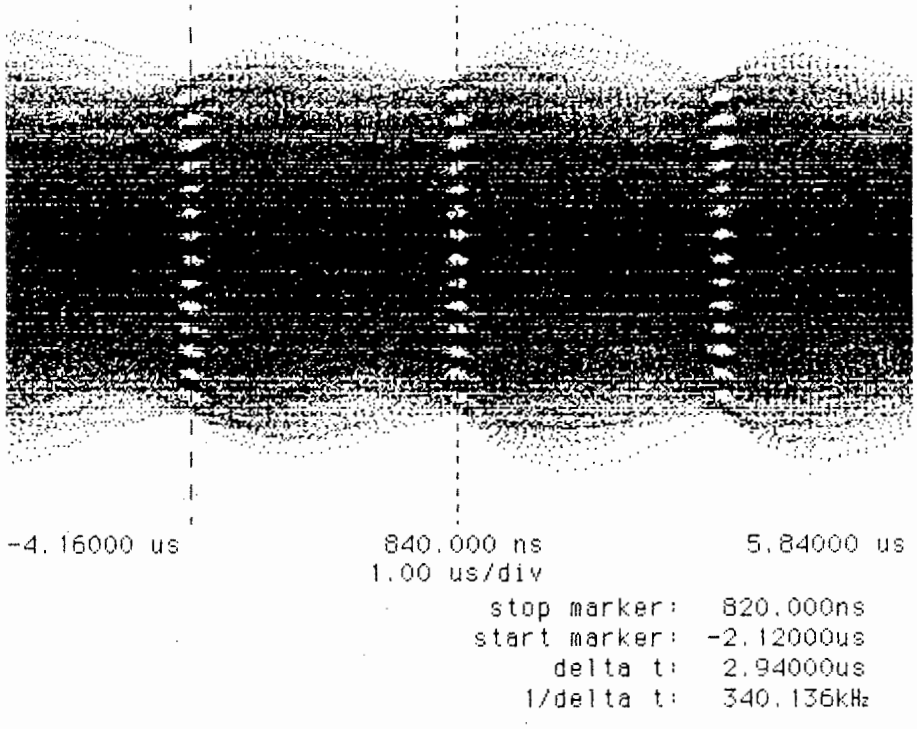

Fig. 4.4 15 Level eye diagram.

The eye diagram of Fig. 4.4 was obtained using the long PRBS, $(2^{20}-1)$. It can be seen that all 15 levels are tested by this sequence. The eye diagram is a 15 level superimposed extension of the class-4 PRS channel impulse response shown in Fig. 2.3(b). The eye diagram is obtained at the input to the slicer. The pilot tone is already present in the signal. Its effect on the eye diagram is discussed in section 4.3.6.

The point of maximum vertical eye opening is the point of maximum S/N and hence the theoretical optimum sampling instant at the slicer.

4.3.2 Data Transition Jitter

Even if the filter designer is successful in designing the required amplitude and phase characteristics of a nearly ideal raised-cosine Nyquist channel (discussed in Chapter 2), this channel may still have significant data transition jitter [4.4]. Data transition jitter is a variation in the zero crossings of the waveform. The peak-to-peak time difference of the zero crossings is known as the peak-to-peak jitter, D_{jpp}. Data transition jitter by itself does not lead to performance degradation. However, data transition jitter combined with symbol clock jitter or clock static offset or both may lead to significant performance degradation.

Data transition jitter was observed in the multilevel impulse train before the DAC. It is reasonable to assume that this jitter propagated through into the channel. It is uncertain though, whether the jitter had significant effect on the performance of the modem.

4.3.3 Vertical Eye Opening

An expanded version of the centre-most eyes (obtained from the digitizing oscilloscope) is shown in Fig. 4.5. The theoretical optimum sampling instant is shown. The threshold levels of the slicer are also shown.

To determine the S/N degradation due to hardware imperfections in the modem, a measurement of the vertical eye opening was taken. Hardware imperfections included amplitude and group delay distortions and circuit layout.

The theoretical maximum vertical eye opening (0.315V) is equal to the twice the decision distance, d. This is the best possible performance i.e., there is no ISI at the sampling instant. A reduction in vertical opening constitutes a degradation in performance (reduced decision distance). The S/N degradation is given by

$$-20 \log \left[\frac{V_1}{0.315} \right] \text{ dB} \qquad (4.1)$$

where V_1 is the measured eye opening. It must be noted that (4.1) places an upper bound on the degradation. Referring to Fig. 4.5, the vertical eye opening is approximately 244mV, and the corresponding upper limit in S/N degradation is -20 log(0.77) = 2.2dB.

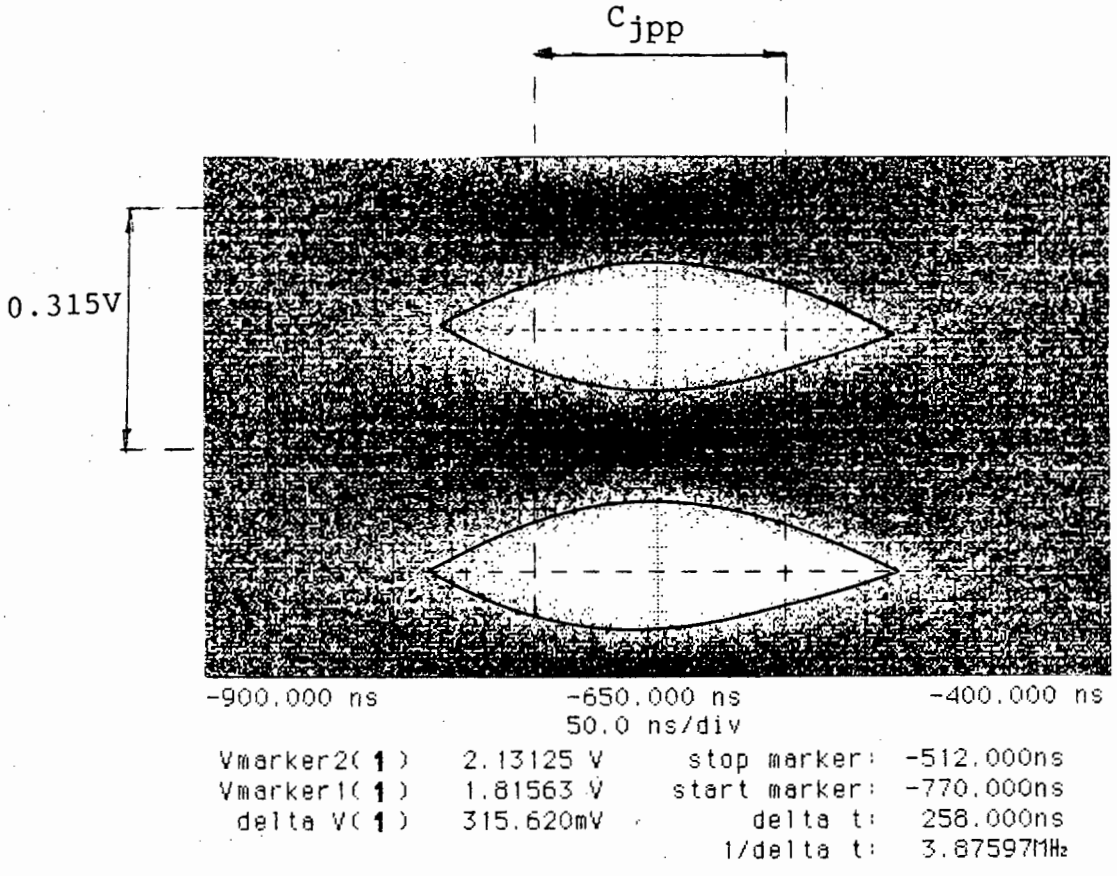

Fig. 4.5 Expanded centre-most eyes.

Prior to connection of the Butterworth filter into the modulator circuit, a vertical eye opening measurement of the elliptic filter channel was taken. The opening was measured to be 20% of the maximum. This corresponded to a degradation in S/N of 14dB. Hence the selection of the Butterworth filter.

4.3.4. Horizontal Eye Opening

For a MB α = 0 filter, class-4 15 PRS operating at the Nyquist rate (6 b/s/Hz) has a maximum horizontal eye opening of $0.048T_s$ or 0.048 x 2.93μsec = 141ns [4.5]. The superiority of PRS over zero memory systems operating at or above the Nyquist rate is clear when one considers the horizontal eye opening. In PRS systems the eye is open whereas in zero memory systems, the eye is theoretically closed. This is the reason for practical zero memory systems having to employ filters with increased roll-off.

Referring to Fig. 4.4, it can be seen that the extreme-level eyes are wider than the eyes near the centre. This is due to the triangular probability distribution of levels for random binary inputs [4.3].

The horizontal eye opening (Fig. 4.5) of the Butterworth channel is approximately 240ns. This can be explained by the increased roll-off of the Butterworth filter (NMB channel) as compared to the ideal α = 0 filter. The horizontal eye opening tends to increase with increased roll-off.

4.3.5 Clock Jitter

It was shown (section 3.5.1.3) how a measurement of the recovered clock jitter could be taken, and reduced to a minimum for the given input PRBS. Figure 4.6 is an illustration of a jittery clock and its corresponding jitter probability density function. The peak-to-peak jitter, $C_{jpp} = x_1 - x_0$ is shown. Figure 4.7 shows a single shot measurement of the recovered symbol clock jitter. It can be seen that the jittery clock has a C_{jpp} of 145ns. C_{jpp} is normally expressed as a percentage of the symbol time. Here C_{jpp} is 145ns/2.93μs x 100 = 4.9%. C_{jpp} for the 7 length PRBS was measured to be 2% of the symbol time.

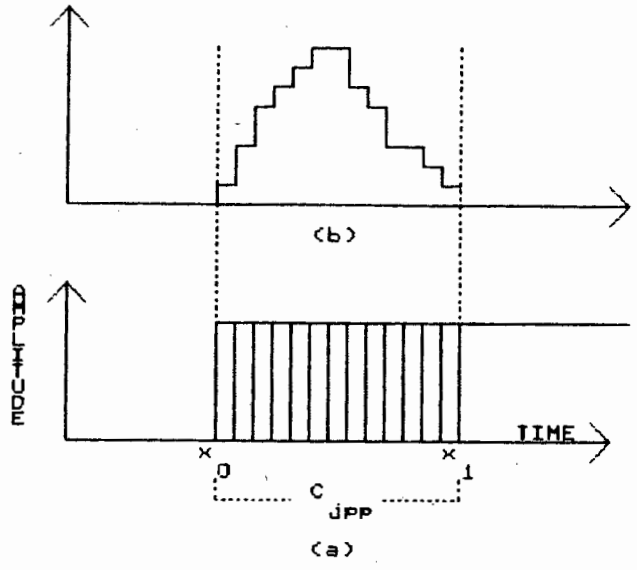

Fig. 4.6 Clock jitter: (a) jittery clock, (b) jitter probability density function.

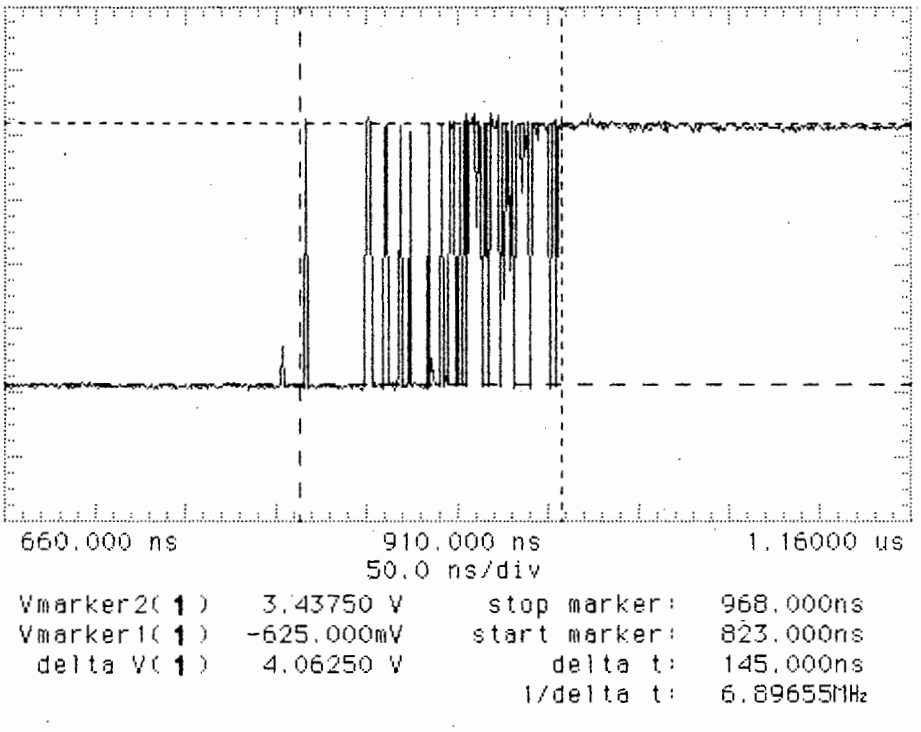

Fig. 4.7 Measured symbol clock jitter.

The upper limit in S/N degradation due to C_{jpp} is determined by the percentage eye closure from the theoretical optimum sampling instant to the peak excursion of the jitter. With reference to Fig. 4.5, it can be seen that the vertical eye opening is reduced by approximately 26.3%. The maximum S/N degradation is -20log(1 - 0.263) = 2.7dB.

4.3.6 Pilot Tone

The phase of the pilot tone was adjusted at the modulator so that its zero crossings occurred at the centre of the eyes. Figure 4.8 shows the eye diagram and pilot tone before the combiner at the modulator. Note how the 170.7 kHz pilot tone passes through half a cycle between two symbols.

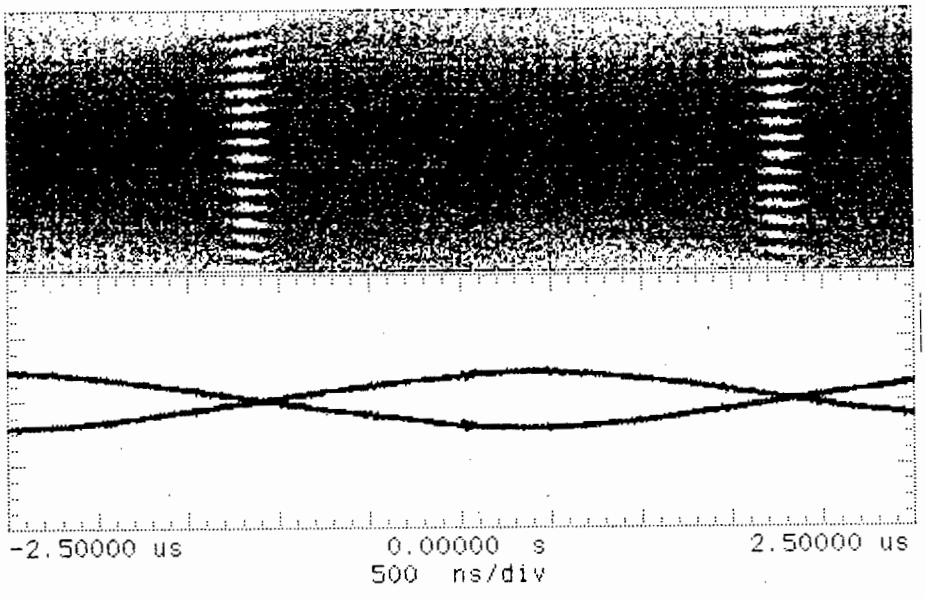

Fig. 4.8 Eye diagram and pilot tone.

Measurements were taken at the slicer of the horizontal and vertical eye openings with and without the addition of the pilot tone. (Recall that the measured PRS signal to pilot tone ratio was 18.8dB.) The results are given in table form below.

Table 4.1 Effect of Pilot Tone on Eyes

Tone	Eye Openings	
	Vertical (mV)	Horizontal (ns)
present	243.75	239
not present	237.50	260

It can be seen that the addition of the pilot tone increases the vertical opening by 6.26mV. This implies that the tone has its zero crossings slightly offset from the centre of the eyes. The difference of 6.25mV constitutes an decrease of 2.6% in vertical eye opening (0.2dB degradation).

When the pilot tone is present, the horizontal opening is reduced by 20ns. This can be attributed to the slight twisting effect of the eye caused by the addition of the pilot tone. For reduced signal to pilot tone power ratios (section 3.4.7.2), this effect could be even more pronounced. The reduction in horizontal opening does degrade performance slightly. However, no exact measurement of degradation was taken.

4.4 Sub-Nyquist Rate Speed Tolerance Test

Speed tolerance is normally defined as the increase above the Nyquist rate which causes at least one eye closure. The speed tolerance for Class-4 15 PRS is given as 1% [4.8]. This figure shows that it is virtually impossible to increase the transmission rate above the Nyquist rate without severe performance degradation. The experimental modem operated well below the Nyquist rate of 6 b/s/Hz. However, a sub-Nyquist rate speed tolerance test performed on the modem gave insight

into its sensitivity due to changes in the transmission rate.

The transmission characteristics of the modem were fixed as if for 1.024 Mb/s data rate, i.e., the -3dB cutoff frequency of the Butterworth filter remained at 170.7 kHz. The crystal oscillator was replaced by a variable-square wave generator. The data sent at the new rate was not recovered at the demodulator because the PLL was not designed to lock onto pilot tones of widely varying frequencies. A measurement of the maximum vertical eye opening was taken at the slicer for each transmission rate. The results are shown in Fig. 4.9. Note that for transmission rates between 1.024 Mb/s and 1.026 Mb/s, the vertical eye opening is at a maximum (244mV corresponds to a 77% opening).

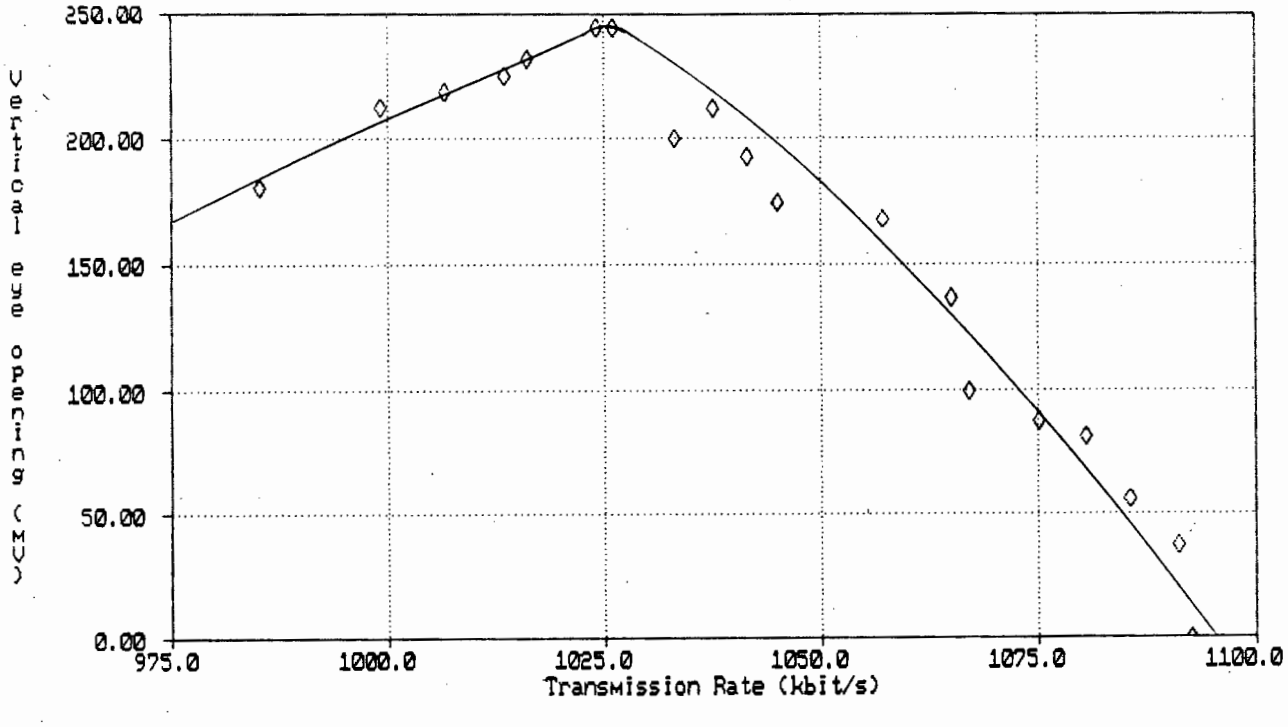

Fig. 4.9 Sub-Nyquist rate speed tolerance test.

As the transmission rate is varied away from the optimum, the vertical eye opening decreases. The eye closes for rates well below 1.024 Mb/s. At 512 kb/s (not shown on the curve), the eyes are open again. However spectral efficiency at a transmission rate of 512 kb/s is 2.14 b/s/Hz.

Above 1.024 Mb/s the vertical eye opening decreases with frequency. At 1.093 Mb/s the eye is closed and we deem the system to have failed. This transmission rate represents an increase of 6.7% above the nominal rate and a spectral efficiency of 4.55 b/s/Hz.

Additionally, these results show that in order to obtain the best possible system performance (at the nominal transmission rate of 1.024 Mb/s), the -3dB cutoff frequency of the low-pass filter must be accurately tuned to the Nyquist frequency.

4.5 Error Performance

4.5.1 Error Probability Theory

The probability of error [4.6] of a precoded PRS system is approximately:

$$P(e) \leq 2(1 - 1/L)\, Q\left[\frac{d}{\sigma_o}\right] \qquad (4.2)$$

where L is the number of output levels (15).
σ_o^2 is the noise variance at the slicer
d is the decision distance (half the level separation = 0.1575V).
and Q is defined in (3.2)

Since the output data are taken modulo-8 from the slicer output, errors which carry the slicer output eight levels away may still be correct modulo-8. The probability of error is an approximation in that this effect is ignored.

It should be noted that the expression for P(e) places an upper bound on the theoretical probability of error. This is a probability of an incorrect decision at the input to the slicer, and hence it is the probability of a symbol error. Also, the formula assumes that the 15 levels are equally spaced (which is the case here).

Expression (4.2) presents information about the likelihood of an incorrect decision but does not characterize the frequency of this event. In digital microwave systems [4.4] the final system is frequently specified in terms of the average probability of error P(e). This is also known as the average bit error rate. For example, a transmission system having an average P(e) of 10^{-6} might have error - containing seconds in every hour or might have error-free seconds throughout 24 hours with the exception of a large error burst. Normally the P(e) specification is given with an error-free second requirement.

On account of the lack of Grey-coding and the method by which errors were measured, the modem was characterized in terms of an average SER (symbol error rate) rather than an average BER (see section 4.5.6). The requirement for error-free second operation had no significance here since no long term field tests were done on the modem.

4.5.2 Error Floors

Most practical transmission systems [4.1] require a higher S/N than illustrated in the theoretical curves. Non-ideal amplitude response and imperfect group delay of practical channel filters may be the cause of performance degradation.

In badly distorted channels, an error-floor may be measured (known as the residual-error rate). Dramatic increase in S/N does not result in a lower P(e). The physical reason for performance degradation is that at the sampling instants, there is a time-variable ISI component in addition to the

desired component. Deviation from the amplitude or ideal phase of a raised-cosine Nyquist channel lead to ISI. Error floors may also occur due to excessive clock jitter or system nonlinearities.

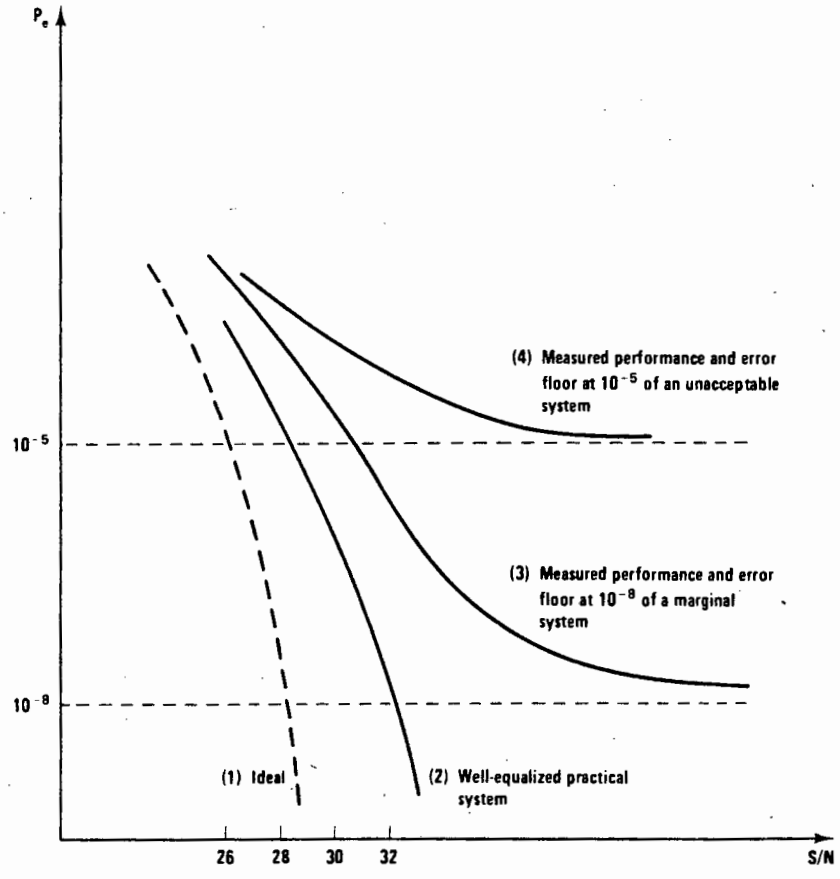

Fig. 4.10 Error floors [4.1].

The error floor effect is illustrated by the curves in Fig. 4.10. Curve (1) is the theoretical performance of a digital communication system. Curve (2) is the performance of a well equalized practical system. Curve (3) is a system which has a noise floor along the dotted line.

4.5.3 Finite Crest Factor Noise [4.1]

Theoretically, an ideal Gaussian noise process has infinitely high peaks; in other words, there is a finite chance that a

peak as high as 7σ (or even higher) will occur, even though this probability is only 10^{-12}.

The crest factor (C) of a waveform is the ratio of the peak voltage to the rms voltage. For example, the crest factor of a sine wave is 2, or 3dB. Noise with a 15dB crest factor is limited in its voltage excursion to peaks 5.6 times the rms value. Figure 4.11 illustrates this point.

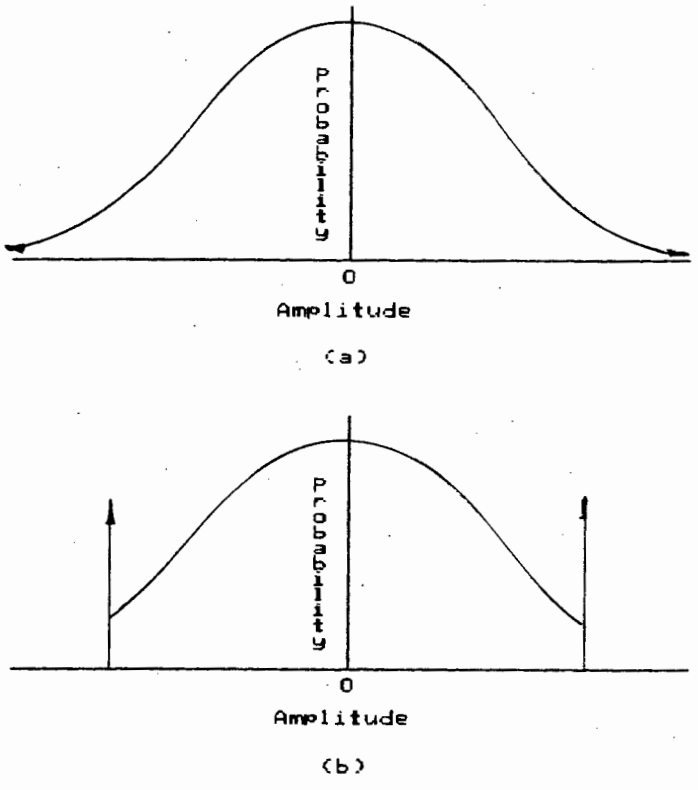

Fig. 4.11 (a) Ideal Gaussian noise, (b) Finite crest factor noise.

Most theoretical curves of P(e) verses S/N assume that the noise has an infinite crest factor. In practical noise measurements, a realizable noise source is limited in amplitude by its power supplies and components. Thus the maximum noise voltage is constrained.

Gaussian noise with an infinite crest factor will always produce a small, but finite BER, no matter how large the S/N is. However, when the crest factor is finite, reducing the noise below a definite threshold (or equivalently) raising the S/N above a definite level makes the BER actually zero. Increasing the noise, (or equivalently) reducing the S/N reduces the crest factor since the ratio of peak voltage to the rms voltage is reduced.

4.5.5 Noise Bandwidth

For impulse transmission [4.1], when filter shaping is divided equally (each $\sqrt{\alpha}$ roll-off), irrespective of the value of $\sqrt{\alpha}$, the noise power is defined as the average noise power in the single-sided Nyquist bandwidth. If this form of filtering had been used, then the average noise power would have been measured in a 170.7 kHz bandwidth.

Since 100% filter shaping was performed at the modulator, the noise bandwidth of the modem was slightly higher than the Nyquist frequency: the equivalent noise bandwidth B_e of the Butterworth channel is calculated from

$$B_e = \frac{1}{2\pi} \int_0^{\infty} \frac{1}{1 + w^{2n}} \, dw \qquad (4.3)$$

where n is the filter order = 6. Here the 3dB bandwidth is normalized to 0.159 Hz. An approximate result to the integral (obtained from MATHCAD(C) software) is B_e = 0.161 Hz. Thus the noise is measured in a

$$\frac{0.161}{0.159} \times 170.7 = 172.8 \text{ kHz}$$

bandwidth and not in the single-sided Nyquist bandwidth of 170.7 kHz.

4.5.4 White Noise Generator

Referring to Fig 4.12, the reverse voltage applied to the emitter of a BC109 will cause the emitter-base junction to break down in an avalanche mode thus forming a noisy zener diode junction. The breakdown voltage is approximately 7V. The noise generated in the junction is wideband and approximately 100μV rms. It is AC coupled so that the rms noise voltage is exactly equal to its standard deviation, σ_i [4.6]. A simple transistor amplifier with a gain of approximately six is used to amplify the noise source.

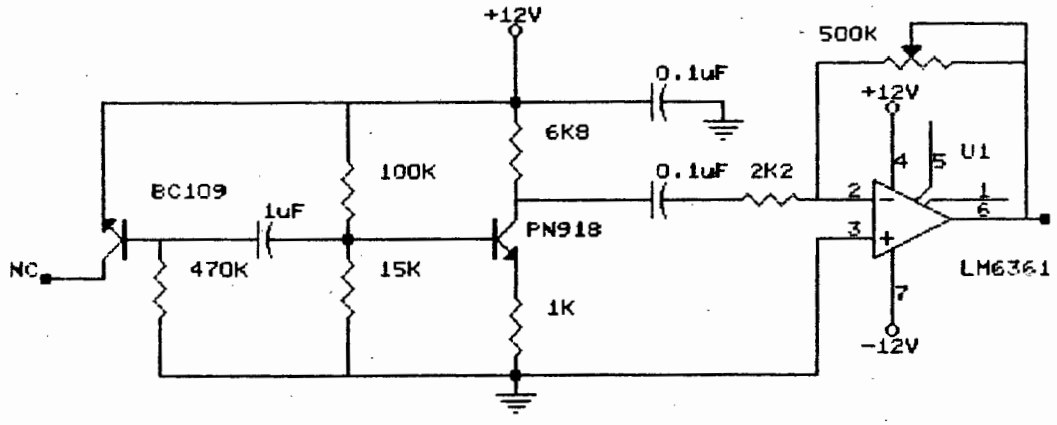

Fig. 4.12 Constructed noise source.

If the noise is to be white to the system, it is required to have a flat power spectral density beyond 240 kHz. The bandwidth of the noise is limited mainly by the frequency response of the power amplifier. For this reason, a high speed op-amp (LM6361) was used as a power amplifier. Manufacturers specifications give it a typical slew rate of 300V/μsec and a unity gain frequency of 50 MHz. It is well behaved and has a typical large signal voltage gain of 750 into a 2kΩ load. The LM6361 was used with gains from 200 to 700 into a 4.7kΩ load. The measured rms noise for a gain of 200 was approximately 40mV rms and for 700, 140mV rms. The

power spectral density of the noise was measured to be flat from DC to a frequency of at least 2 MHz.

The constructed noise source had a finite crest factor. Voltage excursions about zero volts were limited by the power supplies. If it is assumed that the full swing of ±12V was possible, then the crest factor was approximately 24dB when σ_i was 140mV rms. When σ_i was 40mV rms, the crest factor was approximately 50dB.

4.5.6 Error Counter

Several methods of error measurement of a PRS system exist. On account of the correlation properties of PRS waveforms, the data can, to a certain extent, be detected and corrected. The implementation of one such system [4.9] was considered but was not used on account of its complexity.

During experimentation, a more general method was used: the input PRBS was delayed so that it was exactly synchronized to the recovered data at the demodulator. The two sequences could then be compared and an error count taken.

Measurement of time delay through the system was done by connecting the input and output data sequences to a logic analyzer and making a time measurement. The measured delay was 14.56µs. At a data rate of 1.024 Mb/s, 14.56µs is a delay of approximately 14.2 bit periods. The input data stream was delayed for 15 bit periods (14.6µs) by means of 15 SN7496 shift registers. The clock for the shift registers was taken from the crystal oscillator. The small discrepancy of 0.04µs was cancelled out by loading both data streams into D-type latches and clocking them out in the centre of the bits (see Fig 4.13). The outputs of the two latches were connected to an (XOR) exclusive-or gate to make the necessary comparison. Table 4.2 shows how the output logic states of the XOR gate were interpreted.

Table 4.2 XOR Gate Logic

Output Voltage	Logic State	Interpretation
> 4V	1	error
< 0.4V	0	no error

The output of the XOR gate was connected to a frequency counter. The threshold level of the counter was set to approximately 2V (halfway between the two logic levels). The frequency counter was set to an averaging function over a 30 second interval.

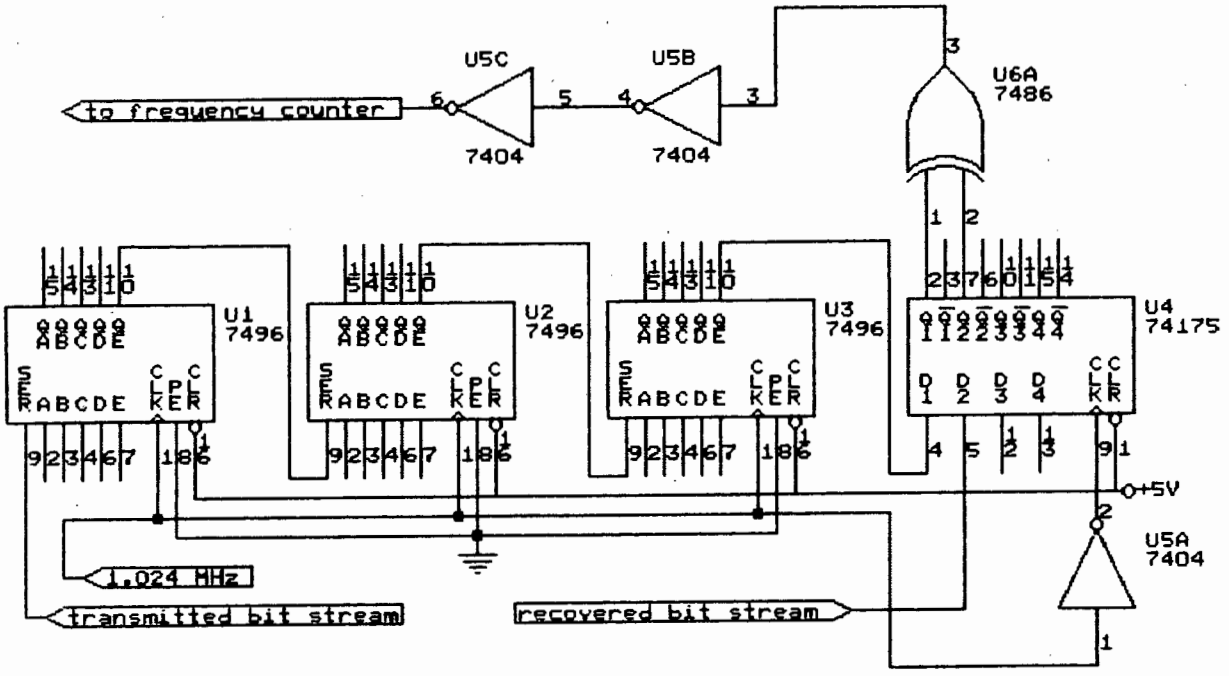

Fig. 4.13 Delay and comparison circuit.

Since no Grey-coding operation was performed, a single error measured by the frequency counter did not necessarily mean that an incorrect decision had been made by the slicer one level away. Two or even three bit errors in succession could have corresponded to a single symbol error, again not necessarily one level away. The frequency counter, being a positive edge sensitive device, detected only positive transitions in the error waveform at the output of the XOR

gate. It can therefore be concluded that the frequency counter provided a better measure of the average SER rather than of the average BER. The BER was higher than the SER by a factor in the range (1..3). Practical SER measurements could be compared to the theoretical values of expression (4.2) with no error-free second requirement. Thus for example, if the frequency counter measured 15.5 Hz after the 30 second averaging period, then the corresponding average P(e) or SER was 15.5 Hz/1.024 x 10^6 Mb/s = 15.1 x 10^{-6}.

There were definite drawbacks to this method of error frequency counting. It was possible, on account of the frequency counter being edge sensitive, that it could have failed to detect many errors (as long as they appeared consecutively). However it was assumed that the probability of long burst errors appearing under test conditions was small.

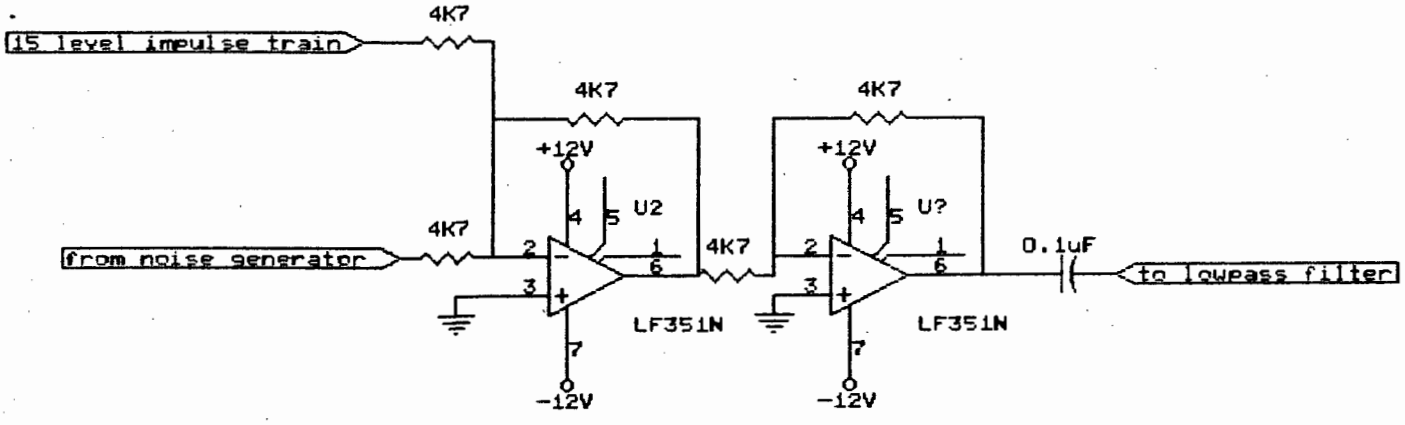

Fig. 4.14 Connection of noise source into the system.

4.5.7 Error Performance Measurements

The white noise generator was connected to the input of the Butterworth low-pass filter as shown in Fig 4.14. A digitizing oscilloscope provided a measure of the rms noise voltage at this point. The time scale on the digitizing

oscilloscope was set to 50 ns/div. This provided the highest possible sampling rate of the noise and hence the most accurate. The delay circuit and frequency counter were connected. A direct connection was made between the modulator and the demodulator. The experimental setup for error measurement is shown in Fig. 4.15.

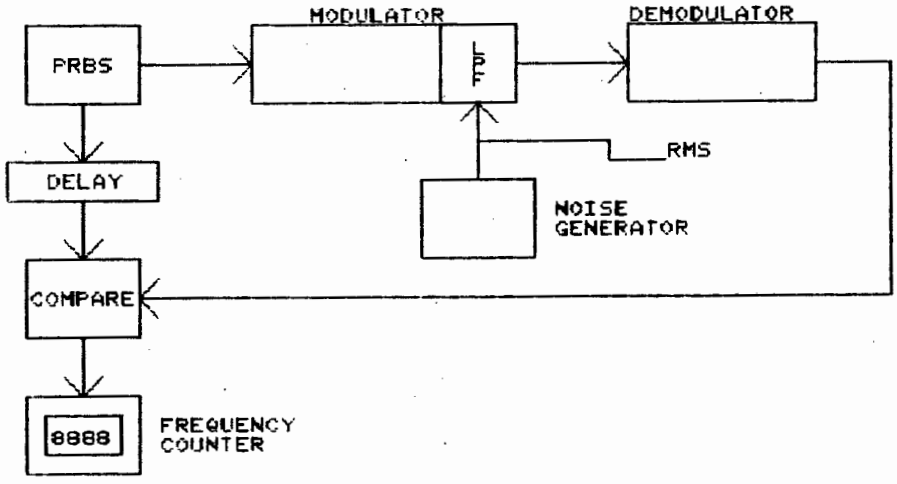

Fig. 4.15 Experimental error measurement setup.

It was extremely difficult to obtain an accurate estimate of rms noise levels (σ_o) at the input to the slicer (the point at which expression (4.2) applied), for any measured σ_i. Although the noise bandwidth of the system was known, it was impossible to determine what percentage of σ_i leaked back into the modulator circuit.

Instead, the following hypothesis was put forward: if the system is linear and saturation does not occur, then the rms noise at the slicer should be a constant fraction of the rms noise at the input to the low-pass filter.

To test this hypothesis, the system was required to operate along the curve given by (4.2). Along this curve, P(e) is determined only by the additive noise (S/N degradation due to hardware imperfections, symbol clock jitter and noise are negligible). The 7 length PRBS was used to approximate such performance. This sequence gave a worst case degradation of

1dB due to clock jitter. It generated a 12 level deterministic signal, negligible ISI at the slicer and negligible multiplicative noise in the modulator circuit.

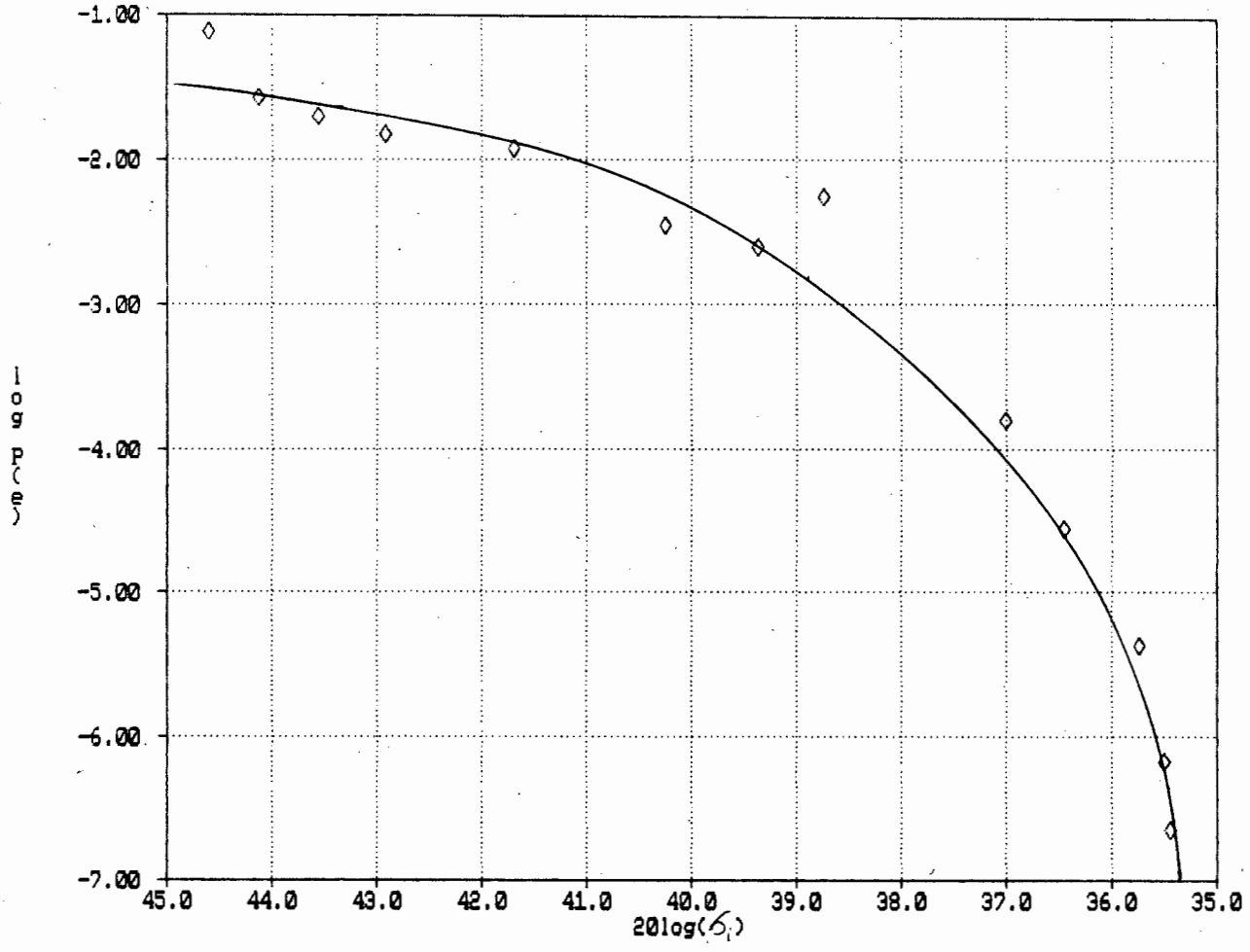

Fig 4.16 Error performance: 7 length PRBS.

At the start of each P(e) test, the PRS waveform amplitude and DC offset at the slicer were finely adjusted to give the lowest possible error frequency count. The static phase of the recovered symbol clock was also finely adjusted to give optimum results.

For each value of σ_i, a corresponding average P(e) was measured after the 30 second interval. A graph of $20\log\sigma_i$ against log P(e) is shown in Fig. 4.16. For each value of

P(e) expression (4.2) gave the corresponding value of d/σ_o. Now, since (d) was known, σ_o could be calculated. An attenuation factor A_t could then be defined as

$$A_t = \frac{\sigma_o}{\sigma_i} \qquad (4.4)$$

The graph of A_t versus σ_i (Fig. 4.17) shows that A_t is approximately constant for all values of σ_i. The average value of A_t calculated for this set of readings is 0.53. A second test verified these results. Thus it was possible to calculate σ_o for any value of σ_i.

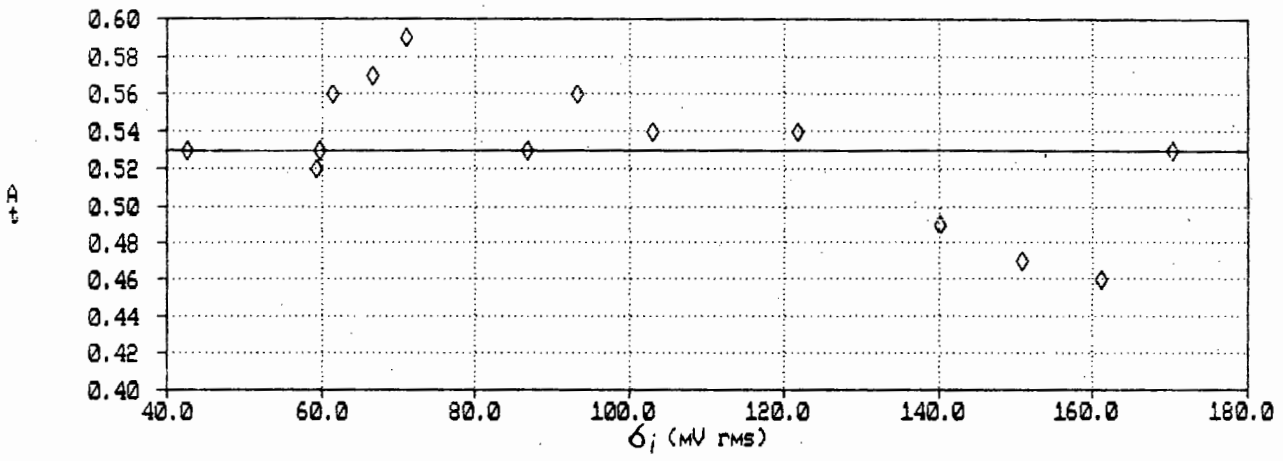

Fig. 4.17 Measurement of noise attenuation factor.

A "true" P(e) test on the modem was performed using the long PRBS. It was found that the optimum sampling instant was slightly offset from the centre of the eye. Expressed as a percentage of the horizontal eye opening, the optimum sampling instant was measured to be 20% (51ns) to the right of centre.

Intuitively it would seem that the optimum threshold level (to minimize the probability of error) is one which passes directly through the centre of the eye. However, this is not the case [4.6]. The threshold levels were fixed by the method of design. Thus the best possible error performance could only be obtained by finely adjusting the amplitude and DC offset of the waveform at the slicer input.

For each measured value of σ_i, σ_o was calculated using the attenuation factor, A_t. The eyes at the input to the slicer started closing as σ_i was increased (this was expected). The graph in Fig. 4.18 shows the best obtainable plot of $20\log(d/\sigma_o)$ against log P(e).

It was impossible to obtain a better P(e) than 5×10^{-6} (error frequency of 5.5 Hz) for the entire period over which the modem was tested. Hence the error floor at 5×10^{-6} (log P(e) = -5.3). The error floor is present for reasons discussed in section 4.5.2. The extreme deviation of the practical curve from the theoretical for decreased values of $20\log(d/\sigma_o)$ can be explained as follows:

(1) Expression (4.2) placed an upper bound on the performance of the modem. It was possible that the measured P(e) was better than the value predicted by the theory.

(2) As the additive noise σ_i increased, its peak excursions were increasingly limited due to the non-constant crest factor of the noise source. Thus the probability of the slicer making an incorrect decision was reduced.

Signal to noise ratio degradation and improvement for various P(e) can be determined from the curves. It can be seen that the S/N is degraded for $P(e) < 3 \times 10^{-5}$ (log P(e) < -4.5) and better than the theoretical for $P(e) > 3 \times 10^{-5}$. At $20\log(d/\sigma_o) = 15$, the degradation is 4dB. (Recall that the worst case degradation caused by eye closure, symbol clock jitter and the pilot tone was 2.2dB + 2.7dB + 0.2dB = 5.1dB).

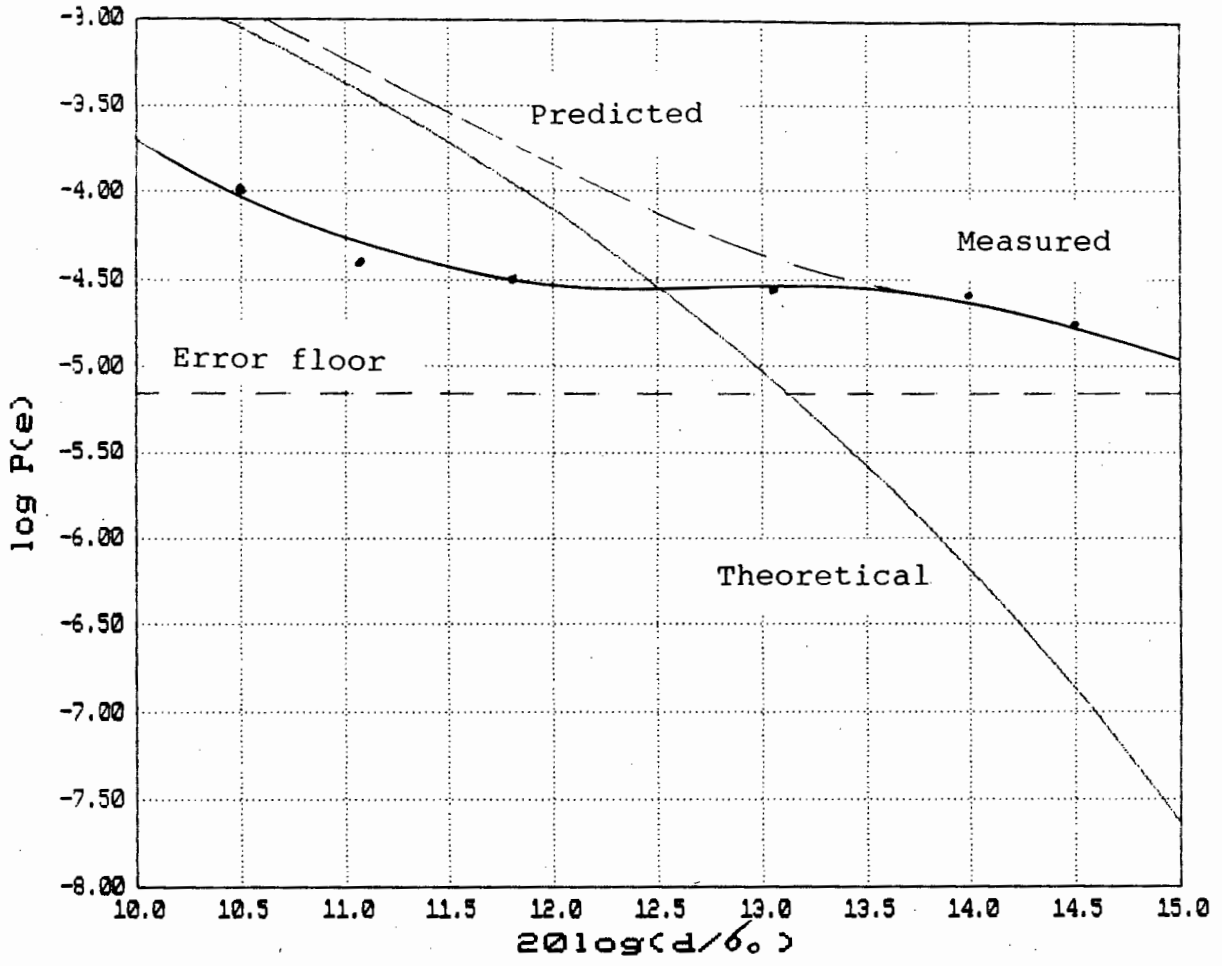

Fig. 4.18 Error performance: 2^{20}-1 length PRBS.

A prediction, based on the discussion in section (4.5.2), of the actual modem performance in the presence of white Gaussian noise is shown in Fig. 4.18. Note that the practical performance is always worse than the theoretical performance.

4.6 Equivalent Signal to Noise Ratio

Although the measurements were taken in a 172.8 kHz bandwidth, it is useful to get an indication of the equivalent S/N as measured in the single-sided Nyquist bandwidth. In the literature most curves of P(e) are plotted

against S/N and not d/σ_o. Expressions (3.1) and (4.2) are nearly equivalent in that they differ only by the constant term in front of the error functions Q. Combining the two, we get:

$$S/N\ (dB) \approx 10\log_{10}\left[\frac{M^2-1}{3}\left[\frac{4d}{\pi\sigma_0}\right]^2\right] \qquad (4.5)$$

Thus, for example, from the curve of Fig. 3.18, for $20\log(d/\sigma_0) = 12.5dB$, the approximate equivalent S/N in the single-sided Nyquist bandwidth is 27.8dB.

REFERENCES

[4.1] Feher, K. and Engineers of HP, **Telecommunications Measurements, Analysis, and Instrumentation**, Prentice-Hall Inc. 1987.

[4.2] Thow, G., Crawford, T. and Scott, P. **Fundamental Limits of Jitter Tolerance in Digital Transmission Systems**, HP Communications Symposium, 1982.

[4.3] Lender, A. Chapter 7 in reference [4.4] below.

[4.4] Feher, K. **Digital Communications: Microwave Applications**, Prentice-Hall Inc., 1981.

[4.5] Smith, B.M. **Some Results for the Eye Patterns of Class 4 Partial Response Data Signals**, IEEE Trans. on Communications, May 1974.

[4.6] Kabal, P. and Pasupathy, S. **Partial Response Signaling**, IEEE Trans. on Communications, Vol. COM-23, No.9, September 1975.

[4.7] Stremler, F.G. **Introduction to Communication Systems**, Second Edition, Addison-Wesley, 1982

[4.8] Wu, K., Sasase, I. and Feher, K. **Class-IV PRS above the Nyquist rate**, Proc. IEE, Vol.135, Pt.F, No.2, April 1988.

[4.9] Gunn, J.F and Lombardi, J.A. **Error Detection for Partial-Response Systems**, IEEE Trans. on Communication Technology, Vol. COM-17, No.6, December 1969.

C H A P T E R 5
CHANNEL IMPAIRMENTS

5.1 Introduction

In practice, supergroup filters (for DIV systems) and the channel (for DUV,DIV and DAV systems) may have significant effect on the overall system performance. This chapter is of a theoretical nature. It gives a discussion of the most common forms of channel impairments and their effect on the impulse response of the channel. The final section of this chapter goes a short way to determine the impairments caused by the Butterworth and elliptic filters designed in Chapter 3.

5.2 Ideal Channel

If the channel is ideal, then a raised-cosine power spectrum is measured at the threshold detector inputs. The performance degradation of QPRS modulated systems is the same as that of their corresponding baseband PRS systems, assuming that the channel filters are symmetrical; that is, the band-pass channel model has an equivalent low-pass model [5.1].

The equivalent [5.2] baseband of the channel distortion transfer function can be expressed as:

$$c(f) = |c(f)|e^{j\phi(f)} \tag{5.1}$$

$$A(f) = |c(f)| \tag{5.2}$$

$$\tau(f) = -\frac{1}{2\pi}\cdot\frac{d\phi}{df} \tag{5.3}$$

The distortionless channel is the standard Nyquist-shaped raised-cosine channel given in expression (2.6).

5.3 Distorted Channel

5.3.1 Amplitude Distortions

To investigate the performance degradation due to residual amplitude distortions, i.e., after adaptive equalization, we assume that the phase distortions are equalized, i.e., $\tau(f)$ = constant. The amplitude distortions are defined as follows

$$A(f) = \begin{cases} L_A f & \text{for linear distortion} \\ P_A f^2 & \text{for parabolic distortion} \\ S_A \cos\left[\frac{2\pi K f}{2 f_{BW}}\right] & \text{for sinusoidal distortion} \end{cases} \tag{5.4}$$

where K is the number of ripples of the sinusoidal distortion in the passband. Here f_{BW} is the system baseband bandwidth and L_A, P_A and S_A are parameters characterizing the amount of amplitude distortion. Here

$$f_{BW} = (1 + \alpha) f_N \tag{5.5}$$

where f_N is the Nyquist frequency

The maximum amplitude distortion A_m is

$$A_m \text{ (dB)} = \begin{cases} L_A\,(2f_{BW}) & \text{linear} \\ P_A\,(f_{BW})^2 & \text{parabolic} \\ S_A & \text{sinusoidal} \end{cases} \tag{5.6}$$

Figure 5.1 shows the residual amplitude distortions of the channel and their corresponding impulse responses. Figure 5.1(a) is the ideal raised-cosine Nyquist channel. The impulse response of this channel has rapidly decaying sidelobes. Parabolic amplitude distortion in the channel produces an impulse response with ringing in the sidelobes. Hence there is an increased probability of ISI in adjacent time slots. Sinusoidal amplitude distortion of the channel

has a corresponding impulse response whose sidelobes are separated by $K/2f_{BW}$.

Research has shown [5.2, 5.4] that for a given value of A_m, sinusoidal amplitude distortion generally causes the worst degradation. Linear and parabolic distortion have less severe effect. Note that all three impulse responses in Fig. 5.1 are symmetrical about τ_0 (constant group delay term).

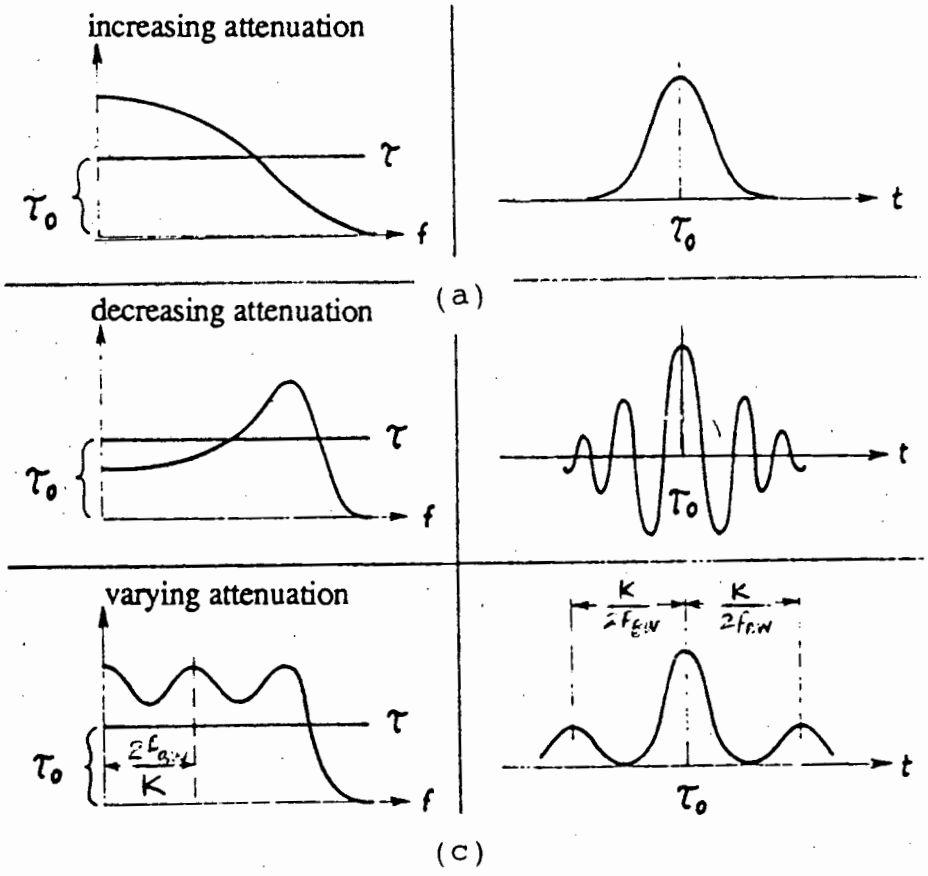

Fig. 5.1 Amplitude distortion functions: (a) ideal raised-cosine Nyquist channel, (b) parabolic, (c) sinusoidal, (linear not shown) [5.3].

5.3.2 Group Delay Distortion

We assume that the amplitude distortions are equalized, i.e. $A(f) = 1$. Again, three different characteristics for group delay distortions are defined

$$\tau(f) = \begin{cases} L_D f & \text{linear} \\ P_D f^2 & \text{parabolic} \\ S_D \cos\left[\frac{2\pi f K}{2f_{BW}}\right] & \text{sinusoidal} \end{cases} \qquad (5.7)$$

where L_D, P_D, S_D are parameters characterizing the amount of group delay, and the rest of the notations are the same as for amplitude distortions. The maximum group delay in each case is τ_m

$$\tau_m = \begin{cases} L_D\ (2f_{BW}) & \text{linear} \\ P_D\ (f_{BW})^2 & \text{parabolic} \\ S_D & \text{sinusoidal} \end{cases} \qquad (5.8)$$

Figure 5.2 shows the residual group delay distortions of the channel and the corresponding impulse responses. Again the ideal channel is the raised-cosine Nyquist channel of Fig. 5.1(a). Linear and parabolic group delay distortions produce channel impulse responses which are symmetrical. Here τ_0 (group delay at DC) is the centre of gravity of the impulse responses. Higher signal frequencies are delayed longer than lower signal frequencies due to increasing group delay. Sinusoidal group delay distortion produces a symmetrical impulse response whose sidelobes are separated from the main lobe by $K/2f_{BW}$.

Computer simulations [5.2, 5.4, 5.5] have shown that linear group delay distortion generally causes the most severe degradation in system performance.

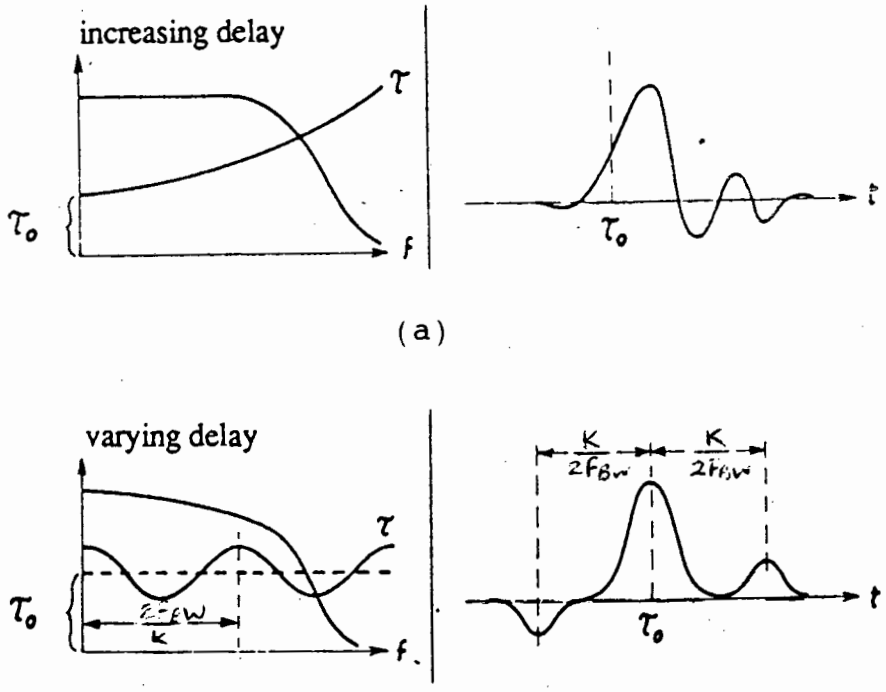

Fig. 5.2 Group delay distortion functions: (a) parabolic, (b) sinusoidal, (linear not shown) [5.3].

5.4 Butterworth and Elliptic Distortion

Referring to Fig. 3.12, it can be seen that the 6th order Butterworth response is similar to Fig. 5.2(a) (except for frequencies above f_N). Thus the impulse response of the Butterworth channel is asymmetrical with a centre of gravity, τ_0 of approximately 3.8μs. The 6th order elliptic response is a combination of 5.1(c) and 5.2(a). The impulse response of this channel is asymmetrical. with $\tau_0 \approx 3\mu s$. The impulse response of the elliptic channel is more distorted than the Butterworth response due to its extreme deviation from the ideal raised-cosine Nyquist channel. These results serve to reinforce the practical measurements taken of vertical eye openings of the two filters. Recall that the Butterworth channel eyes were 77% open, and the elliptic less than 20%.

REFERENCES

[5.1] Feher, K. **Digital Communications: Satellite/Earth Station Engineering**, Prentice-Hall Inc., 1983.

[5.2] Mathiopoulos, P. and Feher, K. **Performance of a 512-QAM system in distorted channels**, Proc. IEE, Vol.133, Pt. F, No.2, April 1986

[5.3] KÜpfmÜller, **Die Systemtheorie der elekr. Nachr.Übertr**, S. Hirzel Stuttgart, 1952

[5.4] Kucar, A.D. and Feher, F. **On 1.544 Mb/s and 2.048 Mb/s Modems for CCITT Supergroup DIV and DAVID Applications**, IEEE ICC, Chicago 1986, pp. 446-451.

[5.5] Hill, T. and Feher, K. **A Performance Study of NLA 64-State QAM**, IEEE, Vol. COM-31, No. 6, June 1983.

CHAPTER 6
CONCLUSION

This chapter starts with a summary of the developments of the previous chapters. Conclusions in section 6.2 are drawn, based on the findings of Chapters 3 and 4. Recommendations for further areas of study are given in section 6.3. Section 6.4 contains concluding remarks.

6.1 Chapter Summary

In Chapter 2, the necessary theory was developed to aid in the understanding of methods employed in the design of the experimental modem. Nyquist's theorems were discussed: it was shown that the raised-cosine Nyquist channel is the channel which the filter designer should attempt to approximate. Theory was developed for PRS schemes with binary input. It was shown how the theory could be extended to multilevel inputs.

Chapter 3 described the design and construction of an experimental class-4 15 PRS baseband modem. The transmission rate was 1.024 Mb/s in a 240 kHz basic supergroup bandwidth. This corresponded to a non-minimum bandwidth modem with a transmission spectral efficiency of 4.27 b/s/Hz. The modem was best suited to DUV applications.

The input to the modem was a binary NRZ stream. A serial-to-parallel converter was used to group every three serial bits into an eight-state symbol (i.e, one of the numbers 0,1,2,3,4,5,6,7) represented by three parallel bits at a symbol rate of 341.3 ksymbols/s. Precoding for error prevention was performed. The class-4 15 PRS encoder and DAC were used to convert the eight-state precoded symbols into a 15 level waveform. The ideal raised-cosine Nyquist channel was approximated by a 6th order Butterworth filter with no phase or amplitude equalization. A pilot tone was added to the PRS signal in the spectral null at 170.7 kHz. The pilot

tone was used to facilitate symbol timing recovery at the demodulator.

The decoder employed 14 slicers (threshold detectors) to quantize the received signal into one of 15 levels. This decoding method was the well known symbol-by-symbol detection. The pilot tone was recovered from the data by means of a high-Q tuned circuit. A PLL was used to recover the clock lines. The parallel binary outputs of the slicers were combined using standard logic gates to give a replica of the serial transmitted data.

Chapter 4 described the test measurements obtained to characterize the performance of the modem. The main results of the chapter are summarized below:

- data test sequence: $2^{20}-1$ PRBS
- transmission rate: 1.024 Mb/s
- bandwidth: 240 kHz (-19dB)
- noise bandwidth: 172.8 kHz
- worst case S/N degradation caused by
  1. data transition jitter: no estimate
  2. filter and hardware imperfections: 2.2dB
  3. recovered symbol clock jitter: 2.7dB
  4. pilot tone: 0.2dB
- maximum increase above nominal transmission rate for one eye closure: 6.7%
- error floor: 5×10^{-6}
- S/N degraded for:
  $P(e) < 3 \times 10^{-5}$ $(\log P(e) < -4.5)$
- S/N better than theoretical for:
  $P(e) > 3 \times 10^{-5}$
- equivalent S/N (in the single-sided Nyquist bandwidth) at $P(e) = 3 \times 10^{-5}$: 27.8dB

Chapter 5 discussed the more common channel distortion functions. It was shown how both amplitude and group delay distortion effect the impulse response of the channel. A

comparison was made between the theory of this chapter and results obtained from measurements of the Butterworth and elliptic filters.

6.2 Discussion of Results

The Butterworth filter had a measured attenuation of 19dB at 240 kHz. At 312 kHz, the lowest supergroup FDM channel, the measured Butterworth attenuation was 32dB. Whether this attenuation is sufficient to prevent CCI remains to be investigated. The elliptic filter had a measured attenuation of 45dB at 240 kHz. This filter is suited to DIV applications where the demands on the out of band attenuation are more stringent. However, the elliptic filter without several orders of phase equalization is of no practical use.

The addition of a pilot tone to the signal to facilitate clock recovery at the demodulator proved to be a useful technique. The estimated worst case degradation due to the pilot tone was 0.2dB. The pilot tone to signal power ratio was chosen to be 1/20. This ratio was sufficiently low so as to prevent distortion (twisting) of the eye diagram. Whether the pilot tone scheme performs better than a non-linear network (discussed in section 3.5.1.) remains to be investigated.

It is impossible to determine whether the $2^{20}-1$ length PRBS approximated the characteristics of live traffic. It is also possible that, on account of the run properties of the PRBS, a live traffic test will give different recovered clock jitter results.

The characteristics of the 7 length PRBS were such that it was possible to obtain near optimum performance from the modem. The noise attenuation factor (A_t) through the system was determined by the use of this sequence.

The measured P(e) curve for the $2^{20}-1$ PRBS sequence bore little resemblance to the theoretical curve. The specification given in Chapter 3 was that the BER be at worst 10^{-8} under noiseless conditions. The error floor of 5×10^{-6} in the SER corresponds to a pessimistic BER of 15×10^{-6} (three bit errors for each symbol error). Thus, the BER is at worst 3.5 orders of magnitude higher than the specification.

The error floor can be attributed to:

- deviation from the characteristics of the ideal raised-cosine Nyquist channel
- hardware imperfections
- clock jitter in the recovered symbol clock
- a time-variable ISI component at the slicer
- multiplicative noise caused by the propagation of the random PRS waveform

The totally false optimistic measured results for P(e) for low values of $20\log(d/\sigma_o)$ could be attributed to the non constant crest factor of the test noise source. A prediction of the actual modem performance in the presence of white Gaussian noise showed that in all cases its performance was worse than the theoretical.

A test noise source will always have a finite crest factor for the reasons discussed in section 4.5.3. Care must be taken to correctly interpret the results of practical measurements.

The immunity of the 7 length PRBS to the crest factor of the noise source for low values of $20\log(d/\sigma_o)$ may be due to its short repetition time and peculiar spectral properties.

6.3 Recommendations for Future Work

From the results of work in this thesis, it can be seen that further development of the experimental modem is necessary for it to be of practical use.

A main avenue for future work should be in the design of data transition jitter-tolerant low-pass filter which meets the requirements given in section 3.4.6. If two such filters, having $\sqrt{\alpha}$ roll-off parameters, are substituted for the present Butterworth filter, a significant improvement in performance can be expected. In the present design, there is approximately 1dB loss in S/N due to 100% filter shaping and further degradation due to amplitude and group delay distortion.

Improvements can be made to hardware layout to minimize performance degradation. Grey-coding should be performed before the precoding operation at the modulator, and decoding after the slicer at the demodulator.

The introduction of low redundancy FEC coding is a practical possibility. There will be an optimum code redundancy [6.1] at the point where the S/N degradation caused by eye closure at the new transmission rate is totally outweighed by the S/N improvement effected by the coding. However, the drawback with FEC coding is that there is increased decoding time at the demodulator.

The use of maximum likelihood sequence estimation instead of symbol-by-symbol detection for a class-4 15 PRS scheme is attractive. The problem is that the hardware implementation of such a scheme is extremely complex [6.2].

In future experimentation, channel distortion functions should be introduced to determine their effect on the system performance. The design of a BATE will be a necessity to equalize for such impairments.

6.4 Concluding Remarks

The advantages of DUV, DIV and DAV(DAVID) hybrid transmission systems were discussed in Chapter 1. The experimental modem is not, it its present form, suitable to operate in one of these hybrid transmission systems. However, with further development, the final product could well find practical application in the existing FDM-FM microwave systems.

REFERENCES

[6.1] Braun, R.M., Golby, J., Joffe, N.R and Mashau, D. **Partial Response Signalling with Forward Error Correction**, Research Review, Dept. Electrical and Electronic Engineering, UCT, Vol. 12, No.4, May 1988.

[6.2] Wu, K., Sasase, I. and Feher, K. **Class-IV PRS above the Nyquist rate**, Proc. IEE, Vol.135, Pt F, No.2, April 1988.

APPENDIX

A P P E N D I X A

SIXTH ORDER ELLIPTIC AND BUTTERWORTH FILTER DESIGN

```
**************************************************************
Eureka: The Solver, Version 1.0
Tuesday September 12, 1989, 1:10 pm.
Name of input file: A:\BIQUAD
**************************************************************

;6th order Biquad Low-Pass Elliptic Filter Design

;Cutoff Frequency is 168 kHz
;Minimum Stopband loss is 50 dB
;Transition width is 0.3513
;Passband Ripple width is 0.1 dB

;

R1 = A/(K*B*C*wc*C1)

R2 = 1/(B*wc*C1)     ;single-turn - adjusts Q, the pole pair related
                     ;to Bwc

R3 = 1/(sqrt(C)*wc*C1)   ;multi-turn pot - adjusts the cutoff freq,

R4 = (A*R7)/(K*C)    ;multi-turn pot - adjusts the notch freq, fz

R5 = 1/(K*sqrt(C)*wc*C2)

R6 = (C1*R3)/C2

R7 = 1/(wc*C1)

K = 1:  Q = sqrt(C)/B

C2 = C1      ;for reasonable values of K and Q

C1 = 10/fc * 1E-06

fz = fc*sqrt(A)     ;notch frequency of the stage

fcs = fc*sqrt(C)    ;cutoff frequency of the stage

wc = 2*pi*fc

pi = 3.141592654

fc = 168E03    ;cutoff frequency of the combined stages

;                A                B                C

{1:}     A =    1.912825 :   B =   1.017329 :    C =    0.399933
{2:}   {A =    3.054375 :   B =   0.526750 :    C =    0.825165}
{3:}   {A =   19.226054 :   B =   0.141167 :    C =    1.088829}
```

```
**********************************************************************
Eureka: The Solver, Version 1.0
Tuesday September 12, 1989, 1:10 pm.        Elliptic - section 1
Name of input file: A:\BIQUAD
**********************************************************************


**********************************************************************

Solution:

 Variables      Values

 A          =      1.9128250

 B          =      1.0173290

 C          =      .39993300

 C1         = 5.9523810e-11

 C2         = 5.9523810e-11

 fc         =      168000.00

 fcs        =      106243.63

 fz         =      232352.26

 K          =      1.0000000

 pi         =      3.1415927

 Q          =      .62163033

 R1         =      74824.997

 R2         =      15644.393

 R3         =      25166.714

 R4         =      76121.639

 R5         =      25166.714

 R6         =      25166.714

 R7         =      15915.494

 wc         =      1055575.1
```

```
**********************************************************************
Eureka:  The Solver,  Version 1.0
Tuesday September 12,  1989,  1:07 pm.          Elliptic - section 2
Name of input file:  A:\BIQUAD
**********************************************************************
```

****

Solution:

Variables		Values
A	=	3.0543750
B	=	.52675000
C	=	.82516500
C1	=	5.9523810e-11
C2	=	5.9523810e-11
fc	=	168000.00
fcs	=	152608.84
fz	=	293609.74
K	=	1.0000000
pi	=	3.1415927
Q	=	1.7245105
R1	=	111840.00
R2	=	30214.512
R3	=	17520.631
R4	=	58911.718
R5	=	17520.631
R6	=	17520.631
R7	=	15915.494
wc	=	1055575.1

```
**********************************************************************
Eureka: The Solver, Version 1.0
Tuesday September 12, 1989, 1:03 pm.       Elliptic - section 3
Name of input file: A:\BIQUAD
**********************************************************************

**********************************************************************

Solution:

 Variables     Values

 A             =      19.226054

 B             =      .14116700

 C             =      1.0888290

 C1            = 5.9523810e-11

 C2            = 5.9523810e-11

 fc            =      168000.00

 fcs           =      175302.91

 fz            =      736638.41

 K             =      1.0000000

 pi            =      3.1415927

 Q             =      7.3917395

 R1            =      1990753.2

 R2            =      112742.31

 R3            =      15252.474

 R4            =      281028.66

 R5            =      15252.474

 R6            =      15252.474

 R7            =      15915.494

 wc            =      1055575.1
```

```
**********************************************************************
Eureka:  The Solver,  Version 1.0
Tuesday September 12,  1989,  1:15 pm.
Name of input file:  A:\BUTTQUAD
**********************************************************************


;6th order Biquad Low-Pass Butterworth Filter Design

;Cutoff Frequency (-3 dB) is 170.667 kHz
;Minimum Stopband loss is 17.8 dB

;


R1 = R4/(K*C)   ;adjusts K

R2 = R4/B       ;adjusts passband response

R3 = R4/C       ;adjusts fc

R4 = 1/(wc*C1)

Q = sqrt(C)/B

C1 = 56E-12     ;approx 10/fc * 1E-06

Km = (2*C*K)/(B*sqrt(4*C-B^2))   ;if B^2/C < 2,
                                 ;the response peaks at fm

fm = fc*sqrt(C-B^2/2)            ;

Kc = (K*C)/(sqrt((C-1)^2+B^2))   ;amplitude of response at fc

wc = 2*pi*fc

pi = 3.141592654

fc = 170.667E03

K=1   ;gain of stage

C=1

  B =  0.517638 ;  stage 1
;  B =  1.414214 ;  stage 2
;  B =  1.931852 ;  stage 3
```

```
**********************************************************************
Eureka:  The Solver,  Version 1.0
Tuesday September 12, 1989, 2:29 pm.     Butterworth - section 2
Name of input file: A:\BUTTQUAD
**********************************************************************

 B           =      1.4142140

 C           =      1.0000000

 C1          = 5.6000000e-11

 fc          =      170667.00

 K           =      1.0000000

 Kc          =      .70710656

 Km          =      1.0000000

 pi          =      3.1415927

 Q           =      .70710656

 R1          =      16652.619

 R2          =      11775.176

 R3          =      16652.619

 R4          =      16652.619

 wc          =      1072332.4
```

```
**********************************************************************
Eureka:  The Solver, Version 1.0
Tuesday September 12, 1989, 1:15 pm.      Butterworth - section 1
Name of input file:  A:\BUTTQUAD
**********************************************************************

 B            =      .51763800

 C            =      1.0000000

 C1           = 5.6000000e-11

 fc           =      170667.00

 fm           =      158823.54

 K            =      1.0000000

 Kc           =      1.9318520

 Km           =      2.0000003

 pi           =      3.1415927

 Q            =      1.9318520

 R1           =      16652.619

 R2           =      32170.395

 R3           =      16652.619

 R4           =      16652.619

 wc           =      1072332.4
```

```
**********************************************************************
Eureka: The Solver, Version 1.0
Tuesday September 12, 1989, 2:26 pm.      Butterworth - section 3
Name of input file: A:\BUTTQUAD
**********************************************************************

 B           =      1.9318520

 C           =      1.0000000

 C1          = 5.6000000e-11

 fc          =      170667.00

 K           =      1.0000000

 Kc          =      .51763800

 Km          =      2.0000047

 pi          =      3.1415927

 Q           =      .51763800

 R1          =      16652.619

 R2          =      8620.0284

 R3          =      16652.619

 R4          =      16652.619

 wc          =      1072332.4
```

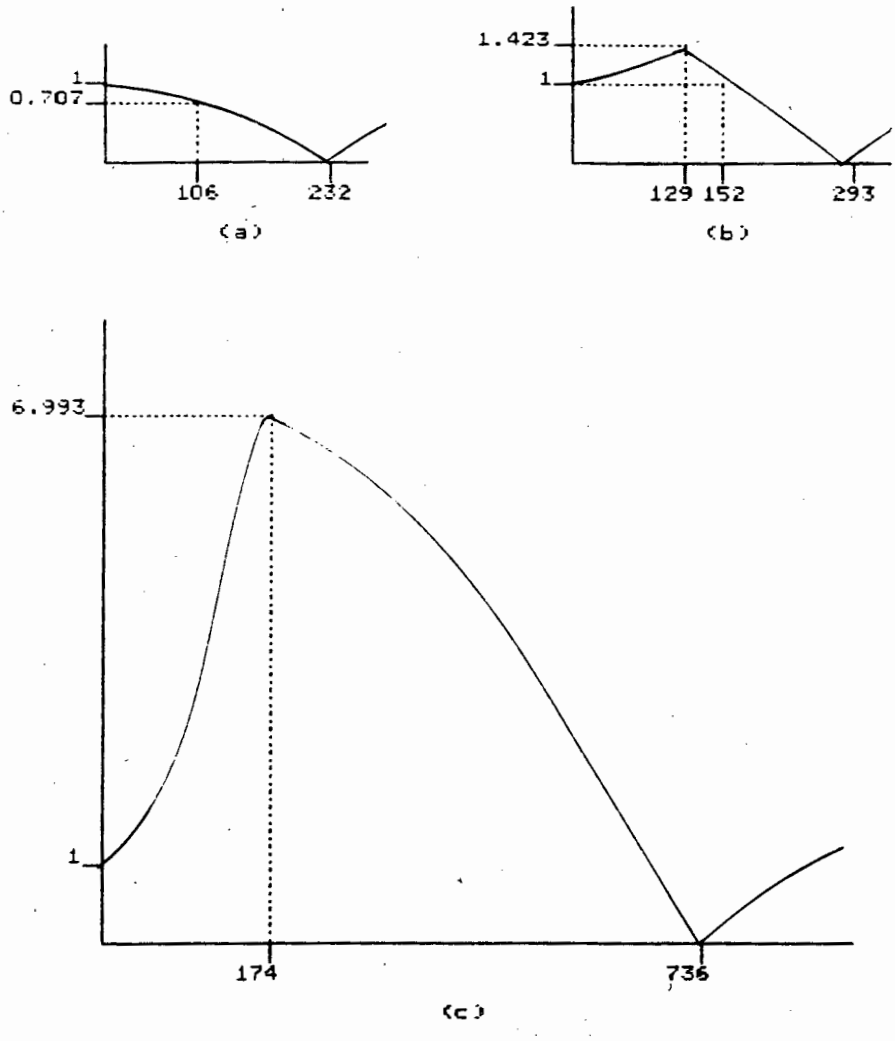

Fig. A.1 Elliptic second order section amplitude responses (vertical axes are normalized to a DC gain of one, horizontal axes are in kHz).

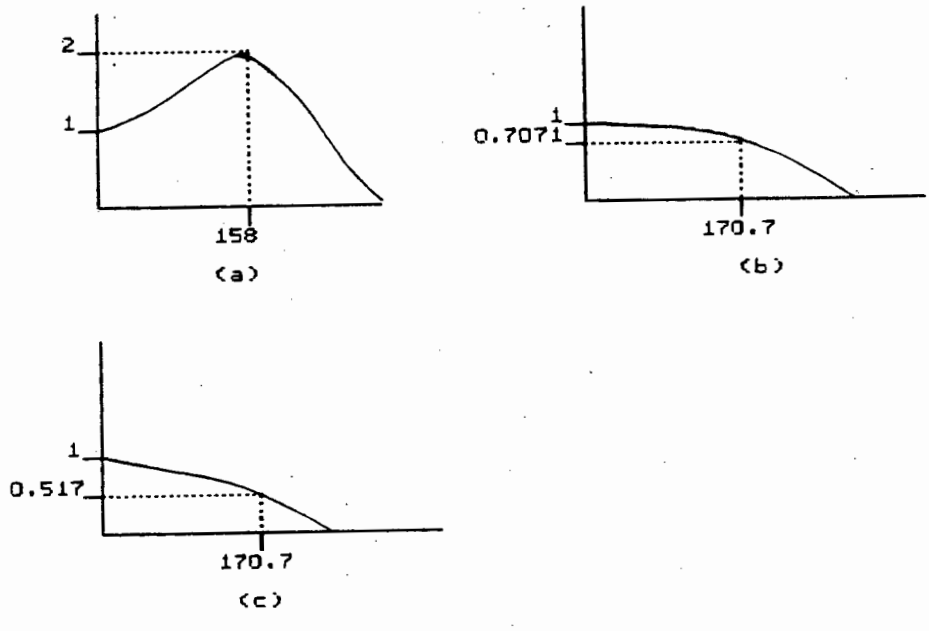

Fig. A.2 Butterworth second order section amplitude responses (vertical axes are normalized to a DC gain of one, horizontal axes are in kHz).

A P P E N D I X B
LINEAR PLL THEORY

With reference to Fig. 3.15, the operation of the PLL circuit can be described as follows:

The phase comparator is basically an analog multiplier that forms the product of the pilot tone input signal, $v_i(t)$, and the reference signal, $v_o(t)$, from the divide-by-two circuit. Assume that the two signals two be multiplied can be described by

$$v_i(t) = V_i \sin(w_i t) \tag{B.1}$$
$$v_o(t) = V_o \sin(w_o t + \theta_e) \tag{B.2}$$

where w_i, w_o and θ_e are the frequency and phase difference (or phase error) characteristics of interest. The product of these two signals is an output voltage given by

$$v_e(t) = V_1 V_o (\sin w_i t)[\sin(w_o t + \theta_e)] \tag{B.3}$$

Note that the amplitude of $v_e(t)$ is directly proportional to the amplitude of the input signal V_i. The two cases of an unlocked loop ($w_i \neq w_o$) and of a locked loop ($w_i = w_o$) are now considered separately.

Unlocked State When the two frequencies to the phase comparator are not synchronized, the loop is not locked. Furthermore the phase angle difference θ_e in (B.2) and (B.3) is meaningless for this case since it can be eliminated by appropriately choosing the time origin.

Using trigonometric identities, (B.3) can be rewritten as

$$v_e(t) = \frac{V_i V_o}{2} [\cos(w_i - w_o)t - \cos(w_i + w_o)t] \tag{B.4}$$

$v_e(t)$ is then scaled by the phase detector conversion constant K_d. When $v_e(t)$ is passed through the low-pass filter, the sum frequency component is removed, leaving

$$v_f(t) = B\cos(w_i - w_o)t \qquad (B.5)$$

where $B = \frac{K_d V_i V_o}{2}$

After amplification (A), the control voltage for the VCO appears as

$$v_d(t) = AB\cos(w_i - w_o)t \qquad (B.6)$$

This equation shows that a beat frequency effect is established between wi and wo causing the VCO's frequency to deviate by ± δw from $6w_o`$ (on account of the divide-by circuit) in proportion to the signal amplitude AB. If the amplitude is sufficiently high and if signal limiting or saturation does not occur, the VCO output frequency will be shifted from $6w_o`$ by some δw until lock is established where

$$w_i = w_o = w_o` \pm \delta w/6 \qquad (B.7)$$

If lock cannot be established, then either V_i is too small to drive the VCO to produce the necessary ± δw deviation or w_i is beyond the dynamic range of the VCO.

Locked State When w_i and w_o are frequency synchronized, the output signal from the phase comparator for $w_i = w_o = w$ and a phase shift of θ_e is

$$\begin{aligned} v_e(t) &= V_i V_o(\sin wt)(\sin wt + \theta_e) \\ &= \frac{V_i V_o}{2}[\cos\theta_e - \cos(2wt - \theta_e)] \end{aligned} \qquad (B.8)$$

The low-pass filter removes the high frequency, AC component of $v_e(t)$, leaving only the DC component. Thus

$$v_f(t) = \frac{V_i V_o}{2} \cos \theta_e \qquad (B.9)$$

After amplification, the DC voltage driving the VCO and maintaining lock within the loop is

$$v_d(t) = AB\cos \theta_e \qquad (B.10)$$

Suppose w_i and w_o are perfectly synchronized to the free-running frequency 6wo`. For this case, $v_d = 0$, indicating that $\theta_e$ must be ± 90°. Thus $v_d$ is proportional to the phase difference or phase error between $\theta_i$ and $\theta_o$ centred about a reference phase angle of ± 90°. If $w_i$ changes slightly from $w_o$`, the first effect will be a change in θ_e from ± 90°. v_d will adjust and settle out to some non-zero value to correct w_o; under this condition frequency lock is maintained with $w_i = w_o$. The phase error will be shifted by some amount $\delta\theta$ from the reference phase angle of ± 90°. This concept can be simplified by redefining θ_e as

$$\theta_e = \theta_r \pm \delta\theta \qquad (B.11)$$

where θ_r is the inherent, reference phase shift of ± 90° and $\delta\theta$ is the departure from the reference value. Now the VCO control voltage becomes

$$v_d = \pm AB\sin\delta\theta \qquad (B.12)$$

Since the sine function is odd, a momentary change in $\delta\theta$ contains information about which way to adjust the VCO frequency to correct and maintain the locked condition. The maximum range over which $\delta\theta$ can be tracked is -90° to +90°. This corresponds to a θ_e range from 0 to 180°.

A P P E N D I X C

PROBABILTITY OF ERROR TABLES FOR 15 PRS

The table given here was generated from expressions (4.2) and (4.5) for given values of d/σ_0. Note that M (no. input levels) = 8 and L (no. ouptut levels) = 15.

Table C.1 Theoretical Probability of Error for 15 PRS

d/σ_o	$20\log(d/\sigma_o)$	Approximate S/N (single-sided Nyquist BW) $\gamma\beta$	$Q(d/\sigma_o)$	P(e) (symbol error)	log P(e)
3.00	9.5	24.9	1.35E-03	2.52E-03	-2.6
3.05	9.7	25.0	1.14E-03	2.13E-03	-2.7
3.10	9.8	25.1	9.68E-03	1.81E-02	-1.7
3.15	10.0	25.3	8.16E-03	1.52E-02	-1.8
3.20	10.1	25.4	6.87E-03	1.28E-02	-1.9
3.25	10.2	25.6	5.77E-03	1.08E-02	-2.0
3.30	10.4	25.7	4.83E-03	9.02E-03	-2.0
3.35	10.5	25.8	4.04E-03	7.54E-03	-2.1
3.40	10.6	25.9	3.37E-03	6.29E-03	-2.2
3.45	10.8	26.1	2.80E-03	5.23E-03	-2.3
3.50	10.9	26.2	2.33E-03	4.35E-03	-2.4
3.55	11.0	26.3	1.93E-04	3.60E-04	-3.4
3.60	11.1	26.4	1.59E-04	2.97E-04	-3.5
3.65	11.2	26.6	1.31E-04	2.45E-04	-3.6
3.70	11.4	26.7	1.08E-04	2.02E-04	-3.7
3.75	11.5	26.8	8.84E-05	1.65E-04	-3.8
3.80	11.6	26.9	7.23E-05	1.35E-04	-3.9
3.85	11.7	27.0	5.91E-05	1.10E-04	-4.0
3.90	11.8	27.1	4.81E-05	8.98E-05	-4.0
3.95	11.9	27.3	3.91E-05	7.30E-05	-4.1
4.00	12.0	27.4	3.17E-05	5.92E-05	-4.2
4.05	12.1	27.5	2.56E-05	4.78E-05	-4.3
4.10	12.3	27.6	2.07E-05	3.86E-05	-4.4
4.15	12.4	27.7	1.66E-05	3.10E-05	-4.5
4.20	12.5	27.8	1.33E-05	2.48E-05	-4.6
4.25	12.6	27.9	1.07E-05	2.00E-05	-4.7
4.30	12.7	28.0	8.54E-06	1.59E-05	-4.8
4.35	12.8	28.1	6.81E-06	1.27E-05	-4.9
4.40	12.9	28.2	5.41E-06	1.01E-05	-5.0
4.45	13.0	28.3	4.29E-06	8.01E-06	-5.1
4.50	13.1	28.4	3.40E-06	6.35E-06	-5.2
4.55	13.2	28.5	2.68E-06	5.00E-06	-5.3
4.60	13.3	28.6	2.11E-06	3.94E-06	-5.4
4.65	13.3	28.7	1.66E-06	3.10E-06	-5.5
4.70	13.4	28.8	1.30E-06	2.43E-06	-5.6
4.75	13.5	28.9	1.02E-06	1.90E-06	-5.7
4.80	13.6	28.9	7.93E-07	1.48E-06	-5.8
4.85	13.7	29.0	6.17E-07	1.15E-06	-5.9
4.90	13.8	29.1	4.79E-07	8.94E-07	-6.0
4.95	13.9	29.2	3.71E-07	6.93E-07	-6.2
5.00	14.0	29.3	2.87E-07	5.36E-07	-6.3
5.05	14.1	29.4	2.21E-07	4.13E-07	-6.4
5.10	14.2	29.5	1.70E-07	3.17E-07	-6.5

d/σ_e	$20\log(d/\sigma_o)$	Approximate S/N (single-sided Nyquist BW) dB	$Q(d/\sigma_o)$	P(e) (symbol error)	log P(e)
5.15	14.2	29.6	1.30E-07	2.43E-07	-6.6
5.20	14.3	29.6	9.96E-08	1.86E-07	-6.7
5.25	14.4	29.7	7.16E-08	1.34E-07	-6.9
5.30	14.5	29.8	5.79E-08	1.08E-07	-7.0
5.35	14.6	29.9	4.40E-08	8.21E-08	-7.1
5.40	14.6	30.0	3.33E-08	6.22E-08	-7.2
5.45	14.7	30.0	2.52E-08	4.70E-08	-7.3
5.50	14.8	30.1	1.90E-08	3.55E-08	-7.5
5.55	14.9	30.2	1.43E-08	2.67E-08	-7.6
5.60	15.0	30.3	1.07E-08	2.00E-08	-7.7
5.65	15.0	30.4	8.03E-09	1.50E-08	-7.8
5.70	15.1	30.4	6.00E-09	1.12E-08	-8.0
5.75	15.2	30.5	4.47E-09	8.34E-09	-8.1
5.80	15.3	30.6	3.32E-09	6.20E-09	-8.2